

Infocommunications Journal

A PUBLICATION OF THE SCIENTIFIC ASSOCIATION FOR INFOCOMMUNICATIONS (HTE)

March 2013

Volume V

Number 1

ISSN 2061-2079

PAPERS

- Global and Local Coverage Maximization in Multi-camera Networks
by Stochastic Optimization *K.K. Reddy and N. Conci* 1
- Receivers Design for OFDM Signals under both High Mobility
and Carrier Frequency Offset *Dong-Hua Chen, Gong-Yi Huang, Yi-Ming Yang* 9
- Applications of a Simplified Protocol of RoboCup 2D Soccer Simulation
N. Bátfai, R. Dóczy, J. Komzsis, A. Mamenyák, Cs. Székelyhídi, J. Zákány, M. Ispány, Gy. Terdik 15

DESIGN STUDIES

- Investigation of the Fault Tolerance of the PIM-SM IP Multicast Routing Protocol
for IPTV Purposes *G. Lencse and I. Derka* 21
- Software Package for Analyzing FSO Links *M. Tatarko, L'. Ovsenik and J. Turán* 29

CALL FOR PAPERS

- Special Issue on Autonomic Communications 37
- Special Issue on Cognitive Infocommunications 38
- Special Issue on Cryptology 39

ADDITIONAL

- Guidelines for our Authors 40

Technically Co-Sponsored by



Editorial Board

Editor-in-Chief: CSABA A. SZABO, Budapest University of Technology and Economics (BME), Hungary

- | | |
|---|---|
| ÖZGÜR B. AKAN
Koc University, Istanbul, Turkey | ANDRZEJ JAJSZCZYK
AGH University of Science and Technology, Krakow, Poland |
| JAVIER ARACIL
Universidad Autónoma de Madrid, Spain | LÁSZLÓ T. KÓCZY
Széchenyi University, Győr, Hungary |
| LUIGI ATZORI
University of Cagliari, Italy | ANDREY KOUCHERYAVY
St. Petersburg State University of Telecommunications, Russia |
| STEFANO BREGNI
Politecnico di Milano, Italy | DÓRA MAROS
Óbuda University, Budapest, Hungary |
| LEVENTE BUTTYÁN
Budapest University of Technology and Economics, Hungary | MAJA MATIJASEVIC
University of Zagreb, Croatia |
| TEREZA CRISTINA CARVALHO
University of Sao Paulo, Brasil | VASHEK MATYAS
Masaryk University, Brno, Czechia |
| TIBOR CINKLER
Budapest University of Technology and Economics, Hungary | OSCAR MAYORA
Create-Net, Trento, Italy |
| FRANCO DAVOLI
University of Genova, Italy | MIKLÓS MOLNÁR
Université Montpellier 2, France |
| VIRGIL DOBROTA
Technical University Cluj, Romania | JAUELICE DE OLIVEIRA
Drexel University, USA |
| KÁROLY FARKAS
Budapest University of Technology and Economics, Hungary | ALGIRDAS PAKSTAS
London Metropolitan University, UK |
| VIKTORIA FODOR
KTH, Royal Institute of Technology, Sweden | MICHAL PIORO
Warsaw Technical University, Poland |
| AURA GANZ
University Massachusetts at Amherst, USA | ROBERTO SARACCO
EIT ICT LABS, Italy |
| EROL GELENBE
Imperial College London, UK | BURKHARD STILLER
University of Zürich, Switzerland |
| MARIO GERLA
UCLA, Los Angeles, USA | JÁNOS SZTRIK
University of Debrecen, Hungary |
| ENRICO GREGORI
CNR IIT, Italy | YUTAKA TAKAHASHI
Kyoto University, Japan |
| CHRISTIAN GUETL
Graz University of Technology, Austria | DAMLA TURGUT
University of Central Florida, USA |
| ASHWIN GUMASTE
Indian Institute of Technology Bombay, India | ESZTER UDVARY
Budapest University of Technology and Economics, Hungary |
| LAJOS HANZO
University of Southampton, UK | SCOTT VALCOURT
University of New Hampshire, USA |
| THOMAS HEISTRACHER
Salzburg University of Applied Sciences, Austria | WENYE WANG
North Carolina State University, USA |
| JUKKA HUHTAMÄKI
Tampere University of Technology, Finland | ADAM WOLISZ
Technical University Berlin, Germany |
| SÁNDOR IMRE
Budapest University of Technology and Economics, Hungary | JINSONG WU
Bell Laboratories, China |
| EBROUL IZGUEIRDO
Queen Mary University of London, UK | GERGELY ZARUBA
University of Texas at Arlington, USA |
| RAJ JAIN
Washington University in St. Lois, USA | HONGGANG ZHANG
Ecole Supérieur d'Electricité, France |

Indexing information

Infocommunications Journal is covered by Inspec, Compendex and Scopus.

Infocommunications Journal

Technically co-sponsored by IEEE Communications Society and IEEE Hungary Section

Editorial Office (Subscription and Advertisements):

Scientific Association for Infocommunications
H-1055 Budapest, Kossuth Lajos tér 6-8, Room: 422
Mail Address: 1372 Budapest Pf. 451. Hungary
Phone: +36 1 353 1027, Fax: +36 1 353 0451
E-mail: info@hte.hu
Web: www.hte.hu

Articles can be sent also to the following address:

Budapest University of Technology and Economics
Department of Networked Systems and Services
Tel.: +36 1 463 3261, Fax: +36 1 463 3263
E-mail: szabo@hit.bme.hu

Subscription rates for foreign subscribers:

4 issues 50 USD, single copies 15 USD + postage

Publisher: PÉTER NAGY • Manager: ANDRÁS DANKÓ

HU ISSN 2061-2079 • Layout: MATT DTP Bt. • Printed by: FOM Media

Global and local coverage maximization in multi-camera networks by stochastic optimization

Krishna Reddy Konda and Nicola Conci

Abstract—In this paper we present a camera positioning and reconfiguration algorithm for complex indoor environments. The algorithm initially optimizes the global coverage of the selected environment in order to maximize the visibility on the entire area. Reconfiguration of the devices is then performed after the camera installation, in order locally optimize coverage according to the application requirements.

Both initial coverage optimization and reconfiguration are achieved using Particle Swarm Optimization (PSO). The proposed solution has been validated in different setups, also taking into account occlusions and blocking introduced by the presence of obstacles. The achieved results confirm the viability of the approach in both positioning and reconfiguration, also in presence of considerably complex environmental geometries.

I. INTRODUCTION

The reduction in price of video sensors and the ever increasing need for security are significantly contributing to the diffusion of video surveillance systems. The large availability of different types of cameras and lenses let the user customize the sensing infrastructure to achieve the desired area coverage not only by choosing the number of sensors to be deployed, but also selecting their features in terms of field-of-view, resolution, frame rate, indoor/outdoor or night/day operating modes. The large availability of different types of devices and the corresponding number of parameters that can be tweaked provide on the one hand a higher degree of flexibility, but at the same time complicate the setup procedures of the acquisition system, often resulting in a suboptimal configuration that could lead to a reduced efficiency of the entire sensing infrastructure [1].

The availability of automatic planners to choose the optimal positioning of the sensors would be of great help for the security personnel, by improving the quality of coverage, minimizing the number of sensors and the black spots, and including in the optimization model also the presence of obstacles, areas subject to privacy constraints, and other personalization factors.

This kind of instruments would be in fact particularly suitable to plan the deployment of fixed installations (buildings, offices, public spaces), but also in need of temporary deployments (e.g., sports events, fairs, exhibitions) where a fast and efficient planning would be highly desirable.

More in general, the goal of a camera planner is to guarantee the maximum coverage of the observed space, minimizing

occlusions, and obtaining the best possible visibility of the areas of major interest.

The problem of coverage maximization can be easily described through the so-called *art gallery problem* (AGP), where the minimum number of guards is to be determined for a given area [2]. A variant of the AGP is known as the *Watchmen Tour Problem* (WTP), where guards are allowed to move inside the polygon [3]. The objective is to determine the optimal number of guards and their route to guarantee the detection of an intruder. However, both AGP and WTP related algorithms are unsuitable for most real-world camera placement applications. Consequently, more sophisticated algorithms have to be adopted to take into account the most important parameters related to the surrounding environment, which include constraints on observability [4], but also camera and illumination parameters. A short overview on the most relevant literature is reported hereafter.

Earlier solutions belong to the so-called *Generate and Test* approaches, in which all the constraints and models are incorporated into a simulation model. The HEAVEN system [5] is one of the earliest tools using such approach. HEAVEN uses a spherical representation to model the sensor configuration. A geodesic dome is created around the object, tessellating the sphere with an icosahedron that is further subdivided in a hierarchical fashion by recursively splitting each triangular face into four new faces. A similar system called ICE (Illumination Control Expert) [6], includes also the planning of illumination sources.

Synthesis approaches model the constraints as analytic functions, and formulating the problem in terms of satisfaction of constraints. Each requirement generates a geometric constraint, which is satisfied in the 3D domain of admissible locations. The admissible domains obtained are then intersected to each other in order to determine locations that satisfy all constraints simultaneously. An early work in this area is proposed by Cowan and Kovesi [7], in which camera locations are generated also with respect to illumination planning. In [8] the authors propose a camera placement algorithm based on a binary optimization technique and using polygonal spaces presented as occupancy grids. In [9] camera views are optimized so as to provide the highest resolution of objects and motions in the scene. The optimal view is defined by the application scenario (e.g., motion recognition, visual metrology).

Expert Systems address instead the high-level aspects of the problem, informing, for instance, about whether front or back illumination is more appropriate for the particular object and the corresponding features to be observed. An expert system is primarily used as an advising tool. A good

Manuscript submitted October 7, 2012, revised February 14, 2013.

Krishna Reddy Konda and Nicola Conci are with the Department of Information Engineering and Computer Science, University of Trento, Via Sommarive 5, Trento, 38123, Italy, {konda, conc}@disi.unitn.it

Global and Local Coverage Maximization in Multi-camera Networks by Stochastic Optimization

example is the system LIGHTING ADVISOR [10], which provides advice regarding the best lighting configurations in given circumstances.

Among the most recent proposals in camera positioning and reconfiguration algorithms, the work by Mittal and Davis [11] presents a probabilistic framework for object visibility in a multi-sensor environment. Piciarelli et al. [12] address the problem of camera networks reconfiguration, by adjusting pan, tilt, and zoom. They use the Expectation Maximization algorithm, in order to maximize the coverage of salient portions of the observed scene, where the saliency is identified by motion activity maps. In [13], the authors propose a framework for target coverage based on the spatial decomposition of the network and optimizing the solution for individual partitions. Erdem and Sclaroff [14] maximize the visibility in multi-camera networks based on radial sweep. In [15] event based network re-configuration of cameras is presented, even though positioning and reconfiguration is foreseen for moving cameras, which is not in line with generic surveillance scenarios, where the absolute position of cameras is generally fixed. Similarly, a reconfiguration algorithm for continuous tracking is proposed in [16]. However, the camera model used in the paper may result too simplistic since it does not consider various camera parameters that might vary based on reconfiguration. Dieber et al. [17] propose an algorithm, which self optimizes the positioning of mobile aerial cameras based on a simple camera model, which assumes fixed coverage for all the cameras. In this paper we propose an automatic camera positioning tool, which aims at addressing both the *global* and the *local* coverage issues, where by *local* we define critical areas in the area like doors, windows, objects of interest. The work stems from an early solution to the optimization problem, presented in [18]. The main novel aspects of this work consists of two main items. The first one is given by the concept of *quality of view* for the camera model, by defining the optimal region in the image plane for the observation of specific objects and targets. Secondly, we also address the issue of sensors reconfiguration after initial positioning, achieved by adjusting the camera parameters on the basis of the requirements imposed by the events occurring in the scene.

II. PARTICLE SWARM OPTIMIZATION

Particle Swarm Optimizer (PSO), developed by Kennedy and Eberhart [19], is a robust stochastic search technique based on the movement and intelligence of swarms. It has demonstrated to be effective in solving complex non-linear multidimensional discontinuous problems in a variety of fields [20]. Unlike other multiple-agent optimization procedures such as Genetic Algorithms (GA) [21], PSO is based on the cooperation among the agents rather than their competition. Three main advantages of the PSO over the GA can be identified. In the first place, PSO requires a reduced algorithmic complexity, since it considers only one simple operator that is the particles velocity updating, while the GA uses three genetic operators and the best configuration among several options of implementation needs to be chosen. Then, PSO parameters are easier to calibrate and to manipulate than the GA ones, whose optimal values must be evaluated among various operators.

Finally, PSO has a major ability to prevent the stagnation of the optimization process than GA, thanks to a more significant level of control of its parameters [22][23].

During PSO optimization procedure, the particles of the swarm iteratively change their positions in the solution space, searching for the best location. The solution space is defined by selecting the parameters to be optimized and assigning them the corresponding range of variation. Consequently, each parameter models a particular dimension of the solution space, and each location in the solution space corresponds to a particular trial solution. The goodness of the trial solutions is evaluated by means of a suitable fitness function, which provides the link between the optimization algorithm and the physical world.

A short pseudocode of the PSO algorithm is shown hereafter, and the corresponding equations to compute and update the velocity of the particles are shown in (1) and (2), respectively. In the algorithm, at every iteration i , $F(j)$ represent the current fitness value for particle j , $pBest$ is the minimum fitness value obtained so far for particle j , and $gBest$ is the overall global best among all the particles.

```

input: Number of Particles
input: Number of Iterations
InitializeParticles;
for  $i \leftarrow 1$  to Number of Iterations do
  for  $j \leftarrow 1$  to Number of Particles do
     $F(j) = \text{Fitness}(j)$ ;
    if  $F(j) < pBest(j)$  then
       $pBest(j) \leftarrow F(j)$ ;
    end
  end
   $gBest = \min(pBest(j))$ ;
  for  $j \leftarrow 1$  to Number of Particles do
    CalculateVelocity( $j$ );
    UpdateVelocity( $j$ );
  end
end

```

Algorithm 1: Pseudocode of the PSO.

$$v(j) = v(j) + c_1 * rand() * (pBest(j) - F(j)) + c_2 * rand() * (gBest - F(j)) \tag{1}$$

$$F(j) = F(j) + v(j) \tag{2}$$

In (1) c_1 and c_2 are configuration parameters defined in literature, and $rand()$ is a random number defined in $[0, 1]$.

III. THE PROPOSED APPROACH

In our approach we propose to optimize the coverage using a global and a local model as an analytic function of the camera parameters (positional degrees of freedom, pan, tilt and zoom), where the global component is defined to take the environment configuration into account, while the local component considers the position of objects of interest in the scene.

Initially, global optimization is achieved finding a suitable positioning of the sensors in the environment. Once the position of the cameras have been fixed, in case of need (e.g., presence of new obstacles, objects, changes in the environment) reconfiguration is run in order to maximize the local coverage.

A. Global coverage

In order to model global coverage, we have defined two different conditions to be met: *pixel density* and *quality of view*.

Pixel density refers to the fact that the information obtained from an image or a video is dependent on the number of pixels per surface area of the environment. Pixel density can be modeled as a function of the field-of-view and the resolution of the camera. In order to model the pixel density, we propose to represent the camera as a point source and each pixel of the CCD as the corresponding ray that emerges from the point source. Accordingly, far away areas in the environment receive less rays, corresponding to lower pixel density, whereas areas closer to the camera will be intersected by a higher number of rays, thus achieving higher resolution. An example about the mapping of the grid in the floor plan to the camera CCD is illustrated in Fig. 1.

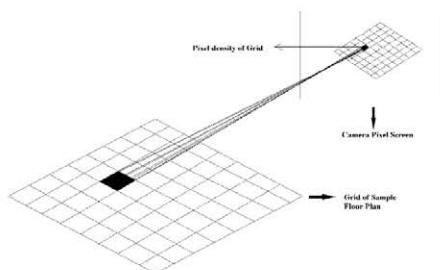


Fig. 1. Pixel Mapping. Each area of the floor plan is captured by a number of pixels that depends on the distance from the camera.

The *quality of view* of a target refers instead to the relationship between feature detectability of the target and the distance from the camera. Given a sensor resolution, the recognition of an object will strongly depend on its distance from the camera: if it is too distant details will be unintelligible; if it is too close, the whole object might not be visible entirely due to the limited field-of-view of the camera. To take into account this parameter, we start from the pixel density information defined in the previous paragraph, so as to model the visibility constraint as a Gaussian distribution that is computed along the ray emerging from the camera (see Fig. 2). The optimal distance is located at the center of the Gaussian, and needs to be specified according to the size and type of the objects to be monitored (e.g., humans, cars), such that they are clearly visible in case they enter the field-of-view of the camera.

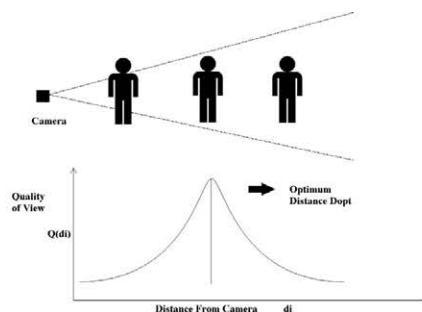


Fig. 2. Quality of view. The optimal distance for observation depends on the kind of objects to be monitored in the specific scene.

B. Local Coverage

As far as the local coverage is concerned, each area of interest (doors, windows, statues, paintings, other objects, etc.) is modeled as a negative exponential function of global coverage at the local target location, and it is expressed as a function normalized between zero and one, as shown in (3). As we can see from the equation the function reaches its maximum when the object is at the cell which has the maximum global coverage. Further details about the parametrization of all the above mentioned elements are provided in next sections.

$$T_k = 1 - \exp(-C_G) \tag{3}$$

C. Camera Model

The parameterization of the camera model, as discussed above, includes both aspects of pixel density, and quality of view.

All simulations we will present are carried out on the ground plane, thus discarding the vertical dimension. From the optimization point of view, the extension to the third dimension is straightforward. However, it is worth noting that in most scenarios the height term is less relevant, because it is common sense to position the cameras either on the ceiling or on the walls, and at the same height. This limits on the one hand the accessibility to non authorized users, and on the other hand it improves the visibility of the area to be monitored.

The quality of view of an object is modeled as a Gaussian distribution, evaluated along the ray emerging from each pixel of the camera, as shown in (4):

$$Q(d_i) = \frac{1}{\sqrt{2\pi}\sigma} \exp\left(-\frac{(d_i - D^{opt})^2}{2\sigma^2}\right) \tag{4}$$

where d_i is the distance of the cell hit by the i -th ray, and D^{opt} is the optimum distance, at which the objects of interest has maximum quality of view. In the current scenario D^{opt} is chosen as a constant.

In order to determine the areas that are visible in the map, we have to define a metric of visibility for the quality of view function. A given cell in a grid is said to be covered if the total quality of view, as defined by summation of $Q(d_i)$ of individual rays that pass through cell, is greater that a certain threshold. The threshold value has been empirically set to 0.5.

Global and Local Coverage Maximization in Multi-camera Networks by Stochastic Optimization

As far as the reconfiguration is concerned, and considering that we model the environment as a 2D plane, the camera parameters we consider for reconfiguration are *pan* and *zoom*, ignoring the *tilt* component. Pan is defined as the horizontal orientation of the camera, and zoom is in general expressed as a combination of two components, namely *optical* and *digital zoom*.

Optical zoom corresponds to imposing a change in the focal length of the camera. Using optical zoom enables us to capture a picture from a near view without any change in image quality. Mapping optical zoom into our model, basically implies to shift the quality of view function by the corresponding amount of zoom applied. For instance if the optical zoom applied is of a factor N the (4) is modified as in (5).

$$Q(d_i) = \frac{1}{\sqrt{2\pi}\sigma} \exp\left(-\frac{(d_i - N * D^{opt})^2}{2\sigma^2}\right) \quad (5)$$

Digital zoom allows instead for a closer view on the target by decreasing the image resolution on the object of interest and resampling. This operation works reasonably well when the object is within a limited distance from the camera and becomes less effective as soon as the object of interest moves far away. In this second case, and in order to be effective, digital zoom is to be used in combination or in cascade with optical zoom.

In our model we simulate zoom by decreasing the field of view of the camera, while keeping the number of rays that correspond to pixels in the camera constant. The rays intersecting the object of interest will then increase.

D. Algorithm

The proposed algorithm can be described in six steps, as explained here after.

Step 1 - Determine the solution space. If the task at hand is initial positioning of cameras, we need to identify the solution space, consisting on the perimetral and internal walls, and defined in terms of position and maximum orientation span. In case the provided map also includes the presence of target objects of interest, given the number of cameras, the algorithm will optimize the position of the devices, by either focusing more on global or local coverage depending on the input requirements.

Similarly, if the task at hand is reconfiguration, the solution space consists of all pan and zoom configuration allowed for the devices, given their initial position.

Step 2 - Compute Global coverage. In order to calculate the global coverage, the environment map is divided into a grid of $N \times N$ pixels. The granularity of the grid is chosen depending on the map scale, as well as on the desired accuracy in positioning. The finer the grid, the more accurate will be the result, at a cost of a higher computational complexity. For each camera, the pixel density (i.e., the number of rays passing through each cell of the grid) is computed. While estimating the number of rays, obstructions caused by the obstacles are also taken into account. The higher the number of rays that

cover a grid cell, the higher the pixel density, as calculated in (6):

$$C(m, n) = \sum_{i=0}^R Q(d_i) \quad (6)$$

where $C(m, n)$ is the final quality of view metric obtained for a specific cell, and m and n give the location of the cell in the map. As can be seen from (6), this metric will weight the quality of view function measured as in (4) considering the number of rays that intersect the cell (R). Conversely, we can say that the number of pixels occupied by a particular cell in the video frame is directly proportional to the number of rays that pass through that cell in the grid.

We then label the cell as “visible” only if the quality of view is higher than a predefined threshold. The global coverage is estimated as the number of visible cells divided by total number cells in the grid (7).

$$C_G = \frac{Cells_{visible}}{Cells_{total}} \quad (7)$$

Step 3 - Include Local coverage. For a given camera position the local coverage is given by (5). Accordingly, the overall local coverage is given by (8):

$$C_T = \frac{1}{T} \sum_{k=0}^T T_k \quad (8)$$

where T is the total number of target objects and T_k is the target coverage given by (3) for the corresponding target.

Step 4 - Fitness Function. We need now to define a suitable fitness function that will be used by the PSO algorithm as a target for the optimization procedure. The proposed fitness function combines both global and local coverage, and each term can be weighted according to the users’ preferences and the application requirements (9).

$$F(C_G, C_T) = (1 - C_G) * w + (1 - C_T) * (1 - w) \quad (9)$$

In (9), C_G represents the global coverage, and C_T models the local (target) coverage; w is the weight used to balance the trade-off between global and local coverage, respectively. We can notice from (9) that, as soon as the global and local coverage approach 1 (maximum coverage), the fitness function converges to zero.

Step 5 - PSO. PSO is applied to the solution space defined in *Step 1*. At each iteration, the particles position and velocity are updated, until convergence. Convergence is usually achieved when the fitness function reaches a minimum, or when a termination criterion is fulfilled (e.g., maximum number of iterations).

Step 6- Check for changes in the environment In case after the initial camera deployment, changes in the environmental conditions occur (thus requiring a reconfiguration of the network) the algorithm can be run again and the optimization will in this case only focus on the pan and zoom parameters.

E. Fitness function

The fitness function is the most critical element of the whole algorithm, as it determines the behavior of the particle

swarm and also the convergence characteristics of the PSO algorithm. Typically an ideal fitness function should have following characteristics

- it should get minimized when the intended output is maximized;
- minimization should be applicable even if only one of the involved parameters is varied while keeping all other parameters constant;
- each and every parameter that is involved in the optimization process should get due representation in the fitness function.

In line with the above requirements our fitness function has been formulated in (9). As can be seen, the fitness function is the weighted summation of local and global coverage. The overall algorithm and the computation of the fitness function is shown by pseudo code in Algorithm 2.

IV. SCENARIOS

Without loss of generality and considering that cameras are usually positioned at the same height, simulations are performed in two dimensions, thus discarding the height coordinate. Moreover, the number of rays corresponding to the pixels is downsampled by a factor 4, in order to make the computational complexity tractable. Considering a standard camera resolution of 640x480 pixels, this implies using 160 rays emitted by each camera, which still represents a fairly dense sampling of the space. The field-of-view is fixed in the range between 5 and 90 degrees and optimum distance for quality of view is fixed at 40 pixels in the map, which corresponds to about 10 meters in the real environment.

In order to assess the validity of our approach, we tested the algorithm on three different maps. As far as the simulation procedure is concerned, we initially determine the cameras position on the map, assuming that no object is present. This is equivalent to optimizing only with respect to global coverage.

After the initial setup, ten different objects of interest are placed in the map. At this point the algorithm is required to re-align the cameras, keeping the positioning of the sensors fixed. This implies that in determining the new camera parameters, only local coverage is considered, thus setting $w = 0$.

The environment maps used for the testing are shown in the left column of respective Fig. 4-6. Cameras can be positioned along internal and perimeter walls of the environment. In the picture we also show the positioning of the targets that will be introduced after the initial setup of the camera infrastructure is found.

V. EXPERIMENTAL RESULTS

As explained in Section IV, we will present the results obtained in the selected scenarios by first illustrating the quality of the global coverage achieved in the initial positioning, and then focusing on reconfiguration for local (target) coverage.

Initially, the environment in which the cameras have to be deployed, do not include targets. Hence, the goal of initial placement is global coverage maximization. In order to do so, we assume that initially cameras are zoomed out (maximum field of view). At this stage, the aim of the algorithm is to find the best position to achieve optimum global coverage. In the maps that will be presented, different colors are used to illustrate the quality of the coverage in over the entire map. For global coverage, areas with maximum coverage (i.e. when $C(m, n)$ is greater than 100) are represented in white, and areas which fall in the range $10 \leq C(m, n) < 100$ are represented in green. Blue indicates areas, which satisfy $0.5 \leq C(m, n) < 10$. Red areas represent zones of the environment, which are visible to cameras but fall below our visibility threshold of 0.5, and black areas are not visible to cameras because they fall out of the field-of-view, or due to the presence of obstacles.

It is worth mentioning that the coverage will in general hardly reach 100%, since the coverage function decreases with the distance of the pixel from the camera position. As an example, to show the effectiveness of the global coverage optimization we have applied our algorithm on a simple map,

```

input : Map  $I$  divided into  $N \times M$  cells of equal
         size
input : Camera Resolution
output: Fitness Value

Initialize Camera Positions from PSO;
Initiate number of rays from camera based on video
resolution;

QOV ;           % Quality of View of the Cell
QOL ;           % Intensity of light perceived by the cell
goodCells = 0 ; % Number of cells with good
coverage
C = 0; % Obtained Coverage for each cell

for  $i \leftarrow 1$  to  $N$  do
    for  $j \leftarrow 1$  to  $M$  do
        pixelDensity  $\leftarrow$  RayIntersect ( $i, j$ );
        QOV  $\leftarrow$  QualityOfView ( $i, j$ );
        QOL  $\leftarrow$  LightIntensity ; % Constant
        C( $i, j$ ) = pixelDensity * QOV * QOL;
        if C( $i, j$ )  $\geq$   $C_{th}$  then
            | goodCells ++ ;
        end
    end
end

 $C_g \leftarrow \frac{\text{goodCells}}{N * M}$  ; % Compute Global Coverage
 $k = T$  ;
while  $k \neq \emptyset$  do
    % Compute Target Coverage
    T( $k$ ) = Gaussian (D,C ( $m, n$ ),QOL) ;
     $C_T = C_T + \frac{T(k)}{T}$ ;
     $k - -$  ;
end

% The final output is a combination of Global and
Local coverage with weights  $w_G$  and  $w_T$ 
 $F(C_G, C_T) \leftarrow w * (1 - C_G) + (1 - w) * (1 - C_T)$ ;
Return  $F(C_G, C_T)$ ;
    
```

Algorithm 2: Fitness Calculation

Global and Local Coverage Maximization in Multi-camera Networks by Stochastic Optimization

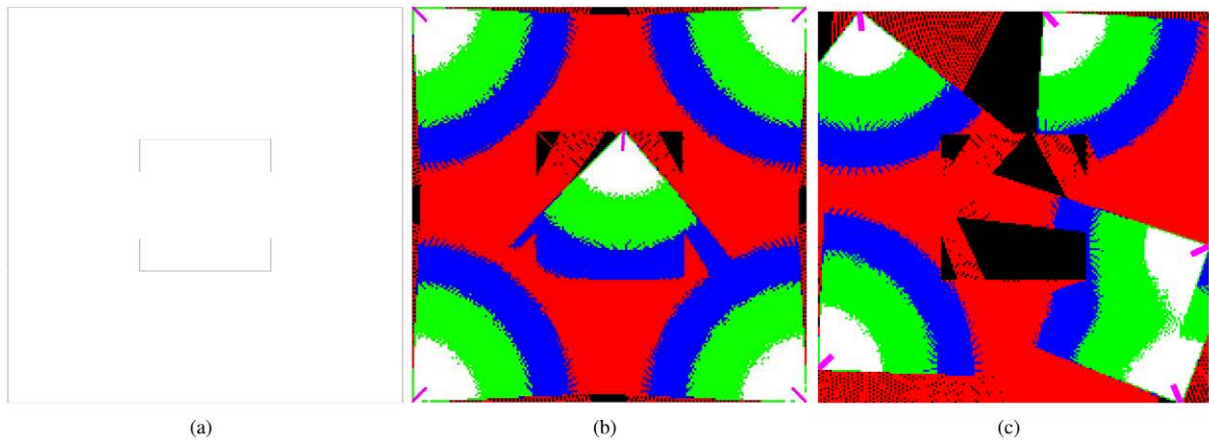


Fig. 3. Global coverage maximization. Sample map (a), optimal coverage (60%), proposed method (52%).

shown in Fig. 3, for which the optimal positioning (about 60%) is known. Through our simulation and after 50 iterations, we could achieve 52%, demonstrating that PSO turns out as a good alternative to deterministic algorithms.

After the initial positioning is completed, targets are randomly distributed over the map. The goal of reconfiguration is to maximize target coverage; however, in most surveillance scenarios camera deployment is fixed and does not allow repositioning after installation, unless PTZ cameras are used. Hence, according to our model the only reconfigurable parameters are pan, and zoom. The algorithm is re-run considering the absolute position of the cameras fixed, thus optimizing target coverage. The input maps used for the three test cases are shown in Fig. 4-6. Initial positioning is performed with the zoom set to 1x, while pan is a free parameter that can be adjusted to obtain maximum coverage. As far as the first map is considered, the coverage level obtained after the initial placement of cameras is shown in Fig. 4(b). In the figure, the environment is overlapped for convenience with the output coverage map obtained from the algorithm. The percentages of global coverage C_G are shown in Table I.

However, we can notice that although the overall coverage percentage is good, this is not optimized when the targets are deployed, and reconfiguration is required.

TABLE I
GLOBAL AND LOCAL (TARGET) COVERAGE FOR THE THREE MAPS USED FOR TESTING.

Map	Config.	C_G	Green	Blue	Red	Black	C_T
1	Initial	0.51	5	1	3	0	0.60
	Final	0.50	5	3	1	1	0.87
2	Initial	0.54	2	1	5	1	0.58
	Final	0.44	7	1	0	1	0.78
3	Initial	0.51	2	3	3	2	0.54
	Final	0.48	7	1	0	2	0.80

As can be seen from the figures in Table I and as depicted in Fig. 4(c), after reconfiguration, C_T has increased quantitatively and qualitatively. In fact, initially three targets are left out with average coverage of 0.60, while after reconfiguration the average coverage has increased to 0.87 by almost 50% with only 2 targets left out.

In a similar fashion, we have conducted the the initial positioning and the re-alignment of the cameras also on the remaining two maps. The obtained maps after initial global coverage optimization are depicted in Fig. 5(b) and Fig. 6(b), respectively. Similarly, the final camera setup after reconfiguration is shown in Fig. 5(c) and Fig. 6(c), respectively. Similarly to the previous experiment, numerical results are presented in Table I.

From the experiments it is reasonable to say that the performance of the algorithm is consistent across different environments, maintaining in all cases more than 50% improvement in the target coverage.

VI. CONCLUSIONS

In this paper we have proposed a tool for automatic positioning and reconfiguration in multi-camera networks using the PSO algorithm. The algorithm aims at dealing with both global and local coverage, that can be set with tunable weights. The coverage is defined as the fulfillment of different quality parameters, including pixel density, quality of view, and the presence of obstacles. The experimental validation carried out on different environmental setups demonstrate the efficiency of the algorithm in achieving a good coverage of the observed space, also in presence of obstacles and targets.

REFERENCES

- [1] Hoerster, E., Lienhart, R.: Optimal placement of multiple visual sensors. In: Multi-Camera Networks. (2008) 117–138
- [2] Chvatal, V.: A combinatorial theorem in plane geometry. (1975) 39–41
- [3] Carlsson, S., J.Nilsson, B., C.Ntafos, S.: Sweeping simple polygons with a chain of guards. (1991) 367–378
- [4] Shafer, S.: Automation and calibration for robot vision systems. Technical report, Technical Report CMU-CS-88-147, Carnegie Mellon University (1988)
- [5] Sakane, S., Ish, M., Kakikura, M.: Occlusion avoidance of visual sensors based on a hand-eye action simulator system: Heaven. Advanced robotics 2 (1987) 149–165
- [6] Sakane, S., Niepold, R., Sato, T., Shirai, Y.: Illumination setup planning for a hand-eye system based on an environmental model. Advanced Robotics 6 (1991) 461–482
- [7] Cowan, C., Bergman, A., Nitzan, D.: Automatic placement of vision sensors. In: 1990 NSF Manufacturing System Research Conference. (1990) 389–395

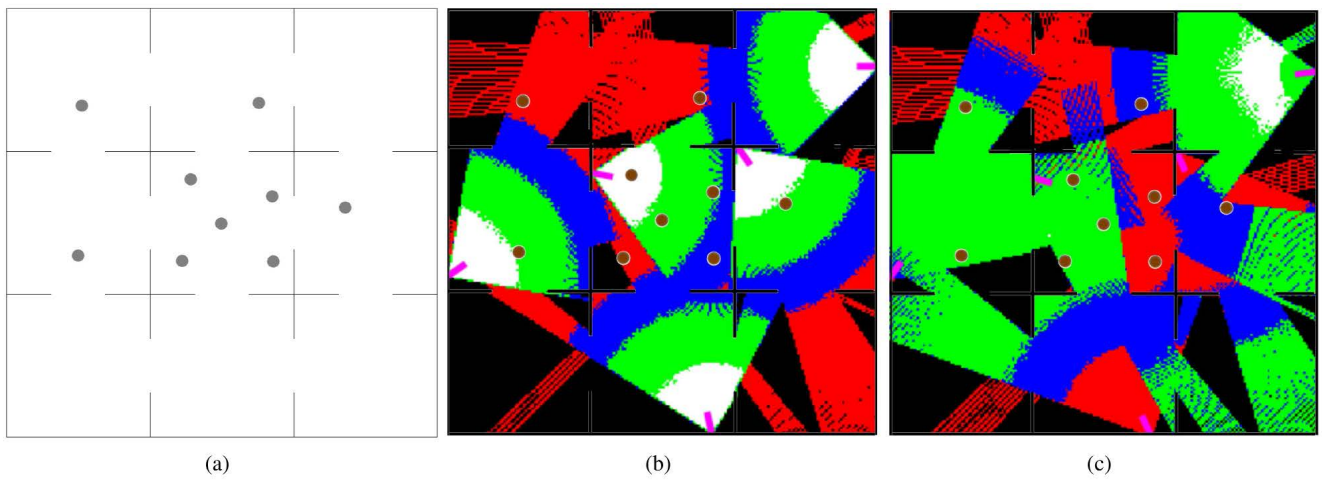


Fig. 4. Map 1 (a), initial positioning (b), and reconfiguration (c).

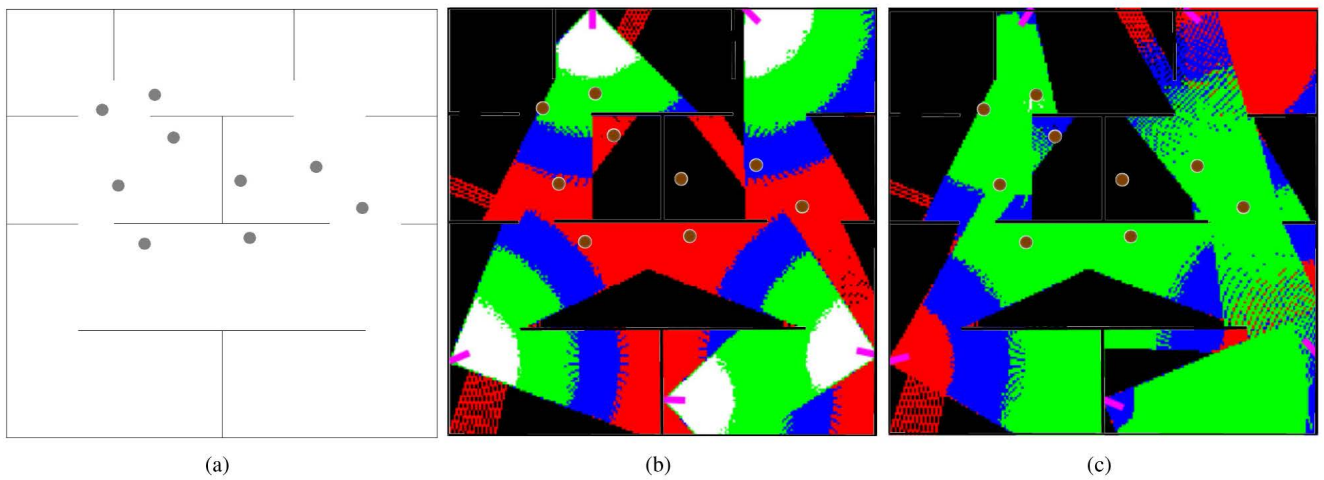


Fig. 5. Map 2 (a), initial positioning (b), and reconfiguration (c).

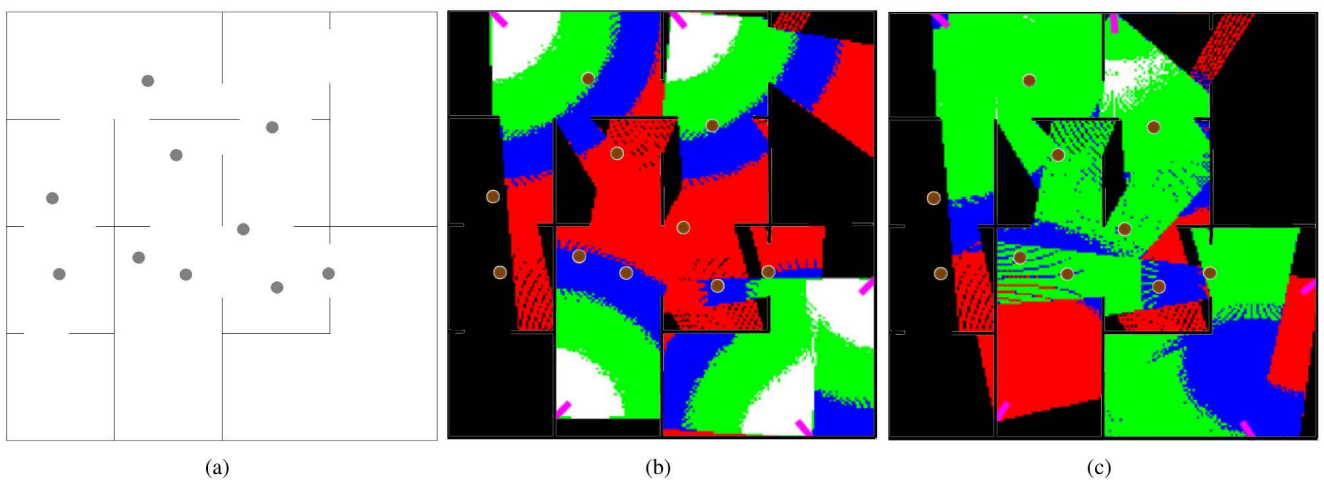


Fig. 6. Map 3 (a), initial positioning (b), and reconfiguration (c).

Global and Local Coverage Maximization in Multi-camera Networks by Stochastic Optimization

- [8] Erdem, U., Sclaroff, S.: Optimal placement of cameras in floorplans to satisfy task requirements and cost constraints. In: OMNIVIS Workshop. (2004)
- [9] Bodor, R., Drenner, A., Schrater, P., Papanikolopoulos, N.: Optimal camera placement for automated surveillance tasks. *Journal of Intelligent & Robotic Systems* **50** (2007) 257–295
- [10] Grimson, W.: Sensing strategies for disambiguating among multiple objects in known poses. *Robotics and Automation, IEEE Journal of* **2** (1986) 196–213
- [11] Mittal, A., Davis, L.: A general method for sensor planning in multi-sensor systems: Extension to random occlusion. *International Journal of Computer Vision* **76** (2008) 31–52
- [12] Piciarelli, C., Micheloni, C., Foresti, G.: Occlusion-aware multiple camera reconfiguration. In: *Proceedings of the Fourth ACM/IEEE International Conference on Distributed Smart Cameras, ACM* (2010) 88–94
- [13] Munishwar, V., Abu-Ghazaleh, N.: Scalable target coverage in smart camera networks. In: *Proceedings of the Fourth ACM/IEEE International Conference on Distributed Smart Cameras, ACM* (2010) 206–213
- [14] Erdem, U., Sclaroff, S.: Automated camera layout to satisfy task-specific and floor plan-specific coverage requirements. *Computer Vision and Image Understanding* **103** (2006) 156–169
- [15] Wittke, M., del Amo Jimenez, A., Radlke, S., Grenz, C., Hahner, J.: Enra: Event-based network reconfiguration algorithm for active camera networks. In: *Distributed Smart Cameras (ICDSC), 2011 Fifth ACM/IEEE International Conference on, IEEE* (2011) 1–6
- [16] Lemon, B., Kulathumani, V.: Local reconfiguration for simultaneous coverage and tracking in a large scale camera network. In: *Technologies for Homeland Security (HST), 2011 IEEE International Conference on, IEEE* (2011) 117–122
- [17] Dieber, B., Micheloni, C., Rinner, B.: Resource-aware coverage and task assignment in visual sensor networks. *Circuits and Systems for Video Technology, IEEE Transactions on* **21** (2011) 1424–1437
- [18] Conci, N., Lizzi, L.: Camera placement using particle swarm optimization in visual surveillance applications. In: *Image Processing (ICIP), 2009 16th IEEE International Conference on, IEEE* (2009) 3485–3488
- [19] Kennedy, J., Eberhart, R.C.: Particle swarm optimization. In: *IEEE Int. Neural. Networks Conf. Volume 4.* (1995) 1942–1948
- [20] Eberhart, R.C., Shi, Y.: Evolving artificial neural networks. In: *1998 Int. Conf. Neural. Networks and Brain.* (1998)
- [21] Goldberg, D.: *Genetic algorithms in search, optimization, and machine learning.* Addison-wesley (1989)
- [22] Robinson, J., Rahmat-Samii, Y.: Particle swarm optimization in electromagnetics. *IEEE Trans. on Antennas and Propagation* **52** (2004) 397–407
- [23] Eberhart, R.C., Shi, Y.: Particle swarm optimization: developments, applications and resources. In: *Congress on Evolutionary Computation.* (2001) 81–86



University of Trento, Italy since 2011. His research interests include video compression, machine vision, and video analytics.



Nicola Conci (S'04-M'08) received the Ph.D in 2007 from the University of Trento, Italy. In 2007 he was visiting student at the Image Processing Lab. at University of California, Santa Barbara. In 2008-2009 he was post-doc researcher in the Multimedia and Vision research group at Queen Mary, University of London (UK). Since 2009 he is assistant professor at the University of Trento, Italy. His research interests are related to machine vision for behavior understanding and human computer interfaces. In 2006 he received the Best Student Paper Award at the international ACM conference Mobimedia held in Alghero (Italy).

Receivers Design for OFDM Signals under both High Mobility and Carrier Frequency Offset

Dong-Hua Chen , Gong-Yi Huang , Yi-Ming Yang

Abstract—In highly mobile scenarios, mobility-induced channel time variation (CTV) will destroy the orthogonality among subcarriers in orthogonal frequency division multiplexing (OFDM) systems, which causes intercarrier interference (ICI) and thus degrades the system performance. On the other hand, carrier frequency offset (CFO) between the oscillators of the transmitter and the receiver also causes ICI. As a result, when the CFO and the channel time variation coexist, ICI caused by the two factors become more severe and thus complicate the receiver design. In order to cope with the ICI caused by these two factors, this paper investigates two receiver structures for OFDM systems. One separately addresses the effects of the CFO and the channel time variation, and the other makes an integrated compensation of the two factors. Performances of the two receivers are studied and compared through numerical simulations. Results obtained from simulations show that the separate receiver takes advantages over the integrated one, and is an appropriate option for OFDM receiver under both high mobility and carrier frequency offset.

Index Terms—orthogonal frequency division multiplexing, carrier frequency offset, time varying channel, equalizer

I. INTRODUCTION

OFDM is a frequency efficient transmission technique owing to its capability of maintaining the subcarriers orthogonality. Moreover, it is computationally efficient as the modulation and demodulation can be realized by using fast discrete Fourier transform (FFT) [1]. Till now, OFDM has become an important transmission technique in various wireless communication standards including IEEE 802.11a, 802.16e, 802.20 and 802.22 etc [2]. The aforementioned merit of such a transmission technique is obtained assuming no channel variation for the duration of an OFDM symbol [3]. In mobile application environments, however, there exist many challenges for this technique to be addressed. For one thing, the channel time variation (CTV) in mobile environments will destroy the orthogonality among subcarriers and result in intercarrier interference (ICI) which thereby degrades the system performance. For the other, carrier frequency offset [4], the frequency discrepancies between the oscillators of the

transmitter and the receiver, will also destroy the subcarrier orthogonality and cause ICI. As a result, the ICI will be severe under both the CFO and the channel time variation, so in order to reduce their effects, associated mitigation method is indispensable.

For mitigating ICI caused by the channel time variation, Stamoulis *et al.* proposed a time-domain equalization approach by designing a series of block ICI-mitigating filters [5]. Compared with the time-domain approach, the method in the frequency domain is more advantageous in the sense of the compromise between system performance and complexity. So rather than still working in the time domain, Choi *et al.* proposed a minimum mean squared error based frequency-domain equalization method [6]. A remarkable feature of this method is its ability of exploiting the inherent time diversity provided by the channel time variation, achieved by using an ordered serial interference cancellation (OSIC) during the MMSE equalization of OFDM symbols. Unfortunately, however, this method has an unaffordable computational load as it involves tedious subcarriers sorting and complex matrix inversion. With the aim of reducing computational complexity of Ref. [6] and based on the observation of ICI diminishing rapidly with subcarrier intervals increasing, Cai and Giannakis proposed a reduced-complexity MMSE equalizer with SIC by neglecting the ICI from subcarriers with far spacing [7]. Compared with Ref. [6], the complexity of Ref. [7] was reduced from $O(N^4)$ to $O(N^2)$, where N is the symbol length in terms of subcarriers, unfortunately however, such a computational load is still high for practical applications. For further reducing the computational complexity, [8]-[10] independently proposed several ICI equalization methods of linear complexity with the symbol length. Fang *et al.* proposed a block turbo MMSE equalizer by exploiting the band structure of the channel frequency domain (CFR) matrix [8]. In Ref. [8], the intensive computations of matrix inversion is lessened by means of a band LDL factorization. In Ref. [9], Schniter proposed a two-stage turbo equalizer also by exploiting the band structure of the CFR matrix. In this algorithm, the first stage used an optimal linear processing filter for windowing the received signal in order to restrict the ICI support. Using the windowed signal, the second stage adopted a serial turbo equalizer to recover the transmit symbols. In addition to the turbo equalizers [8-9], Li *et al.* proposed a one-tap frequency-domain equalizer with parallel ICI cancellation [10]. In the parallel interference cancellation of Ref. [10], only parts of the neighboring ICI are considered in

Manuscript revised February 6, 2013. This work was supported in part by the Natural Science Foundation of Fujian Province of China under Grant No. 2012J05119, the Fundamental Research Funds for the Central Universities under Grant No. 11QZR02, the Scientific Research Fund of Huaqiao University under Grant No. 12BS230.

D.-H. Chen is with Huaqiao University, Xiamen, 361021 China (e-mail: dhchen0@163.com).

Receivers Design for OFDM Signals under both High Mobility and Carrier Frequency Offset

order to reduce the computational complexity which thereby sacrificed the equalization performance. In [11], a CFO compensation technique was proposed to improve the channel estimation reliability using piece-wise models, but its focus is on reducing the ICI impact on the channel estimation.

As stated previously, when the channel time variation and the CFO coexist, the ICI becomes more severe. Existing OFDM receiver designs generally consider only one or neither of the two factors of the CFO and the channel time variation [12-13]. This does not conform to the actual conditions of mobile applications. By now, few literatures addressed the receiver designs for OFDM system under such cases. In this paper, we consider the receiver design for OFDM operating over time varying channels and in the presence of CFO. Two types of receivers, the hybrid time-frequency domain receiver and the pure frequency domain receiver, are investigated and compared under the considered cases. The hybrid time-frequency domain receiver works in two stages. In the first stage, the effect of CFO is compensated from the received signals in the time domain. As the CFO has been compensated in the first stage, the second stage only needs to cope with the channel time variation. Specifically, the received signals after CFO compensation are firstly converted into the frequency domain, and then feeds into an ICI equalizer to recover the transmit symbols. The frequency domain receiver, as its name indicates, only works in the frequency domain. After converting the overall received signal from the time domain to the frequency domain, it jointly equalizes the channel time variation and the CFO. In order to evaluate the two receivers, comparisons in terms of system performance and complexity are made through numerical simulations.

The rest of the paper is organized as follows. Section II presents the system model for OFDM under the effect of both time varying channels and CFO. Section III addresses the receiver design for OFDM affected by time varying channels and CFO. Section IV presents some simulations to evaluate the receiver performance. Finally, section V concludes with a summary of some key results.

II. SYSTEM MODEL WITH BOTH CFO AND CTV

In the transmitter, the bit streams are mapped into complex symbols $X(k)$ according to the adopted modulation scheme such as QPSK. After a serial to parallel conversion, the QPSK symbols are converted into the time domain by using an N -point inverse DFT. The resulting OFDM modulated signal is given by

$$x(n) = \frac{1}{\sqrt{N}} \sum_{k=0}^{N-1} X(k) \exp(j2\pi kn / N) \quad n = -G, \dots, N-1, \quad (1)$$

where N and $X(k)$ are the OFDM symbol length in terms of subcarriers number and the data modulated on the k th subcarrier, respectively. G is the cyclic prefix (CP) length bigger than the maximal channel delay. The OFDM signals

$\{x(n), n=-G, \dots, N-1\}$ are transmitted over doubly selective channels. After removing CP samples at the receiver, we get the received signal in the time domain [7]

$$r(n) = e^{j2\pi \frac{\varepsilon n}{N}} \sum_{l=0}^{L-1} h(n,l)x(n-l) + w(n), \quad (2)$$

where ε is the CFO between the oscillators of the transmitter and the receiver; $h(n, l)$ is the channel impulse response (CIR) corresponding to the l th transmission path at time n ; $w(n)$ is the additive white Gaussian noise (AWGN) with zeros mean and variance of σ^2 . After discarding the CP and performing an N -point DFT to the received signal, we arrive at [7]

$$\begin{aligned} R(k) &= \frac{1}{\sqrt{N}} \sum_{n=0}^{N-1} r(n) \exp(-j2\pi kn / N) \\ &= H(k,k)X(k) + \sum_{u=0, k \neq u}^{N-1} H(k,u)X(u) + W(k), \end{aligned} \quad (3)$$

where $R(k)$ and $H(k, k)$ are the received signal in the frequency domain and the associated channel complex gains on the k th subcarrier, respectively; $W(k)$ is the additive noise in the frequency domain. The second term in the right hand side (RHS) of (3) is the ICI superimposed on the k th subcarrier and $H(k, u)$ denotes the weighted ICI coefficient from the u th subcarrier. The formulas of $H(k, k)$ and $H(k, u)$ are given by

$$H(k, k) = \sum_{l=0}^{L-1} \bar{h}(l) \exp(-j2\pi kl / N) \quad (4)$$

and

$$H(k, u) = \sum_{l=0}^{L-1} \left(\frac{1}{N} \sum_{n=0}^{N-1} h(n,l) e^{-j\frac{2\pi}{N}(k-u-\varepsilon)n} \right) e^{-j\frac{2\pi}{N}ul}, \quad (5)$$

respectively. $\bar{h}(l)$ in (4) is defined as the time-averaged product of the CIR and the CFO over a symbol:

$$\bar{h}(l) = \frac{1}{N} \sum_{n=0}^{N-1} h(n,l) \exp(j2\pi \varepsilon n / N). \quad (6)$$

When the channel is static and the CFO is zero, $H(k, u)=0$ for any $k \neq u$, i.e., ICI no longer exist under time invariant channels and perfect carrier synchronization. If the channel is static, $H(k, u)$ becomes [4,14-15]

$$H(k, u) = \frac{\sin(\pi\varepsilon)}{N \sin\left(\frac{\pi(\varepsilon + u - k)}{N}\right)} \exp\left(\frac{j\pi(N-1)\varepsilon - u + k}{N}\right). \quad (7)$$

For the convenience of derivations, (3) can be further written in a vector form [7]:

$$\mathbf{R} = \mathbf{H}\mathbf{X} + \mathbf{W}, \quad (8)$$

where $\mathbf{R} = [R(0), R(1), \dots, R(N-1)]^T$ is defined as the received signal vector; $\mathbf{X} = [X(0), X(1), \dots, X(N-1)]^T$ is the transmitted symbol vector and $\mathbf{W} = [W(0), W(1), \dots, W(N-1)]^T$ is the superimposed noise vector. \mathbf{H} is an $N \times N$ channel frequency response matrix:

$$\mathbf{H} = \begin{bmatrix} H(1,1) & H(1,2) & \dots & H(1,N) \\ H(2,1) & H(2,2) & \dots & H(2,N) \\ \vdots & \vdots & \ddots & \vdots \\ H(N,1) & H(N,2) & \dots & H(N,N) \end{bmatrix}. \quad (9)$$

As can be seen from (9), non-zero elements on the non-diagonal matrix \mathbf{H} incur ICI that need be addressed in the receiver designing.

III. OFDM RECEIVERS DESIGN UNDER BOTH CFO AND CTV

Based on the signal models derived in Section 2, this section investigates two types of receivers, the hybrid time-frequency domain receiver and the pure frequency domain receiver, in presence of both the CFO and the CTV. In the hybrid receiver, effects of the CFO and the channel time variation are compensated separately. Specifically, the CFO is firstly removed from the received time-domain signals. The resultant received signals are then converted from the time domain into the frequency domain. Finally the ICI only caused by the channel time variation are mitigated in the frequency domain. As compared with the hybrid/separate receiver, the pure frequency receiver works in a different manner. It jointly addresses the effects of the two factors in the frequency domain. For the convenience of discussion, two receivers of the separate and the joint/integrated are denoted by the type-I receiver and the type-II receiver respectively.

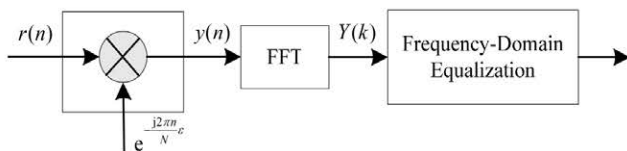


Fig. 1. Hybrid time-frequency domain receiver.

A. Hybrid time-frequency domain receiver

The hybrid time-frequency domain receiver, as shown in Fig 1, is based on the received signal model (2). In this structure, the CFO is firstly removed by multiplying the received signal (2) with sequences $\exp(-j2\pi\epsilon n/N), n = 0, \dots, N-1$. The resulting received signal after CFO compensation is given by

$$y(n) = \sum_{l=0}^{L-1} h(n,l)x(n-l) + v(n), \quad (10)$$

where $v(n) = w(n)\exp(-j2\pi\epsilon n/N)$. As $w(n)$ is identically and independently distributed (*i.i.d.*), $v(n)$ is also *i.i.d.* and has the identical distributions as $w(n)$. Performing an N -point DFT to (10), we arrive at

$$Y(k) = \frac{1}{\sqrt{N}} \sum_{n=0}^{N-1} y(n) \exp(-j2\pi kn/N) \\ = G(k,k)X(k) + \sum_{u=0, k \neq u}^{N-1} G(k,u)X(u) + V(k), \quad (11)$$

where $G(k,k)$ and $G(k,u)$ are the special cases of $H(k,k)$ and $H(k,u)$, respectively, with the exception of $\epsilon = 0$.

Similar as (8), for the derivation convenience, (11) can be written in a vector form by (12)

$$\mathbf{Y} = \mathbf{G}\mathbf{X} + \mathbf{V}, \quad (12)$$

where \mathbf{G} is the ICI coupling matrix defined as

$$\mathbf{G} = \begin{bmatrix} G(1,1) & G(1,2) & \dots & G(1,N) \\ G(2,1) & G(2,2) & \dots & G(2,N) \\ \vdots & \vdots & \ddots & \vdots \\ G(N,1) & G(N,2) & \dots & G(N,N) \end{bmatrix}. \quad (13)$$

Comparing (12) with (8), we find they are in a similar form with exception that the ICI coefficients in the ICI coupling matrix \mathbf{G} are caused only by the CTV while in \mathbf{H} they are caused by both the CFO and the CTV. As the received signal is only affected by the CTV, the following task of the receiver is to mitigate the CTV induced ICI in the frequency domain. From (12), the equalized symbol \mathbf{X} based on the MMSE criteria is given by

$$\mathbf{X} = (\mathbf{G}^H \mathbf{G} + \sigma^2 \mathbf{I})^{-1} \mathbf{G}^H \mathbf{Y}, \quad (14)$$

where \mathbf{I} is an $N \times N$ diagonal identity matrix. As can be seen from (14), direct MMSE equalization in the presence of ICI involves $N \times N$ matrix inversion which is a heavily computational task for practical realization. Fortunately, previous study has shown that the ICI caused by only CTV diminishes rapidly with the increasing of subcarrier intervals. Based on this observation, the frequency domain equalization can be realized in a low complexity, by considering ICI only from neighboring subcarriers, without obvious performance degradation.

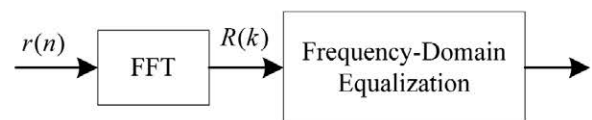


Fig. 2. Pure frequency domain receiver.

Receivers Design for OFDM Signals under both High Mobility and Carrier Frequency Offset

B. Pure frequency-domain receiver

Different from the hybrid receiver, the pure frequency-domain receiver, as shown in Fig 2, is derived on the basis of signal model (8). It jointly compensates the ICI induced by both the CFO and the channel time variation. The transmitted symbol can also be recovered by using MMSE equalization:

$$\mathbf{X} = (\mathbf{H}^H \mathbf{H} + \sigma^2 \mathbf{I})^{-1} \mathbf{H}^H \mathbf{R}. \quad (15)$$

As (15) takes on the form of (14), so the type-II receiver can also be realized in a low complexity so long as the ICI induced by both the CFO and the CTV decrease rapidly with the increasing of subcarrier intervals.

In order to reveal the ICI distributions in the ICI coupling matrix, we illustrate in Fig 3 the normalized amplitude of ICI coefficients $|H(k,u)|$ versus the subcarrier interval for a typical OFDM system with $N=64$. Transmission channels consist of 6 independent paths with exponential power delay profile generated by Jakes model [17]. The CIR of each path varies with time and the channel time variation speed is measured by the normalized (by subcarrier spacing) Doppler frequency f_d . Fig 3 considered three cases: (1) Only CFO exists (denoted by “only CFO”); (2) Only channel time variation exists (denoted as “only CTV”); (3) Both CFO and channel time variation exist (denoted as “both CTV and CFO”). We see from Fig 3 that in all cases, the ICI power decreases sharply with the increasing subcarrier spacing, and moreover, when the CFO and channel time variation coexist, the ICI becomes more severe than the case of only CFO or channel time variation presents.

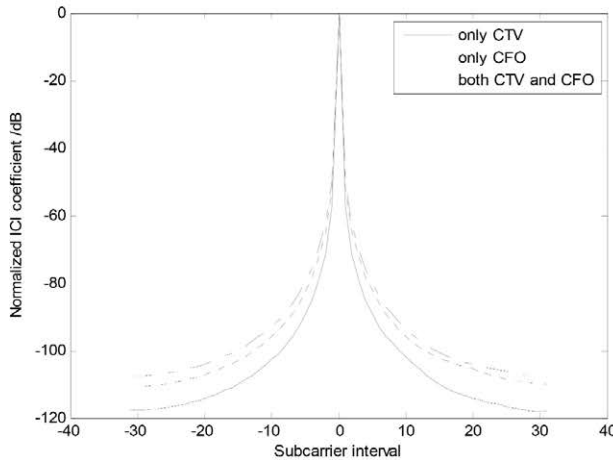


Fig. 3a. Illustration of the ICI distributions ($f_d=0.1$, $\epsilon=0.1$)

Although both the receivers can be realized with low complexity, the type-II may involve more computations than the type-I, as the ICI induced by two factors is more severe than by only one, and a bigger bandwidth of banded matrix may be assumed in type-II receiver to maintain the same performance as that of the type-I receiver. In the next section, we will evaluate the system performance of these two receivers through numerical simulations.

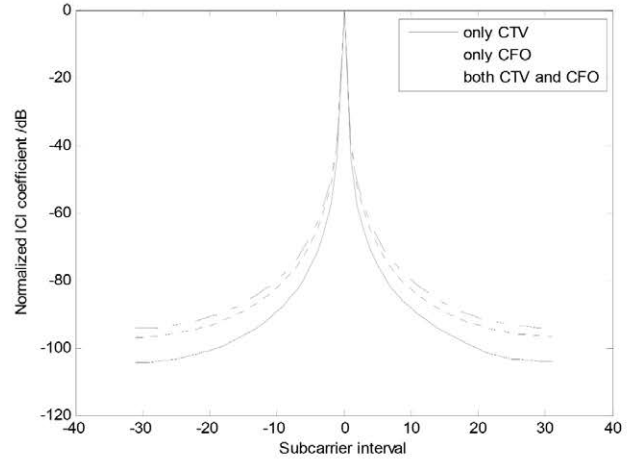


Fig. 3b. Illustration of the ICI distributions ($f_d=0.2$, $\epsilon=0.2$)

C. Complexity-Reduced Equalization

Owing to the approximate band structure of CFR matrix, there exists many low-complexity equalization methods such as the complexity-reduced MMSE equalizer with ordered SIC (MMSE-OSIC) [16]. Next we take the MMSE-OSIC [16] as an example to illustrate how to use the band structure of CFR matrix for reducing computational complexity. For the convenience of formulation, we define the vectors: $\mathbf{Y}_k = [Y(k-D), \dots, Y(k+D)]^T$, $\mathbf{X}_k = [X(k-2D), \dots, X(k+2D)]^T$, $\mathbf{W}_k = [W(k-D), \dots, W(k+D)]^T$, and the matrix:

$$\mathbf{H}_k = \begin{bmatrix} H(k-D, k-2D) & \cdots & H(k-D, k+2D) \\ \vdots & \ddots & \vdots \\ H(k+D, k-2D) & \cdots & H(k+D, k+2D) \end{bmatrix}, \quad (16)$$

where D is the number of considered ICI terms. It is worth noting that the indexes in above expressions of this subsection are all taken by modulo- N operation. For properly selected parameter D , \mathbf{Y}_k can be approximated as

$$\mathbf{Y}_k = \mathbf{H}_k \mathbf{X}_k + \mathbf{W}_k. \quad (17)$$

From (17), the MMSE estimate of $X(k)$ can be obtained as

$$\hat{X}(k) = \mathbf{H}_k^H(:, k) (\mathbf{H}_k \mathbf{H}_k^H + \sigma^2 \mathbf{I}_k)^{-1} \mathbf{Y}_k, \quad (18)$$

where $\mathbf{H}_k^H(:, k)$ is the $(2D+1)$ th column of \mathbf{H}_k and \mathbf{I}_k denotes a $(2D+1) \times (2D+1)$ identity matrix. In order to improve detection performance, the ICI caused by $X(k)$ is subsequently subtracted from the received signal. This operation is the so called SIC. Although the SIC can improve detection performance to some extent, the performance improvement is restricted by error propagation inherent in the SIC. In response, the authors in [16] proposed a simple yet effective ordering method based on Frobenius norm of the column vector of matrix \mathbf{H}_k to relief the error propagation of SIC. The overall complexity-reduced MMSE-OSIC detection procedure proposed in [16] is summarized as follows:

Step 1. Obtain the subcarrier index k for which the subcarrier is detected by (19)

$$k = \arg \max_m \|\mathbf{H}_m(:, m)\|_F, \quad (19)$$

where $\|\cdot\|_F$ denotes the Frobenius norm operator.

Step 2. Obtain the MMSE estimate of $X(k)$ using (18) and then make a decision according to the modulation constellation adopted.

Step 3. Perform SIC: $\mathbf{Y} = \mathbf{Y} - \mathbf{H}(:, k)X(k)$, where $\mathbf{H}(:, k)$ is the k th column of the CFR matrix \mathbf{H} .

Step 4. Set $\mathbf{H}(:, k) = \mathbf{0}$.

Step 5. Go to step 1 until all subcarriers have been detected.

According to the discussion of [16], the complexity-reduced MMSE-OSIC equalizer is advantageous over the MMSE equalizer with full CFR matrix in terms of both performance and complexity.

IV. NUMERICAL SIMULATIONS

We consider an OFDM system with 64 subcarriers per symbol. Each symbol appends a CP of 16 samples to avoid intersymbol interference. Transmission channels consist of 6 independently paths with exponential power delay profile, and the CIR of each path are Rayleigh distributed samples generated according to the classic Jakes model [17]. In the simulations the normalized Doppler frequency f_d is set to be 0.1 and 0.2, and the CFO are also chosen to be 0.1 and 0.2. Other simulation parameters are the same as in Section 3. In order to reduce the receiver complexity, we use the complexity-reduced MMSE-OSIC method [16] to perform ICI equalization in the frequency domain. The parameter D of the MMSE-OSIC is chosen to be 4. Moreover, the MMSE equalizer with full CFR (i.e., all ICI are considered) is used to benchmark the equalization performance. We also assumed perfect knowledge of CFO and channel state information at the receiver.

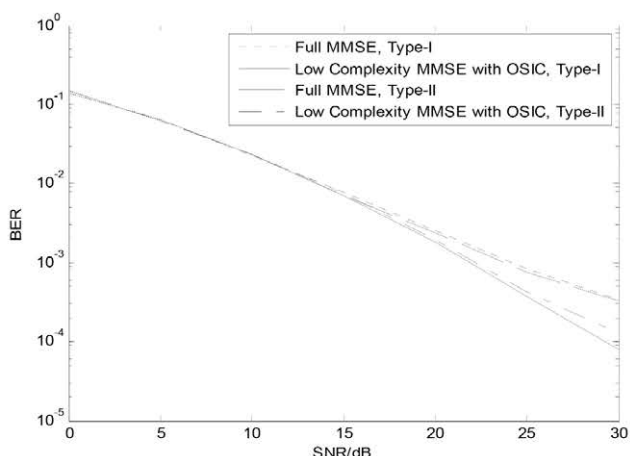


Fig. 4a. BER Performance under both CFO and CTV ($f_d=0.1, \epsilon=0.1$).

Fig 4 shows the bit error rate (BER) versus signal to noise ratio (SNR) using the two type receivers. In these plots, “Full MMSE” denotes the MMSE equalizer with full CFR and “Low

Receivers Design for OFDM Signals under both High Mobility and Carrier Frequency Offset

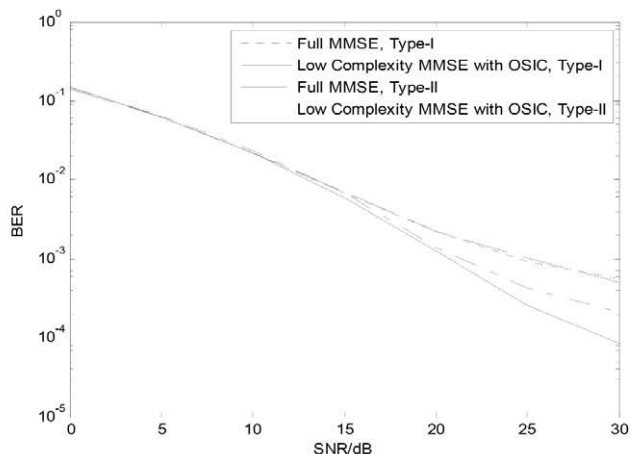


Fig. 4b. BER Performance under both CFO and CTV ($f_d=0.2, \epsilon=0.2$).

complexity MMSE with OSIC” the low-complexity MMSE equalizer with ordered serial interference cancellation [14]. We see from these plots that under various conditions and for both receivers the MMSE equalizer with OSIC is superior to the full MMSE equalizer. This may contribute to the diversity induced by the channel time variation. Due to the channel time variation, the power of each subcarrier is distributed over all subcarriers of a symbol, which produce potential diversity gains that thus be exploited through collecting the scattered subcarrier energies by the MMSE equalizer with OSIC. On the other hand, under severe ICI, the MMSE equalizer cannot fully exploit this diversity and can only mitigate the ICI to some extent.

Further more, we see from Fig 4 that under various conditions and under the MMSE equalization with OSIC, the type-I outperforms the type-II, especially in the case of large CFO. For instance, at a high SNR of 30 dB and under CTV and CFO values of $f_d=0.1$ and $\epsilon=0.1$, the BER of the type-II is 1.6 times the BER of the type-I, while at the same SNR and under large CTV and CFO values of $f_d=0.2$ and $\epsilon=0.2$, the BER of the type-II is 2.5 times that of the type-I.

In order to discover the reason why the type-I outperforms the type-II in the case of, especially large, CFO, we need resort to insight analysis of the effects of the CFO on the OFDM signals. Although in the presence of CFO the power of each subcarrier is also distributed over all subcarriers which also means a possible diversity, unfortunately however, the ICI distributions in this case make the CFR matrix highly correlated as (7) indicates. Actually, given a k , the CFR $H(k, u)$ for any value of u are the same when the channels is flat and static. As is well known, matrix with correlated elements means an ill conditioned matrix which thereby leading poor performance of the type-II receiver.

To corroborate this claim, Fig 5 shows the simulation results for the type II receiver where there is no CTV and only CFO exists. It is seen from the simulations that the performance of MMSE equalization with OSIC is even inferior to that of the MMSE equalization with full CFR. This is due to the ill conditioned CFR matrix \mathbf{H} caused by the CFO and the resulting diversity suppression.

Receivers Design for OFDM Signals under both High Mobility and Carrier Frequency Offset

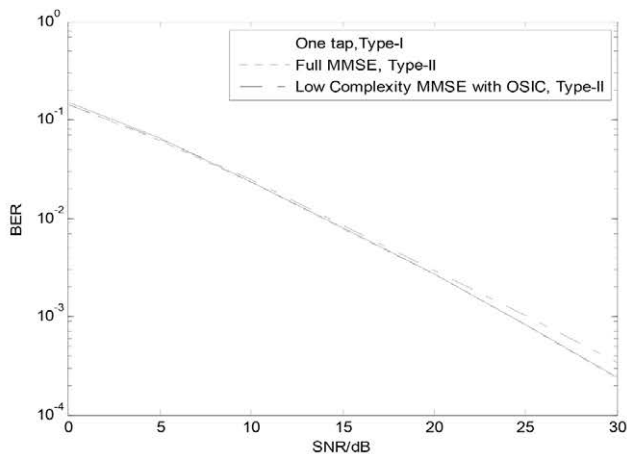


Fig. 5a. BER performance with only CFO ($\epsilon = 0.1$)

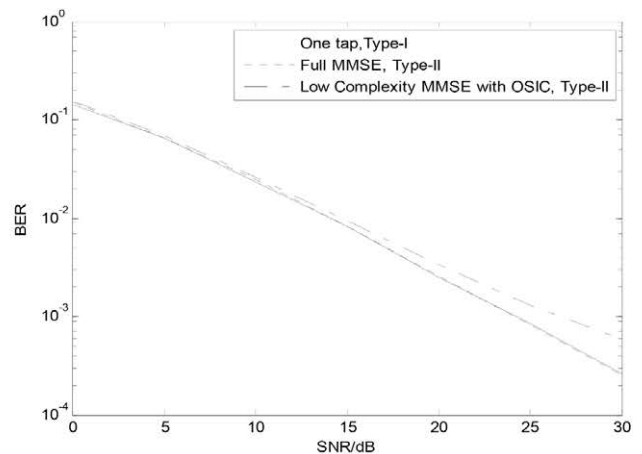


Fig. 5b. BER performance with only CFO ($\epsilon = 0.2$)

On the other hand, for the type-I receiver, the effect of CFO is compensated before the MMSE equalization with OSIC, so ill conditioned CFR matrix no longer exists in this case, and as a result the diversity gain can be exploited by the MMSE equalizer with the OSIC. The analysis above makes us naturally conclude that it is inappropriate for OFDM system to compensate the CFO in the frequency domain.

V. CONCLUSION

This paper investigates the receiver design for OFDM system operating over both the CFO and the channel time variation. The ICI under such cases becomes severe and the receiver confronts challenges of intensive computations and performance degradation. For solving this problem, this paper investigates two receive schemes, denoted by the separate scheme and the integrated scheme respectively, for OFDM system operating in such conditions. Performance of these two receivers are studied and compared through numerical simulations. Results obtained from the simulations show that the separate scheme outperforms the integrated one in terms of the BER performance, and is a more appropriate option for OFDM system operating over both the CFO and the channel time variation.

REFERENCES

[1] Y. Li, G. Stuber, *Orthogonal Frequency Division Multiplexing for Wireless Communications*. Boston, MA: Springer-Verlag, 2006.
 [2] T. Hwang, C. Yang, G. Wu, et al., "OFDM and Its Wireless Applications: A Survey," *IEEE Transactions on Vehicular Technology*, vol. 58, no. 4, pp. 1673-1694, 2009.
 [3] C.-Y. Hsu, W.-R. Wu, "Low-Complexity ICI Mitigation Methods for High-Mobility SISO/MIMO-OFDM Systems," *IEEE Transactions on Vehicular Technology*, vol. 58, no. 6, pp. 2755 – 2768, 2009.
 [4] P. H. Moose, "A Technique for Orthogonal Frequency Division Multiplexing Frequency Offset Correction," *IEEE Transactions on Communications*, vol. 42, no. 10, pp. 2908-2914, 1994.
 [5] A. Stamoulis, S. N. Diggavi, N. Al-Dhahir, "Intercarrier Interference in MIMO OFDM," *IEEE Transactions on Signal Processing*, vol. 50, no. 10, pp. 2451-2464, 2002.
 [6] Y. S. Choi, P. J. Voltz, F. A. Cassara, "On Channel Estimation and Detection for Multicarrier Signals in Fast and Selective Rayleigh Fading Channels," *IEEE Transactions on Communications*, vol. 49, no. 8, pp. 1375-1387, 2001.

[7] X. Cai, G. B. Giannakis, "Bounding Performance and Suppressing Inter-Carrier Interference in Wireless Mobile OFDM," *IEEE Transactions on Communications*, vol. 51, no. 12, pp. 2047-2056, 2003.
 [8] K. Fang, L. Rugini, G. Leus, "Low-Complexity Block Turbo Equalization for OFDM Systems in Time-Varying Channels," *IEEE Transactions on Signal Processing*, vol. 56, no. 11, pp. 5555-5556, 2008.
 [9] P. Schniter, "Low-Complexity Equalization of OFDM in Doubly Selective Channels," *IEEE Transactions on Signal Processing*, vol. 52, no. 4, pp. 1002-1011, 2004.
 [10] R. Li, Y. Li, B. Vucetic, "Iterative Receiver for MIMO-OFDM Systems with Joint ICI Cancellation and Channel Estimation," in *Proc. of 2008 IEEE Wireless Communications and Networking Conference*. Las Vegas, 2008, pp. 7-12.
 [11] T. Suryani, G. Hendratoro, "ICI Mitigation with CFO Compensation for OFDM in Mobile-to-Mobile Channel", *Proc. of IEEE ICTC 2011*, pp. 430-435, 2011.
 [12] S. U. Hwang, J. H. Lee, J. Seo, "Low Complexity Iterative ICI Cancellation and Equalization for OFDM Systems over Doubly Selective Channels," *IEEE Transactions on Broadcasting*, vol. 55, no. 1, pp. 132-139, 2009.
 [13] R. Chen, J. D. Li, C. L. Li, W. Liu, "Joint Transceiver Design for OFDM Systems," *China Communications*, vol. 9, no. 2, pp. 43-51, 2012.
 [14] Y. Zhao, S. G. Haggman, "Intercarrier Interference Self-Cancellation Scheme for OFDM Mobile Communication Systems," *IEEE Transactions on Communications*, vol. 49, no. 7, pp. 1185-1191, 2001.
 [15] W. Qin, Q. C. Peng, "Improved ICI Self-Cancellation Scheme for OFDM System Based on Symbol Transform," *Journal of University of Electronic Science and Technology of China*, vol. 37, no. 5, pp. 641-644, 2008.
 [16] X. P. Xi, C. Zhang, "Complexity-reduced ICI cancellation for OFDM system over doubly-selective channels," *High Technology Letters*, vol. 15 2, pp. 181-186, 2009.
 [17] P. Dent, G. Bottomley, T. Croft, "Jakes fading model revisited," *IEE Electronics Letters*, pp.1162-1163, 1993



Dong-Hua Chen was born in 1977. He received his Ph.D. degree in Communication and Information Systems from Xidian University in 2011. Now he is a lecturer in Huaqiao University, Xiamen, China. His research interests are in the area of channel estimation and equalization for wideband wireless communications over doubly selective channels, resources allocation for cognitive wireless networks.

Gong-Yi Huang was born in 1972. He received his B.S. degree in Micro Electronics from Xian Jiao Tong University in 1995. He is a lecturer in Huaqiao University, Xiamen, China. His research interests are in the area of data communication and security for the information networks.

Yi-Ming Yang was born in 1957. Now he is an associate professor in Huaqiao University, Xiamen, China. His research interests include digital signal processing for wireless communications, soft-defined radio and digital receiver design.

Applications of a simplified protocol of RoboCup 2D Soccer Simulation

Norbert Bátfai, Roland Dóczy, János Komzsik, András Mamenyák, Csaba Székelyhídi, József Zákány,
Márton Ispány and György Terdik

Abstract—The RoboCup 2D Soccer Simulation (RCSS) is a sophisticated soccer simulation environment introduced in [1] and implemented in [2], [3]. For educational and other sport science purposes, we have simplified the protocol of the RCSS. With raw phrasing we would say that we have eliminated the main AI part of the AI-based RCSS simulation model in order that it can be used easily in sport science and in education of programming. In compliance with this aim, we must modify the RCSS environment. In our terminology, the suitable modified rcssserver is referred to as "lighter RCSS" [4], [5]. In this paper, the experiences of our first "lighter teams" will be presented.

Index Terms—RoboCup 2D Soccer Simulation, rcssserver/sam-plecient, Lighter RCSS, sport science soccer simulations, Football Avatar, education of programming.

I. INTRODUCTION

The purpose of this paper is twofold. First, we are developing a simulation based decision making support expert system for professional soccer in the framework of an industrial project called Football Avatar. It involves the investigation of the existing soccer simulation environment of the sport science point of view. Second, whereas our part of the development is taking place in university environment, we need to prep students to participate in the development of the mentioned industrial project. The present paper can be seen as a step towards this twofold purpose.

A. Sport Science Purpose

The initiative for development of a sport science simulation based system came from the FerSML (Footballer and Football Simulation Markup Language) platform [6] introduced in the paper [7]. In the terminology of FerSML, the abstractions of soccer players, coaches and matches are called avatars. The avatars contain all information required to play such simulated soccer matches with probability properties corresponding to real matches of the abstracted players and coaches. In the special case of Football World Cups, an introductory statistical comparison of real and simulated matches can be found in [8]. The used simulation engine is based on our former mobile soccer game [9] and absolutely independent from the RoboCup (Robot World Cup) introduced in [1]. This is not surprising, because RoboCup focuses on AI, and it is purely AI in such sense that agents have to build up themselves, from scratch,

the simulated world from their very limited sensory input. In contrast, the FerSML avatars are automatically fully aware of the following data: the exact position of the ball, players and parts of the pitch, the used tactics, etc. Accordingly, the building of this sort of knowledge would be a superfluous process for the purpose of an avatar based simulation, because avatars are apriori aware of this knowledge. In parallel, using the artificially limited sensory input may be waived for "sport science" avatars that will be defined on a much higher abstraction level. However, the RCSS environment is a sophisticated collection of GPLed open source software components (like rcssserver, rcssmonitor or rcsslogplayer [2]). The simulation is made inside the rcssserver, the client agents are connected to it over UDP/IP. The rcssmonitor and the rcsslogplayer are visual software interfaces to the simulation. So it would also be useful to investigate the modification of the RCSS environment in order to serve our sport science or educational purposes easily. In summary, our motivation is to try to eliminate the artificial intelligence-specific limitations from the RCSS environment. The mathematician, Gregory Chaitin, wrote in his book [10], "you understand something only if you can program it. (You, not someone else!) Otherwise you don't really understand it, you only think you understand it." In the spirit of this, although we are early in the investigation of soccer simulation models, we have modified the software of the RCSS environment. This paper is built on a modification of the rcssserver. In parallel, we worked on a modification of rcsslogplayer, where the Brillinger potential field [11]-based model are applied for RCSS matches [12].

B. Educational Purpose

Programming RCSS agents is a hard task because they have a very limited sensory input. For example, the following log snippet shows what can be seen by an agent at every 150 millisecond:

```
(see 0 ((f c b) 23.1 38 0 0) ((f r b) 54.6
-35) ((f p r b) ...
```

where the letter f denotes the appropriate circular flag shown in Fig. 1. A classical RCSS agent must determine its position only from this information. But we are interested in building agents that know, for example, their own position on the pitch, rather than classical agents. In compliance with this, in the lecture notes [4], [5] we introduce a new client protocol command (`pos x y power`), which will move the agent towards the (x, y) position of the pitch with the velocity

N. Bátfai is with the Department of Information Technology, University of Debrecen, H-4010 Debrecen PO Box 12, Hungary, e-mail: batfai.norbert@inf.unideb.hu.

R. Dóczy, J. Komzsik, A. Mamenyák, Cs. Székelyhídi, J. Zákány, M. Ispány and Gy. Terdik are with the University of Debrecen.

Applications of a Simplified Protocol of RoboCup 2D Soccer Simulation

derived from the given power. And vice versa, if the command line option `server::light_response` is switched on, the "lighter RCSS server" returns the x, y coords of an agent. Applying these and similar modifications makes it rather easy to use RCSS environment to investigate sport science questions or to use it in education of programming.



Fig. 1. The RCSS field of play in the program rcssmonitor.

C. Comparison with Existing Works

It is important to note that we have no aim to create classical RCSS 2D robocup agents. Our key motivation is to consider a relaxation of the agents' very limited sensory input together with the RCSS protocol, because the limitations of RCSS environment are unnecessary from the point of view of sport science. The sub-objective of our research is to have a better understanding of server operations. On the one hand, if we begin from scratch, the development time of such robocup team that can apply tactics (in the sense of the sport science) is many years. More recently, a good example of a multiannual development is the Romanian team OXSY [13]. On the other hand, we may customize a ready-made agent by using the GPLed Agent2D sources [14], for example, as some successful teams (e.g. EdInferno.2D [15]) have already did. But in our case, it would raise licensing questions and concerns for the mentioned industry project.

II. THE SIMPLIFICATION OF THE RCSS AND THE FIRST "LIGHTER TEAMS"

In this section, we present the first teams which already use the "lighter RCSS" protocol. The Debrecen Round Forest FC++ team is one of the many educational teams of the book [4], [5]. It introduces the usage of the "lighter RCSS" environment. The other presented teams are developed by students. These teams are based on the educational teams. This kind of student teams can be regarded successful if it can confidently win against the educational teams. The development of the teams, titled "Kő papír metál FC", "Rozsdás FC" and "Deadly Team", satisfy that condition.

In particular, the "lighter teams" can be tested easily because these teams are packaged together with the "lighter RCSS"

server. In addition, we will emphasize some video links where the teams in question can be seen during the matches, as well as associated RCG (record game) files are available for all teams. Based on these classical RCG files the matches are reproduced exactly by rcsslogplayer [2].

A. Debrecen Round Forest FC++

The Debrecen Round Forest FC++ team is the last example of the lecture notes [4], [5]. Here we should remark that [4] is a Hungarian language book and it is ready to be published, but the English translation [5] is only in work in progress state at this moment. But of course, the package of the modified (i.e. the lighter) RCSS server is available for download from <http://www.inf.unideb.hu/~nbatfai/rcssserver-15.1.0.light5.rf.tar.bz2>. This package is based on the classical RCSS distribution and it contains some modifications to implement the new positioning command and contains a few other files to implement the behavior of a lighter sample team called Debrecen Round Forest FC++. The exactly detailed description of changes can be found in the file NEWS in the distribution of the package. This team is gradually developed by simpler examples like "Bolyongó SE", "Bolyongó FC++", "Debreceni Lobogó FC++", "Debreceni Egyetértés FC++", "Debreceni Hivatás FC++", "Light FC++", "Debrecen Great Forest FC++" and "Debrecen Deep Forest FC++". In that order these teams give a programmed introduction to building a C++ based RoboCup team. All teams are based on rcssserver (15.1.0) [2] and its sample client [3]. They are simple threaded versions of client.cpp of [2], [3], but all of them have their own lexer part to analyse sensory data. The "Bolyongó SE" starts from scratch to control the behavior of agents. The Light FC++ is the first lighter team. The mentioned teams can be downloaded from the links contained in the lecture notes [4], [5].

The Debrecen Round Forest FC++ and the "lighter RCSS" server can be found directly at URL <http://www.inf.unideb.hu/~nbatfai/rcssserver-15.1.0.light5.rf.tar.bz2>

B. The simplified server

We have modified some source files in the original rcssserver [2] to implement the simplification. (A description of the modifications can be found in the file NEWS in the distribution of the package at URL <http://www.inf.unideb.hu/~nbatfai/rcssserver-15.1.0.light5.rf.tar.bz2>.) As a result the rcssserver can be started with the following options:

- If the optional command line option `server::light_response` is set to true, the x and y coordinates of the client agent will be inserted into the server's response. (To be more precise, into the client sensor response see [3].)
- If the optional command line option `server::light_response_with_angle` is set to true, the x and y coordinates and the body angle of the client agent will be inserted into the server's response.
- If the optional command line option `server::light_response_with_angles` is set to true, the x and y coordinates and the body and neck angles of the client agent will be inserted into the server's response.

- In all the three cases, the server can interpret the newly introduced client control command (`pos X Y power`).

The implemented command `pos` has the same uses as the original client control commands. And of course, the simplified server can work with original teams transparently without any change.

C. Deadly Team

Our team is developed by András Mamenyák and János Komzsik. The team is based on the Debreceni Hivatásos FC++ team. The strenght of the team comes from the ability to pass the ball from one agent to the other. To perform a pass, we need the coordinates of the players. The coordinates can be calculated easily if we know the position of our agent and the distance to the flags. These are recieved from the server automatically, so the only thing needed is the angle the agent is standing. We calculate this as seen on Fig. 2.

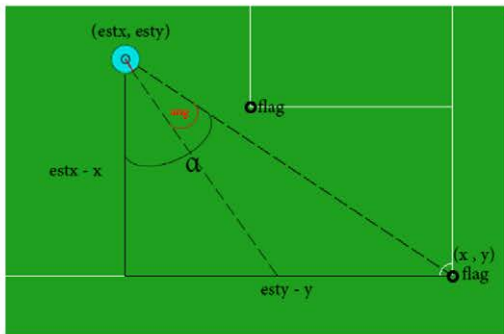


Fig. 2. The calculation of the body angle.

After this we rely on this universal passing method:

```

/*
 * pass the ball to the given x, y coordinates
 */
void deadlyPassXY(float x, float y) {

    float dist = std::sqrt(
        std::pow(dl.estx - x, 2) +
        std::pow(dl.esty - y, 2)
    );

    float power = dist * 5.0 / 2.0;

    float angle = std::atan((dl.esty - y) / (dl.estx - x));
    angle *= 180.0 / pi;
    angle -= dl.esta;

    if (x < dl.estx)
        angle += 180.0;
    if (angle > 180.0)
        angle -= 360.0;

    char buf[64];
    std::sprintf(buf, 64, "(kick_%f_%f)", power, angle);
    sndCmd(buf);
}
    
```

We now need to decide to which players to pass to, and to which players not to pass to. A teammate not receiving a pass is based on two things: there is an opponent player near our teammate or there is an opponent player close to the the path of the pass. If there is no one to pass to, then the player can dash with the ball if there are no opponent players near. If an opponent player is near, our player will try to go past him. If

there are too many opponents near, then our player will turn around, and look for other teammates to pass to.

Meanwhile the other players seek their predefined attacking or defensive positions if not involved in a pass. If the opposite team is attacking, the players try to mark the attackers or tackle if close enough. To determine the possession of the ball, we utilize the possibility to communicate, so our players tell each other which tactic to use.

The main weakness of our team is simply stamina. The players get exhausted quickly because they run too much, but sometimes they are running a bit slowly, because they are constantly adjusting their positions to the ball.

The development of the presented team took more than two months, but it is continuously improved and future developments are planned.

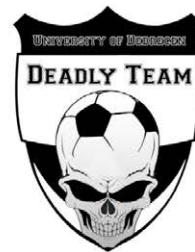


Fig. 3. The logo of the Deadly Team.

D. Tortoise Formation FC

As we played matches against the famous HELIOS (more precisely, the HELIOS_base [14]), we discovered its weakness, so this resulted in creating a team, based on the core of the Deadly Team. This team is called Tortoise Formation FC, because it uses a tactic in which the players surround the ball, creating an impenetrable fortification for the HELIOS players. This way, the players can simply march with the ball, and score, if they are close enough to the goal. The success of the Tortoise Formation FC demonstrates that, using the positioning command of the "lighter RCSS", the teams' approaches to the game may be formed very easily. But it has no sport scientific importance, as shown in the video at http://youtu.be/5ng5W_2Rofs, and in Figure 4.

The teams can be downloaded at the URL <http://robocup.inf.unideb.hu/~andras/RoboCup/Teams/>.

E. KőPapírMetál FC

The first KőPapírMetál FC was developed by Roland Dóczy and Tamás Józsi. This team was an Atan [16] (Java language) based team and it was developed to take place in two local RoboCup events. After this, one of the teammates left the team and it is rewritten in C++ as a DForest based team, which supports the simplified protocol of RoboCup2D Soccer Simulation. The advantages of the new protocol are used by the team. With this, the team has coordinate geometry based methods.

When the ball is not near, the agents try to stay in their correct positions. When it is near the goal, the goalkeeper

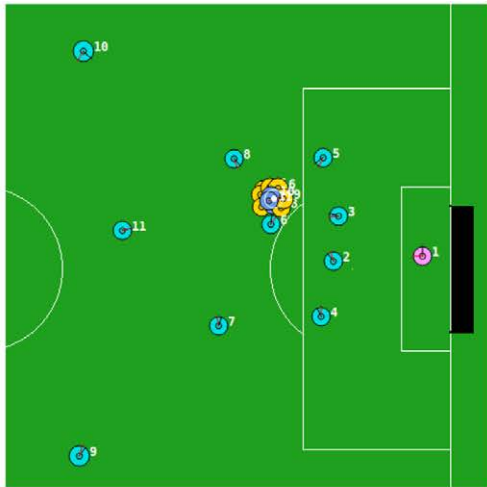


Fig. 4. The Tortoise Formation FC's approach to the game.

rushes for the ball and tries to catch it. The defenders stand before the attackers to block them getting the ball. After this, the defenders pass the ball to the furthest attacker. The midfielders do the same. When an attacker agent gets the ball, it rushes in the direction of the goal, and when the agent is close enough, it tries to score. The target is the furthest goalpost from the goalkeeper.

The main advantage of the team lies in the attacking strategy, but it has its disadvantages too. The goalkeeper can not analyze the situations as fast as it should and because of this, we concede more goals.



Fig. 5. The logo of the KőPapírMetál FC.

The team can be downloaded at the URL <http://shrek.unideb.hu/~roland10/RoboCup2D/team/>

F. Rozsdás FC

The Rozsdás FC is developed by József Zákány. The team was born in a Java environment, based on Atan [16] framework. Thanks to the simplified protocol of RoboCup 2D Soccer Simulation, it could reborn as a C++ team, with the advantages of the new protocol. It is based on the Debrecen Great Forest FC++. The development lasted nearly a month. In this work, the individual behaviour of players was focused. For example, there is an imaginary circle around the middle goal flag. If the goalkeeper crosses the (red) circle line, he goes back to his place, in front of the goal. This can be calculated easily from the coordinates of the goalkeeper, and the equation of the circle.

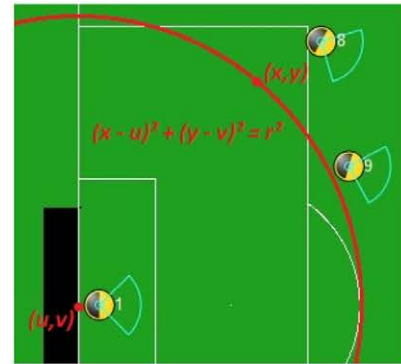


Fig. 6. Positioning of the goalie.

The team is basically built on defensive tactics. The defensive players stay on their own half of the field, they do not take part in the attack at all. They try to keep the ball away from the goal. If one of them gets the ball, he tries to pass it to a teammate, or just kick it into the direction of the opponent goal. The midfielders are playing similar like the defensive players, but they go forward and they help with the attack. And finally, the attackers wait for the ball on the opponent side. They pass the ball between each other, and if they have the chance they try to score.

The team can be downloaded at the URL <http://shrek.unideb.hu/~joe42/RoboCup2D/rcsserver-15.1.0.light4.gf.tar.bz2>.

G. NimFC

The NimFC is based on the Debrecen Round Forest FC++. The work was much easier with the lighter server. The NimFC is functionally divided into defenders, midfielders, strikers and goalkeeper. The methods of passing and positioning and the kicking habits of strikers were changed compared to the original RForest FC++.

The team can be downloaded at the URL <http://web.unideb.hu/~szekelyhidi/rcsserver-15.1.0.light5.rf.tar.bz2>.

III. CONCLUSION

How efficient and effective are the developed teams? In this environment, it is essential to survey the matches. For example, the playing style of our teams can be seen in the following YouTube videos or by viewing the standard rcg (record game) files of the next subsections.

DeadlyTeam:

<http://www.youtube.com/watch?v=DsDnNwj78pw>
<http://www.youtube.com/watch?v=NZeP8BoOQxQ>

Tortoise Formation FC:

http://www.youtube.com/watch?v=5ng5W_2Rofs

A. Results

The match results against each other can be found in the Table I. The Table II shows our match results against the world's best teams. In this latter table, the HELIOSbase [14] is a

TABLE I
RESULTS AGAINST EACH OTHER

Match	Result
GreatForest vs DeadlyTeam	0 9
GreatForest vs DeadlyTeam	2 12
DeadlyTeam vs GreatForest	11 3
DForest vs DeadlyTeam	1 9
DForest vs DeadlyTeam	1 8
RForestFC++ vs DeadlyTeam	3 8
RForestFC++ vs DeadlyTeam	0 12
DeadlyTeam vs RForestFC++	12 2
DeadlyTeam vs RForestFC++	16 1
KoPaparMetal vs DeadlyTeam	2 5
KoPaparMetal vs DeadlyTeam	3 7
DeadlyTeam vs KoPaparMetal	14 3
RozsdasFC vs DeadlyTeam	1 4
NimFC vs DeadlyTeam	1 12
KoPaparMetal vs RozsdasFC	1 7

TABLE II
RESULTS AGAINST THE WORLD’S BEST TEAMS

Match	Lighter	Result
HELIOS_base vs TortoiseFormation	Enabled	5 0
TortoiseFormation vs HELIOS_base	Enabled	2 12
KoPaparMetal vs HELIOS2010	Enabled	0 48
KoPaparMetal vs HELIOS2010	Enabled	0 46
RozsdasFC vs HELIOS2010	Enabled	0 35
HELIOS2010 vs RozsdasFC	Enabled	17 0
RozsdasFC vs HELIOS2010	Enabled	0 34
HELIOS2010 vs RozsdasFC	Enabled	21 0
HELIOS_base vs DeadlyTeam	Enabled	31 0
DeadlyTeam vs WrightEagle	Enabled	0 42
DeadlyTeam vs WrightEagle	Disabled	0 48
RForestFC++ vs WrightEagle	Disabled	0 50
DeadlyTeam vs Dainamite	Disabled	0 23

base team of the famous HELIOS2010 [17] and HELIOS2011 [18], which can be found at URL <http://sourceforge.jp/projects/rctools/downloads/55186/agent2d-3.1.1.tar.gz/>. The WrightEagle [19], the HELIOS2011 and the Dainamite [20] participated in the Competition RoboCup2011 Soccer Simulation 2D in Istanbul, Turkey, where the Chinese WrightEagle team won this championship, the Japanese team HELIOS2011 reached the second place and the Dainamite team from Germany caught the 14-th place. The WrightEagle, HELIOS2011 and Dainamite teams can be downloaded at URL <http://www.socsim.roboocup.org/files/2D/binary/RoboCup2011/>.

All rcg files of the matches of aforementioned tables can be downloaded at the URL <http://roboocup.inf.unideb.hu/~andras/RoboCup/RCG/>.

B. Teaching Experiences

We have been using (Atan [16]) Java and (rcsserver [2]/sample client [3]) C++ based RCSS client agents [4], [5],

[21] in the education of programming for two years in Software Information Technology and Engineering Information Technology BSc regular courses at the University of Debrecen. The use of the "lighter RCSS" has started this year and we have very good experience with it. The lighter student teams are proved better than the last year’s teams.

The development of "lighter teams" requires around 1-3 months. Considering that the developers was first year BSc students, it is a short period of time. But we have no sufficient experience for making a precise global comparison, because we build RoboCup teams only in the context of the investigation of soccer simulations.

C. Summary and Further Work

Regarding the mentioned industrial simulation project, we have no plans to use the classical nor the "lighter RCSS" environment. Partially based on the experience of this work, we can decide that the simulator of Football Avatar will be developed from scratch. In the future, we plan to develop a football avatar to "lighter RCSS" agent conversion software. In addition, it is notable that we are using RCSS data to test mathematical models of sport science [12].

ACKNOWLEDGMENT

The publication was supported by the TÁMOP-4.2.2.C-11/1/KONV-2012-0001 project. The project has been supported by the European Union, co-financed by the European Social Fund.

REFERENCES

- [1] H. Kitano, M. Asada, Y. Kuniyoshi, I. Noda, and E. Osawa, "Robocup: The robot world cup initiative," in *Proceedings of the first international conference on Autonomous agents*, ser. AGENTS '97. ACM, 1997, pp. 340–347. [Online]. Available: <http://doi.acm.org/10.1145/267658.267738>
- [2] The RoboCup Soccer Simulator Maintenance Committee, "The robocup soccer simulator," 2001-2012. [Online]. Available: <http://sourceforge.net/projects/sserver/>
- [3] M. Chen, K. Dorer, E. Foroughi, F. Heintz, Z. Huang, S. Kapetanakis, K. Kostiadis, J. Kummeneje, J. Murray, I. Noda, O. Obst, P. Riley, T. Steffens, Y. Wang, and X. Yin, "Users manual robocup soccer server for soccer server version 7.07 and later," 2003. [Online]. Available: <https://sourceforge.net/projects/sserver/files/rcssmanual/>
- [4] N. Bártfai, *Programozó Páternoszter újrátöltve: C, C++, Java, Python és AspectJ esettanulmányok*. author’s edition, 2012. [Online]. Available: <http://www.inf.unideb.hu/~nbatfai/konyvek/PROP/prop.book.xml.pdf>
- [5] —, *Paternoster of Programmers Reloaded: C, C++, Java, Python and AspectJ Case Studies*. author’s edition, 2012. [Online]. Available: <http://www.inf.unideb.hu/~nbatfai/konyvek/POPR/popr.book.xml.pdf>
- [6] —, "Football(er) simulation markup language," 2010-2012. [Online]. Available: <http://sourceforge.net/projects/footballerml/>
- [7] —, "Footballer and football simulation markup language and related simulation software development," *Journal of Computer Science and Control Systems*, vol. 3, no. 1, pp. 13–18, 2010.
- [8] —, "The soccer force," *CoRR*, vol. abs/1004.2003, 2010.
- [9] N. Bártfai, E. Bártfai, and I. Pšenáková, "Jávacska one: Open source mobile games to revolutionize education of programming," *Journal of Computer Science and Control Systems*, vol. 3, no. 2, pp. 5–10, 2010.
- [10] G. J. Chaitin, *Meta Math! The Quest for Omega*, 2004. [Online]. Available: <http://arxiv.org/abs/math/0404335>
- [11] D. R. Brillinger, "A potential function approach to the flow of play in soccer," *Journal of Quantitative Analysis in Sports*, vol. 3, no. 1, 2007. [Online]. Available: <http://www.stat.berkeley.edu/~brill/Papers/jqas.pdf>

Applications of a Simplified Protocol of RoboCup 2D Soccer Simulation

[12] N. Bátfai and Gy. Terdik, "The application of the data of RoboCup 2D Soccer Simulation League to test several sport science results (submitted manuscript)," 2012. [Online]. Available: <http://robocup.inf.unideb.hu/fersml/assr/>

[13] S. Marian, D. Luca, B. Sarac, and O. Cotarlea, "Oxsy 2010 team description," 2010. [Online]. Available: http://www.socsim.robocup.org/files/2D/tdp/RoboCup2010/2D_TDP_Oxsy.pdf

[14] H. Akiyama and H. Shimora, "Helios_base - agent2d-3.1.1," 2012. [Online]. Available: http://en.sourceforge.jp/projects/rctools/releases/?package_id=4887

[15] M. Hawasly and S. Ramamoorthy, "Team description paper for robocup 2011 2d soccer simulation league," 2011. [Online]. Available: <http://wcms.inf.ed.ac.uk/ipab/robocup/research/TDP-Edinferno2D.pdf>

[16] N. James and D. Wood, "Atan - robocup 2d soccer server java interface," 2012. [Online]. Available: <https://github.com/robocup-atan/atan/>

[17] H. Akiyama and H. Shimora, "Helios2010 team description," 2010. [Online]. Available: http://www.socsim.robocup.org/files/2D/tdp/RoboCup2010/2D_TDP_HELIOS.pdf

[18] H. Akiyama, H. Shimora, T. Nakashima, Y. Narimoto, and T. Okayama, "Helios2011 team description," 2011. [Online]. Available: <http://www.socsim.robocup.org/files/2D/tdp/>

[19] A. Bai, G. Lu, H. Zhang, and X. Chen, "Wrighteagle 2d soccer simulation team description 2011," 2011. [Online]. Available: http://ai.ustc.edu.cn/en/robocup/2D/tdps/WrightEagle2011_2D_Soccer_Simulation_Team_Description_Paper.pdf

[20] H. Endert, T. Karbe, J. Krahmann, F. Trollmann, and N. Kuhnen, "The dainamite 2008 team description," 2008. [Online]. Available: http://www.socsim.robocup.org/files/2D/tdp/RoboCup2008/2D_TDP_DAlnamite.pdf

[21] N. Bátfai, *Mesterséges intelligencia a gyakorlatban: bevezetés a robotfoci programozásba*. author's edition, 2012. [Online]. Available: <http://www.inf.unideb.hu/~nbatfai/konyvek/MIRC/mirc.book.xml.pdf>



Norbert Bátfai is working as an assistant professor in Faculty of Informatics at the University of Debrecen, Hungary. He received his M.Sc. (summa cum laude) in Computer Science at 1998 from the Kossuth Lajos University (KLTE), Debrecen, Hungary. In 1999, he won the first prize in the Java Programming Contest organized by Hungarian Java Alliance: Sun, IBM, Oracle, Novell and IQSoft. In 2004, his company won the first prize in the Hungarian Mobile Java Developer Contest organized by Sun Hungary and Nokia Hungary. In 2008, the Hungarian Chief Information Officers' Association has selected him as an IT trainer of the year. He received the Ph.D degree in 2011. He won the Pollák-Virág award from Scientific Association for Infocommunications Hungary in 2012.



András Mamenyák is mayor in Engineering Information Technology BSc at the University of Debrecen, Hungary. He is a part of the World Football - Modelling and Visualizing Research Group and the Football Avatar Project at the University of Debrecen. He took part in the Romanian national physics competition final and in the Vermes Miklós International Physics competition final. He also took part several times in the Hungarian Gordius national mathematics competition final.



János Komzsik is mayor in Engineering Information Technology BSc at the University of Debrecen, Hungary. He is a member of the World Football - Modelling and Visualizing Research Group at the University of Debrecen. He is also a member of the Football Avatar Project.



József Zákány is mayor in Engineering Information Technology BSc at University of Debrecen, Hungary. He is a part of the World Football - Modelling and Visualizing Research Group and the Football Avatar Project at the University of Debrecen.



Csaba Székelyhídi is mayor in Software Information Technology, BSc at the University of Debrecen, Hungary. He is a member of World Football Modelling and Visualizing Research Group. In 2011 he graduated from Mihály Fazekas High School of Debrecen, Hungary.



Roland Dóczy is mayor in Engineering Information Technology BSc at University of Debrecen, Hungary. He is a part of the World Football - Modelling and Visualizing Research Group and the Football Avatar Project at the University of Debrecen.



Márton Ispány received his Ph.D. degree from the Kossuth Lajos University, Hungary. He is an associate professor at the Department of Information Technology at the University of Debrecen, Hungary. Dr. Ispány's research areas include integer valued time series analysis, branching processes, and data mining.



György Terdik received his Ph.D. degree from the Kossuth Lajos University, Hungary. He is a member of the editorial board of the quarterly Publications Mathematicae Debrecen. He is a professor and Head of the Department of Information Technology at the University of Debrecen, Hungary. Dr. Terdik's research areas include nonlinear, non-Gaussian time series analysis, Lévy processes, and high speed network modeling.

Investigation of the Fault Tolerance of the PIM-SM IP Multicast Routing Protocol for IPTV Purposes

Gábor Lencse, István Derka

Abstract—IPTV services should use an IP multicast solution for a network bandwidth efficient delivery of the media contents. PIM-SM is the most commonly used IP multicast routing protocol in IPTV systems. A short introduction to the operation of PIM-SM is given. Its fault tolerance is examined by experimenting on a mesh topology multicast test network built up by XORP routers in a virtualized environment. Different fault scenarios are played and different parameters of PIM-SM and OSPF are examined if they influence and how they influence the outage time of an IPTV service. A formal model is given for the service outage time of the IPTV service on the basis of the results of the experiments.

Index Terms—IPTV, IP multicast protocols, PIM-SM, OSPF, fault tolerance, mesh networks, simulation models.

I. INTRODUCTION

The global number of IPTV subscribers is growing rapidly [1]. As we have shown in [2], instead of IP unicast, an IP multicast solution should be used in IPTV systems that have a high number of active subscribers (except for the video-on-demand service). There were a number of IP multicast protocols invented, e.g. Distance Vector Multicast Routing Protocol (DVMRP, RFC 1075), Multicast Open Shortest Path First (MOSPF, RFC 1581), Core-Based Trees [3] (RFC 2189), Protocol Independent Multicast – Dense Mode (PIM-DM, RFC 3973) and Protocol Independent Multicast – Sparse Mode [4] (PIM-SM, RFC 4601). From these protocols, PIM-SM is the one that is commonly used in IPTV systems.

The probability of the failure of at least one element (e.g. router) of a network grows with the number of elements of the network. Large networks have redundant routers and transmission lines that are used for building alternate data paths in case of failures. The multicast routing should also support this solution. For example, a fault tolerant solution for the Core-Based Trees was proposed in [5].

As for PIM-SM, the Rendezvous Point (RP, see explanation later) was identified as a single point of failure, as PIM-SM allows only one RP per multicast groups [6]. PIM version 2 introduced a standards-based mechanism for the RP fault tolerance and scalability using the Bootstrap Routers [7]. This mechanism makes possible for a multicast based IPTV system to survive the failure of the RP; however the switching over to the new RP is not always invisible for the customers, but may cause service outage for a certain amount of time. In our current research, we are interested in

the length of the service outage time and the parameters it may depend on. Different scenarios were investigated and parameters were tested whether they have an influence on the length of the service outage time, and if so, how they influence it.

We expect that our results will be useful for both

1. the appropriate choice of the parameters of PIM-SM based multicast subsystems for IPTV systems and
2. building simulation models of the failure behaviour of the PIM-SM multicast protocol.

The second one is very important, because simulation (that is experimenting with a computerized model of the system) is a powerful tool for the performance and fault tolerance analysis of complex ICT (Information and Communication Technology) systems [8]; and measurement data gained with our experimenting with a real system is essential in the model building stage of a simulation project.

The remainder of this paper is organised as follows. First, an introduction to the operation of PIM-SM is presented (for more information see [9] or RFC 4601). Second, a very brief summary of IPTV is given. Third, the test environment is described. Fourth, the different kinds of experiments are presented and the results are interpreted. Fifth, formal models are given for the service outage time of the IPTV system in the function of certain parameters of PIM-SM and OSPF. Finally our conclusions are given.

II. THE OPERATION OF PIM-SM

Protocol Independent Multicast builds multicast trees on the basis of routing information obtained from a unicast routing protocol (e.g. RIP, OSPF) – this is why PIM is called “protocol independent”. It has four variants, from which the two most important ones are:

1. *PIM – Dense Mode* (RFC 3973) builds the multicast trees by flooding the whole network by multicast traffic and then pruning back the branches of the traffic distribution tree where no receivers of the multicast traffic are present.
2. *PIM – Sparse Mode* (RFC 4601) does not suppose group members everywhere thus sends multicast traffic into those directions where it has been requested using unidirectional *shared trees* rooted at the *Rendezvous Point*. It may optionally use shortest path trees per source.

In the rest of this paper, we use PIM-SM. PIM-SM does not have an own topology discovery method, but uses the Routing Information Base (RIB) of the unicast routing protocol applied in the *Autonomous System* (AS). With the help of this “outer” *Routing Information Base* (RIB), PIM-SM

Manuscript submitted Aug. 13, revised Dec. 31, 2012. This research was supported by the TÁMOP-4.2.2/B-10/1-2010-0010 project.

Gábor Lencse is with the Department of Telecommunications, Széchenyi István University, 9026 Győr, Egyetem tér 1, Hungary. phone: +36-30-409-56-60, fax: +36-96-613-646, e-mail: lencse@sze.hu

István Derka is with the Department of Telecommunications, Széchenyi István University

Investigation of the Fault Tolerance of the PIM-SM IP Multicast Routing Protocol for IPTV Purposes

builds its own *Multicast Routing Information Base* (MRIB). Unlike unicast RIB (that specifies the next router towards the destination of the packets) MRIB specifies the reverse path from the subnet to the router.

As PIM-SM is an *Any-Source Multicast* (ASM) protocol, the receivers need to find the source(s). The so-called *Rendezvous Point* (RP) is used for this purpose. The RP can be set statically by the administrator of the AS, or it can be elected from among the RP candidate routers.

There can be only one RP per multicast groups in the AS (or multicast domain) at a time. Note that there is a technique called *Anycast RP* (RFC 4610) that uses multiple instances of the RP in a single multicast domain using the same IP address (anycast addressing) and sharing their information about the sources with the Multicast Source Discovery Protocol (MSDP, RFC 3618). However, the failure of an instance of the RP still requires some kind of switching over to another instance and this switchover also causes outage in the IPTV service, so in this paper, we have chosen the clearer way of having one RP only and electing a new one if it fails.

The operation of PIM-SM has three phases. Now, we briefly describe what happens in these phases.

A. Phase One: RP-Tree

The *Rendezvous Point Tree* (RP-tree) is being built in the following way. The receivers send their *IGMP* (or *MLD*) *Join* messages with the required group address as destination IP address. The *Designated Router* (DR) of the receiver (that was elected from among the local routers before) receives the *IGMP Join* message and sends a *PIM Join* message to the RP of the required multicast group. This *PIM Join* message travels through the routers in the network and the visited routers prepare the appropriate MRIB entries thus the *RP-tree* is being built. The *PIM Join* messages have the marking: $(*, G)$, where the first element is the IP address of the streaming source and the second one is the IP address of the multicast group. The star (“*”) means that when a receiver joins a group, it will receive the traffic from all the sources that send steam to multicast group G. The *PIM Join* messages do not need to travel until the RP; it is enough to reach a point where the RP-tree has already been built. (The RP-tree is also called *shared tree* because the multicast traffic from all the sources uses the same tree.) The *PIM Join* messages are resent periodically while there is at least a single member in the group. When the last receiver of a leaf network leaves the group then DR sends a $(*, G)$ *PIM Prune* message towards the RP so as to cut back the tree until the point where there are other active receivers connected.

When an S data source starts sending to a group, the first hop router (DR) of the source encapsulates the data packets of the source into unicast messages called *Register* messages and send them to the RP. The RP router knows from the Register messages that the source is ready to send the stream. The RP decapsulates the Register messages, and forwards the contained streaming data message to the appropriate multicast group (if it has at least a single member) using the RP-tree. The whole process is illustrated in Fig. 1.

Note that the multicasting is fully functional at end of phase one; the following two phases serve efficiency purposes only.

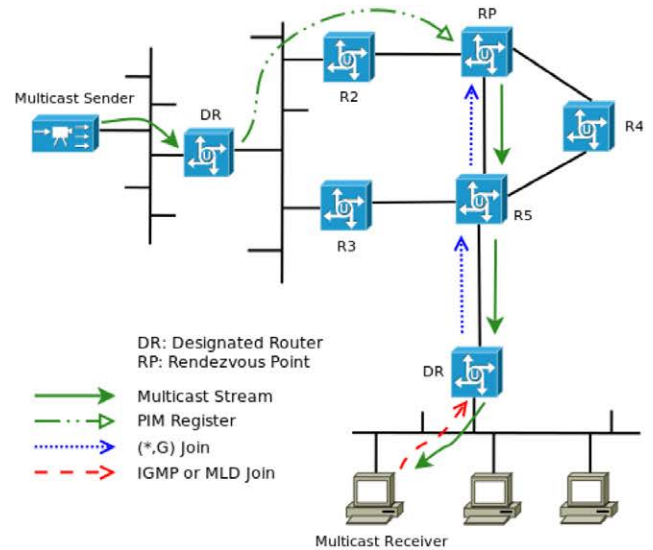


Fig. 1. The Operation of PIM-SM – Phase One

B. Phase Two: Register-Stop

The RP sends an (S, G) Join message to the source. As this message travels to the source, the routers along its path register the (S, G) pair to their MRIB (if they do not have it yet). When this Join message arrives to the subnet of the source (S) or to a router that already has an (S, G) pair registered in its MRIB, then the streaming data start flowing from the S source to the RP by multicast routing. Now, a *source-specific multicast tree* between the S source and the RP was built. After that, the RP sends a *Register-Stop* message to indicate that the first hop router of the source does not need to send Register messages (encapsulating the multicast data packets into unicast messages). Phase two is illustrated in Fig. 2.

C. Phase Three: Shortest-Path Tree

The path of the packets from the source to the receivers through the RP may be not optimal. To eliminate this, the DR of the receiver may initiate the building of a *source*

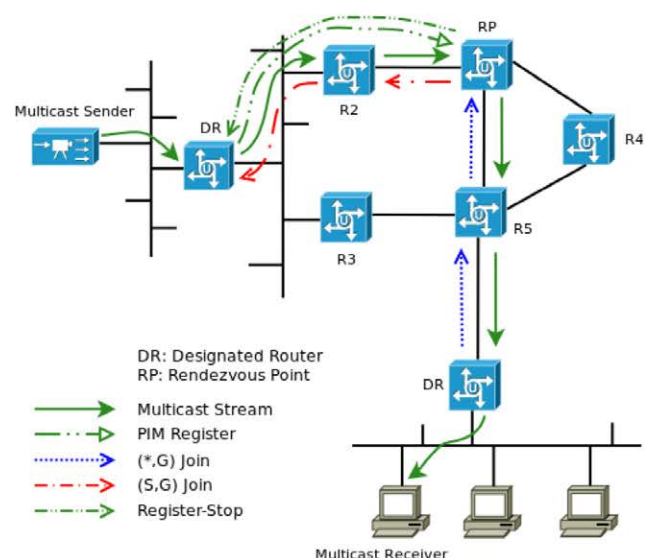


Fig. 2. The Operation of PIM-SM – Phase Two

specific shortest-path tree (SPT) towards the source (in this way possibly leaving out RP from the path). To do this, DR sends an (S, G) Join message to S. When this message arrives to the subnet of S or to a router that already has an (S, G) pair, then the streaming data start flowing from S to the receiver using this new SPT.

Now, the receiver receives all the streaming data packets twice. To eliminate this, the DR of the receiver sends an (S, G) Prune message towards the RP. (This is also known as an (S, G, rpt) Prune.) This message will prune the unnecessary tree parts and the streaming data will not arrive to the receiver through the RP-Tree any more. See Fig. 3.

D. The Built-in Fault Tolerance Mechanism of PIM-SM

It is an important element of the fault tolerance of PIM-SM that the RP does not need to be set up manually, it can be automatically elected from among those PIM-SM routers that were configured Candidate RP (C-RP).

The election uses the bootstrap mechanism described in RFC 5059. The BSR router is elected dynamically from among the PIM-SM routers that were configured Candidate BSR (C-BSR). All the C-BSR routers flood the multicast domain with their Bootstrap messages (BSM). The one with the higher priority wins. During the BSR election all the routers – including C-RP routers – learn the IP address of the BSR. After that, all the C-RP routers send their Candidate-RP-Advertisement (C-RP-Adv) messages to the BSR periodically. (The C-RP-Adv messages are sent in every C_RP_Adv_Period seconds, the default value is 60 seconds.) The BSR collects these messages, builds an RP list and advertises it also periodically for all the routers. The list is encapsulated into a BSM and is sent in every BS_Period seconds. All the routers – including the BSR and the C-RPs – can decide the winner RP¹ by the priority of the C-RPs. If the current RP fails to send its C-RP-Adv message to the BSR within RP Holdtime (a value included in the C-RP-Adv message) then BSR decides that it is dead and starts advertising the new RP list leaving out the dead one.

Notes:

1. RFC 5059 says that the RP candidate routers should set RP Holdtime to a value that is not less than $2.5 * \max\{BS_Period, C_RP_Adv_Period\}$ so that the system is able to tolerate the loss of some Bootstrap messages and/or C-RP-Adv messages.
2. The C-BSR routers also take care if the elected BSR fails, but that is not addressed in this paper.

E. The Choice of the Underlying Unicast Routing Protocol

As PIM-SM is protocol independent, there is a certain freedom in the choice of the underlying unicast routing protocol. The two most widely used protocols are the Routing Information Protocol (RIPv2, RFC 2453) and the Open Shortest Path First (OSPFv2, RFC 2328) for routing within a single autonomous system. Even though RIP is much simpler and more widely used in LANs than OSPF, it is not scalable and therefore it is not appropriate for the size of networks that are often used for providing IPTV services. This is why OSPF was chosen for our test network.

¹There can be different RP-s for different multicast groups; RP-s are advertised together with the group address and netmask.

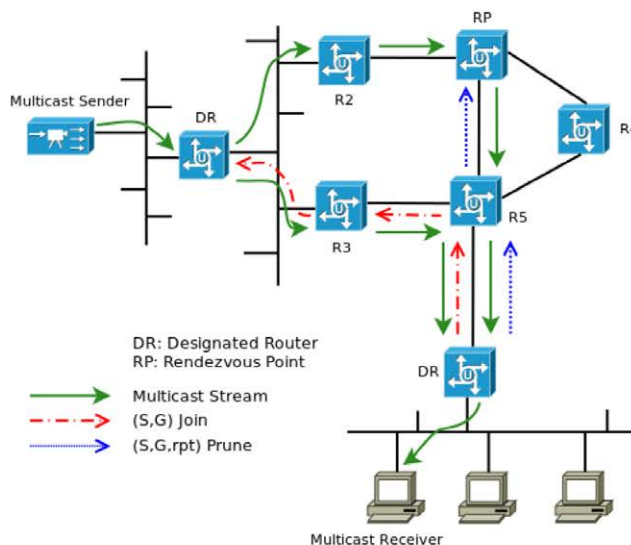


Fig. 3. The Operation of PIM-SM – Phase Three

Note that OSPF also uses a fault tolerance mechanism but it is much simpler than that of PIM-SM. The OSPF routers take care for their neighbours only. All the OSPF routers send Hello messages in every Hello Interval seconds to their neighbours. If they do not see a Hello message from a neighbour within the so called Dead Interval time they consider the given neighbour dead and they calculate new routes leaving out the dead neighbor.

III. IPTV IN A NUTSHELL

Nowadays, several data transmission technologies are available to transmit digital data (that may represent various media types, e.g. video, audio, text, etc. – the standard handles them in a uniform way) over different channels such as DVB-S/S2 via satellite, DVB-T/T2 via terrestrial, DVB-C/C2 via cable TV links and so on. In the TCP/IP based networks, the commonly used solution for delivering the digital video, audio and auxiliary data is based on the DVB-IPTV [10].

A general property of the above mentioned technologies is that they use the same MPEG2 Transport Stream (MPEG2-TS) format to organize the digital data (video, audio, etc) and additional service informations (SI/PSI tables) into a common frame. Basically, two types of MPEG2-TSs are available: the Single Program Transport Stream (SPTS), which includes only one service (e.g. TV program) and the Multiple Program Transport Stream (MPTS).

The MPEG2-TS (SPTS or MPTS) is divided into 188 bytes long packets (4 bytes header and 184 bytes data). In the IPTV environment, usually seven TS packets are embedded into one IP/UDP or IP/UDP/RTP packet and they are sent through the network. Unlike other DVB technologies, IPTV does not use broadcasting to deliver these packets. Instead, it uses IP multicast for the live or online streaming (e.g. live TV) and unicast for the offline services, for example VoD or Timeshift.

When a subscriber would like to watch the selected IPTV program his/her receiver joins to the TV program's preprogrammed IP multicast group. After the join process (a few seconds) the receiver will get continuously the

Investigation of the Fault Tolerance of the PIM-SM IP Multicast Routing Protocol for IPTV Purposes

MPEG2-SPTS packets of the TV program through the IP multicast enabled network. If the subscriber switches over to another IPTV program then the receiver will leave the current one and join to the next IP multicast group.

IV. TEST ENVIRONMENT

In order to have a test network of reasonable size, a virtualization environment was used. The virtualization software was VmWare ESXi running on an IBM eServer BladeCenter LS20 using 5 blades having each 4GB RAM and two dual core AMD Opteron CPUs running at 2.2 GHz. The storage was mounted through NFS using Gigabit Ethernet network connection.

The topology of the test network was a mesh. It is not a typical topology for the commercial IPTV networks, but it was considered suitable for our experiments because it contains several redundant paths with equal costs. The mesh network contained 4 times 4 virtual routers interconnected by Layer 2 virtual switches. The virtual routers were built of virtual computers (1 virtual CPU, 512MB RAM, 10GB HDD) running Ubuntu 10.04 LTS operating system. The well known and widely used XORP [11] routing platform was chosen to implement both OSPF and PIM-SM for unicast and multicast routing, respectively. Two further virtual computers with the same configuration and operating system were added to the mesh network for the purposes of media streaming server and playing client. The VLC software of VideoLAN was used for both server and client purposes.

Note that our test system contained altogether 18 virtual computers and two Layer 2 virtual switches powered by 20 (5 times 4) CPU cores, thus each logical device had its own physical CPU and enough memory. Except for the moderate computing requirement of media streaming, all the other nodes had low computing requirements. In this way, it was ensured that the application of virtualization would not garble our results.

A. IP Configuration

Private IP addresses were used from the 192.168.0.0/16 network. The IP addresses of the virtual computers were configured manually as shown in Fig. 4. The network segments between two routers displayed by horizontal and vertical lines got IP addresses from 192.168.{1-12}.0/24 and 192.168.{13-24}.0/24 networks respectively. The last octets of the IP addresses of the interfaces are written next to the interfaces. The IP addresses of the network segments connecting the server and the client virtual computers are displayed in a similar manner.

B. OSPF Configuration

Because of the nature of the mesh, the OSPF protocol could be configured by the definition of peer-to-peer connections (it can be done if the neighbouring routers are interconnected by point-to-point links). A typical configuration fragment for an interface looks like follows:

```
ospf4 {
  router-id: 192.168.1.1
  area 1.1.1.1 {
    area-type: "normal"
    interface eth0 {
      link-type: "p2p"
      vif eth0 {
        address 192.168.1.1 {
          interface-cost: 1
          neighbor 192.168.1.2 {
            router-id: 192.168.1.2
          }
        }
      }
    }
  }
  ...
}
```

Configuring OSPF in this way made the network fully connected: unicast IP packets can be sent from anywhere to anywhere. Note that PIM-SM uses the unicast routing table (RIB) when building its own multicast routing table (MRIB).

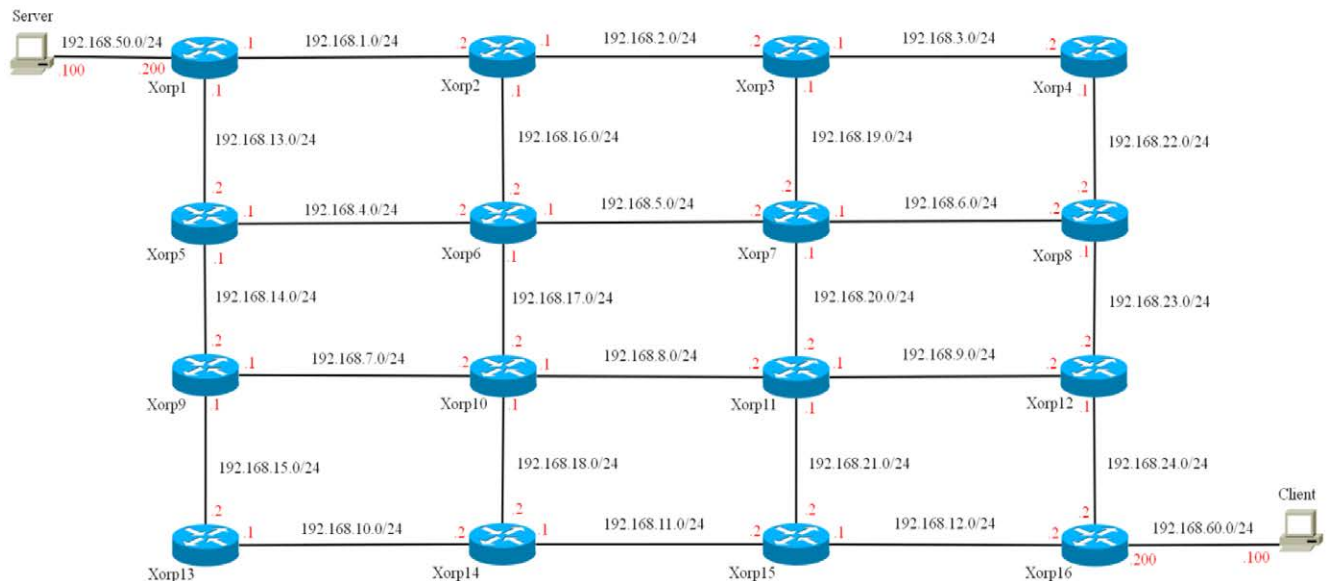


Fig. 4. Topology of the Test Network

C. PIM-SM Configuration

For PIM-SM, those and only those interfaces should be configured where PIM-SM has to handle multicast traffic. A typical configuration for an interface looks like follows:

```
pimsm4 {
  disable: false
  interface eth0 {
    vif eth0 {
      disable: false
      dr-priority: 101
      hello-period: 30
      hello-triggered-delay: 5
    }
  }
}
...

```

In order to be able to experiment with the fault tolerance of PIM-SM, the dynamic election of the RP was used. This required us to configure some routers as C-RP and at least one router as C-BSR. Routers **xorp2**, **xorp4** and **xorp14** were configured as both C-RP and C-BSR but with different priorities². The **xorp2** router was the highest priority C-RP, the **xorp4** was the second highest priority one; **xorp14** was the highest priority C-BSR. A typical configuration for a router that was set as both C-RP and C-BSR looks like follows:

```
bootstrap {
  disable: false
  cand-bsr {
    scope-zone 224.0.0.0/4 {
      cand-bsr-by-vif-name: "eth0"
      bsr-priority: 102
    }
  }
  cand-rp {
    group-prefix 224.0.0.0/4 {
      cand-rp-by-vif-name: "eth0"
      rp-priority: 102
    }
  }
}

```

Considering the fact that in phase three there is no need for the RP, but a source-specific shortest path tree (SPT) is used for the transmission of the stream (that may not contain RP, or even if it contains RP then RP acts like a simple multicast router only), PIM-SM was configured so that it would never enter phase three. (The XORP implementation of PIM-SM gives three possible parameters for the control of switching to SPT, the simplest way is just to disable it.)

```
switch-to-spt-threshold {
  disable: true
  interval: 100
  bytes: 1024000
}

```

D. Time Synchronization

The important events of the measurements were logged into text files. In order to be able to compare the timestamps of the events occurred on different virtual computers, the system times of the other virtual computers were synchronized to **xorp1** using the standard NTP protocol.

²As it is commonly used in Unix like systems, the lower numeric value means higher priority.

E. Streaming

A single program transport stream (SPTS) – that was demodulated and demultiplexed from a Hungarian DVB-T multiplex – was pre-recorded and used for all the measurements. The VLC server sent the stream to the 230.1.1.1 multicast IP group address using UDP. The VLC client received the stream and the standard **tcpdump** program was used to monitor (capture and record for offline analysis) the stream on the receiver side.

V. EXPERIMENTS AND RESULTS

A. Testing the Failure of the RP

Hypothesis 1: Killing the RP on **xorp2** router will stop the stream for a while, but the stream will be restored when a new RP is elected. The length of the service outage time likely depends on how much time elapsed from the last Candidate-RP-Advertisement (C-RP-Adv) message when the RP is killed.

The measurements were controlled by a script executed on **xorp2** router. This script did the following: after starting XORP and the streaming, it made sure that **xorp2** is the actual RP. Then it waited until XORP sent a C-RP-Adv message. From that time it waited until a *predefined delay* (it was a parameter, see later). After that it started the **measure.sh** scripts both on the DR of the server and on the DR of the client (these scripts recorded the IP address of the actual RP in every second) and sent a marker (ICMP echo request) to the client and killed the RP.

The *predefined delay* was increased from 5 seconds to 55 seconds in 5 seconds steps. (As C-RP-Adv is sent in every 60 seconds by the defaults settings of XORP, there would be no point in increasing the delay above 55 seconds.) The whole measurement was executed 11 times.

The results of the measurements can be found in Fig. 5. Here, and also in all the following figures the standard deviation is displayed by a vertical section: the Y coordinates of the two ends of the section are set as:

$$(average - std. dev, average + std. dev.)$$

The service outage time values justify hypothesis 1: even though they show large fluctuations, there is a visible tendency that a larger delay from the last C-RP-Adv usually results in shorter service outage time.

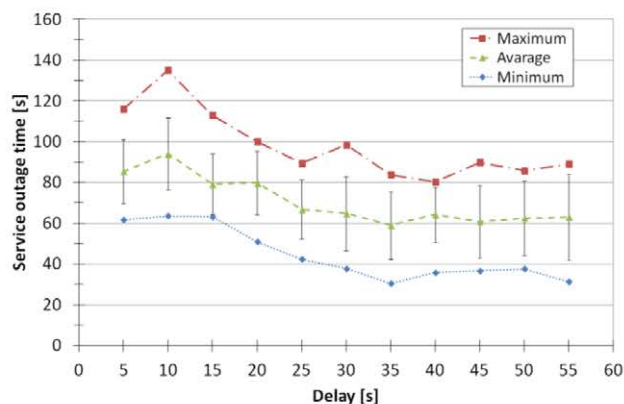


Fig. 5. Service Outage Times in the Function of the Delay from the Last C-RP-Adv Message to the Stopping of the RP on **xorp2** Router

Investigation of the Fault Tolerance of the PIM-SM IP Multicast Routing Protocol for IPTV Purposes

B. Testing the Failure of the Complete PIM-SM router

Hypothesis 2: Switching off the operation of the complete XORP on **xorp2** router will stop the stream for a while, but the stream will be restored when the underlying unicast routing (OSPF) finds new route (that does not contain **xorp2** router) from the DR of the server to the DR of the client.

This process will result in shorter service outage time as the default timeout values of OSPF are shorter than that ones of PIM-SM. We also expect that the length of the outage time will show no correlation with the time elapsed from the last C-RP-Adv message when the RP is killed.

The measurements were taken in a similar way than before. The results can be found in Fig 6. They justify hypothesis 2: the service outage times are much shorter and

they show no correlation with the time elapsed from the last C-RP-Adv message. Both prove that *no new RP is necessary for the restoration of the stream.*

Hypothesis 3: The length of service outage time caused by the switching off the operation of the complete XORP on **xorp2** router depends on the time elapsed from the last Hello message of the OSPF protocol.

The default values of the OSPF *Hello Interval* and *Dead Interval* are 10 seconds and 40 seconds respectively. For testing purposes, the first one was raised to 35 seconds and similar series of the measurements were performed in the way that the delay from the last OSPF *Hello message* before the stopping of XORP was increased from 5 seconds to 30 seconds in 5 seconds steps. The results can be found in Fig. 7. They justify hypothesis 3: the average service outage times are very close to the time that was left from the *Dead Interval* of OSPF at the time of stopping XORP. (The stream was restored because OSPF calculated a new route that did not contain the **xorp2** router.)

C. Limiting the service outage time by parameter tuning

As we have shown in section B, if the service outage was caused by the complete failure of a multicast routing node³ which is an element of the path from the DR of the server to the DR of the client then the service outage time was determined by the parameters of the underlying unicast routing protocol. In our experiments, the service outage time was upper bounded by the *Dead Interval* of OSPF. The actual value of the service outage time depended on the elapsed time from the last OSPF *Hello message* at the time of the failure of XORP.

Hypothesis 4: The service outage time caused by the complete failure of a XORP router can be limited by an appropriate setting of the OSPF *Dead Interval* parameter.

The measurements were taken in the usual way but using 20 seconds and 15 seconds as OSPF *Dead Interval* and *Hello Interval*, respectively. The values of delay from the last OSPF *Hello message* to the failure the XORP were 5 and 10 seconds. The results can be found in Table 1. They justify hypothesis 4.

The significance of the findings of hypotheses 4 is that the time of the service outage caused by the complete failure

³It can be the RP, but it is not necessarily the RP.

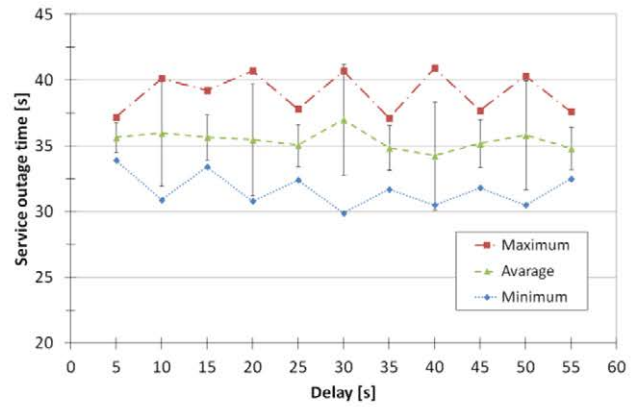


Fig. 6. Service Outage Times in the Function of the Delay from the Last C-RP-Adv Message to the Stopping of XORP on xorp2 Router

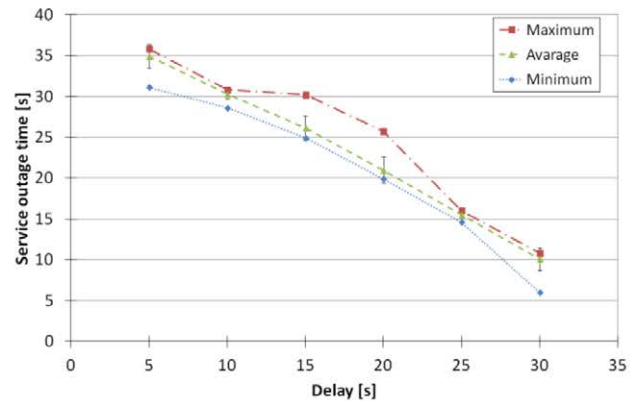


Fig. 7. Service Outage Times in the Function of the Delay from the Last OSPF Hello Message to the Stopping of XORP on xorp2 Router

TABLE 1. SERVICE OUTAGE TIMES IN THE FUNCTION OF THE DELAY FROM THE LAST OSPF HELLO MESSAGE TO THE STOPPING OF XORP ON XORP2 ROUTER USING 20 SECONDS OSPF DEAD INTERVAL

Delay [s]	Service outage time [s]			
	min	max	average	std. dev.
5	14,8	15,8	15,45	0,39
10	9,8	10,8	10,45	0,38

of a multicast node can be limited by the appropriate choice of the *Dead Interval* parameter of OSPF. Note that the service outage time cannot be arbitrarily decreased in this way for at least two reasons:

1. The choice of the *Dead Interval* parameter of OSPF has a consequence on the frequency of the OSPF Hello messages. This frequency should not be too high as these messages consume both network and router capacity.
2. The exchange of the topology information and the recreation of the routing tables in OSPF require a certain amount of time. Though this time was negligible in our experiments due to the small size of our test network, the situation can be different in the case of a real life multicast network for IPTV.

Finding a similar way of limiting the service outage time caused by the failure of the RP only would be a natural idea, however it is much more difficult.

Hypothesis 5: The service outage time caused by the failure of the RP only (but XORP remained working) can not be efficiently limited by the choice of the PIM-SM *RP Holdtime* parameter.

In the fifth series of measurement, the value of the PIM-SM *RP Holdtime* parameter was changed from its default value of 150 seconds to 75 seconds. As the XORP platform does not provide a method for modifying the value of *C_RP_Adv_Period*, its value was left 60 seconds. Note that these settings do not comply with RFC 5059 (see Note 1. in section II.D. of this paper), but in our small test network the loss of *C_RP_Adv* or BSM messages is not a serious issue.

The results of the measurements can be found in Fig. 8. They justify hypothesis 5: the service outage time values are not significantly smaller than in Fig. 5 and the results show similar fluctuations as they did it in Fig. 5.

The reason of this behaviour and especially of the fluctuations can be found in the operation of the fault tolerance mechanism of PIM-SM. Two independent and unsynchronised timers are used for measuring *C_RP_Adv_Period* and *BS_Period* in the C-RP routers and in the Bootstrap router, respectively. If the killing of the RP is synchronized to one of them, the unpredictable value of the other one causes “random” fluctuations in the service outage time.

Hypothesis 6: Repeating the first series of measurements of killing the RP on *xorp2* router but measuring the delay from the last BSM message received (instead of from the last C-RP-Adv message) when the RP is killed will produce similar results that is the longer delays result in shortest service outage time – at least in tendency –, but there will be similar fluctuations.

The results in Fig. 9 justify hypothesis 6: the average service outage times show a decreasing tendency in the function of the delay from the last BSM, but they are not monotonous and the measured values show similar fluctuations as it could be seen in Fig. 5.

The findings of hypotheses 5 and 6 deserve some discussion. These results do not give us a straight forward way of limiting the service outage time in the case if the RP fails. However they give us an important lesson: it is worth entering the third phase of PIM-SM not only for efficiency reasons (that is using SPT for faster delivery) but also for achieving shorter service outage time in case of the failure of a multicast router due to the faster recovery of OSPF (see hypotheses 3 and 4).

Note that even though the failure of the RP could be easily simulated for experimenting purposes using the *xorpsh* interface of the XORP routing platform; in practice, the complete failure of a router is much more typical than the failure of its RP functionality only.

VI. TOWARDS A FORMAL MODEL FOR THE SERVICE OUTAGE TIME

As the simulation of large and complex systems may require a huge amount of memory and processing power, the

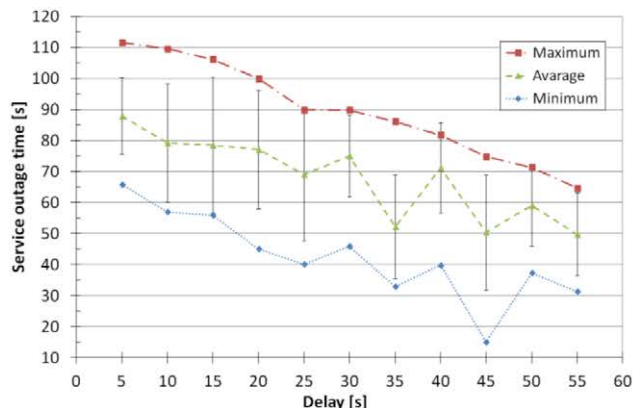


Fig. 8. Service Outage Times in the Function of the Delay from the Last C-RP-Adv Message to the Stopping of the RP on *xorp2* Router using 75 Seconds PIM-SM *RP Holdtime*

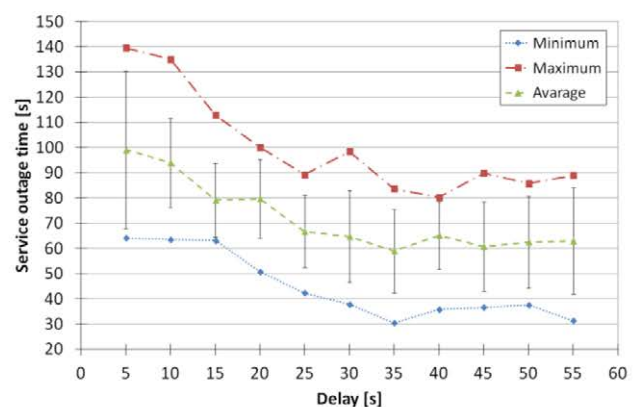


Fig. 9. Service Outage Times in the Function of the Delay from the Time of the Last BSM Received to the Stopping of the RP on *xorp2* Router

models used for simulation should contain only the details that are relevant for the purposes of the simulation [12].

For example, when the focus is placed on certain networking applications, the detailed behaviour of the lower layer components of the network (e.g. the 1-persistent CSMA/CD protocol played by Ethernet NICs at MAC layer) are usually omitted or if they have an important influence on the communication they are modelled by a much simpler phenomenon (e.g. the packet loss due to collisions is modelled by random drop of packets with a fixed or traffic volume dependent packet loss ratio).

The service outage time caused by the complete failure of a XORP router can be modelled as follows:

$$t_{SO} = ODI - DLH + t_{D\&R}$$

Where t_{SO} , ODI , DLH and $t_{D\&R}$ denote the time of service outage, the length of OSPF *Dead Interval*, the delay from the last OSPF *Hello* message at the time of the failure of the XORP router and the time OSPF uses for the distribution of topology information and for the recalculation of the routes, respectively. Note that $t_{D\&R}$ is not negligible in general, as it depends from the size of the network. In a practical simulation model for a given fix size of network, $t_{D\&R}$ can be approximated by a constant.

As for the two other values, ODI is a constant parameter of OSPF, and DLH can be modelled by random variable that

Investigation of the Fault Tolerance of the PIM-SM IP Multicast Routing Protocol for IPTV Purposes

takes its values from $[0, \text{OSPF Hello Interval}]$ according to uniform distribution.

The service outage time caused by the failure of the RP only could be formally modelled as follows:

$$t_{SO} = PRH - f_1(DLC) - f_2(DLB) + t_{NRP}$$

Where t_{SO} , PRH, DLC, DLB and t_{NRP} denote the time of service outage, PIM-SM *RP Holdtime*, the delay from the last PIM-SM C-RP-Adv message of the RP at the time of the failure of the RP, the delay from the last PIM-SM BSM received at the time of the failure of the RP and the time necessary for the designated router of the source and of the server for switching over to the new RP, respectively. The $f_1(\cdot)$ and $f_2(\cdot)$ functions are necessary because in spite of the fluctuations it can be clearly seen in Fig. 5 and Fig. 10 that the service outage time was decreased by less than the value of DLC and DLB. They could be estimated, however because of the before mentioned rare nature of the failure of the RP only the estimation probably does not worth the effort.

VII. DIRECTIONS OF FUTURE RESEARCH

The formal model for the service outage time presented above should be validated. This is planned to be done among the next year PhD research tasks of the second author of this paper.

VIII. CONCLUSIONS

The operation and the fault tolerance mechanism of PIM-SM were introduced. A mesh topology test network of virtual computers running the XORP router software was built. In different series of experiments, the service outage time of an IPTV system was measured in the function of different parameters of PIM-SM and OSPF in the second phase of the PIM-SM protocol.

It was shown that in case of the complete failure of the RP or any router in the path of the multicast stream from the DR of the server to the DR of the client the service outage time depends on the OSPF Dead Interval parameter and the delay elapsed from the last OSPF Hello message at the time of the failure. A formal model was also given for the service outage time. It was also shown that in the much less common case of the failure of the RP functionality only (not the failure of the complete router that serves actually as the RP) the service outage time depends on a number of different factors and it cannot be easily limited by parameter tuning due to the unpredictable conditions of two unsynchronised timers. A formal model was also given for the service outage time in this case.

We conclude that it is worth switching to the third phase of PIM-SM for fault tolerance considerations, because in that phase the service outage time is shorter, predictable and can be limited by the appropriate selection of the Dead Interval parameter of OSPF.

IX. REFERENCES

[1] International Television Expert Group, "Global IPTV market (2009-2013)" http://www.international-television.org/tv_market_data/global-iptv-forecast-2009-2013.html

[2] G. Lencse and B. Steierlein, "Quality of service and quality of experience measurements on IP multicast based IPTV systems", *Acta Technica Jaurinensis*, Vol. 5, No. 1, pp. 55-66. 2012.

[3] A. J. Ballardie, P. F. Francis, and J. Crowcroft, "Core Based Trees", *ACM SIGCOMM Computer Communication Review* Vol. 23, No. 4, pp. 85-95. August 1993. DOI:10.1145/167954.166246.

[4] S. Deering, D. Estrin, D. Farinacci, V. Jacobson, C. Liu, L. Wei, "The PIM architecture for wide-area multicast routing", *IEEE/ACM Transactions on Networking*, Vol. 4, No. 2, pp. 153-162. April 1996. DOI:10.1.1.39.7251

[5] Weijia Jia, Wei Zhao, Dong Xuan, Gaochao Xu: "An efficient fault-tolerant multicast routing protocol with core-based tree techniques", *IEEE Transactions on Parallel and Distributed Systems*, Vol. 10, No. 10, pp. 984-1000. 1999. DOI:10.1.1.74.157

[6] M. Sola, M. Ohta and T. Maeno: "Scalability of internet multicast protocols", in: *Proc. of INET'98*, Geneva, Switzerland, July 1998.

[7] Silvano Da Ros, *Content Networking Fundamentals*, Cisco Press, 2006, ISBN: 1-58705-240-7

[8] L. Muka and G. Muka, "Creating and using key network-performance indicators to support the design and change of enterprise infocommunication infrastructure", in: *Proc. of 2012 International Symposium on Performance Evaluation of Computer and Telecommunication Systems (SPECTS 2012)*, Genoa, Italy, July 8-11, 2012, Volume 44, Books 12, ISBN: 978-1-61839-982-3, pp. 737-742.

[9] Beau Williamson, *Developing IP multicast networks*, Volume 1, Cisco Press, 2000, Indianapolis, IN, USA. ISBN: 1-57870-077-9

[10] Digital Video Broadcasting (DVB); Transport of MPEG-2 TS Based DVB Services over IP Based Networks, ETSI TS 102 034 V1.4.1 (2009-08)

[11] XORP Inc. and individual contributors, XORP user manual, Version 1.8-CT, 2010.

[12] G. Lencse and L. Muka, "Managing the resolution of simulation models", in: *Proc. of the 2008 European Simulation and Modelling Conference (ESM'2008)*, Le Havre, France, Oct. 27-29, 2008, EUROSIS-ETI, ISBN: 978-90-77381-44-1, pp. 38-42.



Gábor Lencse received his MSc in electrical engineering and computer systems at the Technical University of Budapest in 1994, and his PhD in 2001. He has been working for the Department of Telecommunications, Széchenyi István University in Győr since 1997. He teaches Computer networks, Computer architectures, IP based telecommunication systems and the Linux operating system. Now, he is an Associate Professor. He is responsible for the specialization of the information and communication technology of the BSc level electrical engineering education. He is a founding member of the Multidisciplinary Doctoral School of Engineering Sciences, Széchenyi István University. The area of his research includes discrete-event simulation methodology and performance analysis of computer networks. Dr. Lencse has been working part time for the Department of Telecommunications, Budapest University of Technology and Economics (the former Technical University of Budapest) since 2005. There he teaches Computer architectures and Media communication networks.



István Derka received his Msc at Faculty of Electrical Engineering and Informatics at the Technical University of Budapest in 1995. He worked for the Department of Informatics from 1999 to 2003 and since then has been working for Department of Telecommunications, Széchenyi István University in Győr. He teaches Programming of communication systems and Interactive TV systems. He is an Assistant Professor. The area of his research includes multicast routing protocols and IPTV services in large scale networks.

Software package for analyze FSO links

M. Tatarko, L. Ovseník and J. Turán

Abstract—This paper describes a software package called FSO System Simulator (FSO SystSim), which was designed and implemented at KEMT FEI TUKE (Department of Electronic and Multimedia Communications, Faculty of Electronics and Informatics, Technical University of Košice). Simulation of FSO communication link is very important in designing and understanding the context of such connection depending on various parameters (technically and continually changing atmospheric parameters of the transmission optical channel). FSO System Simulator consists of two basic parts. First part is about Steady model and second part is about Statistical model. Paper briefly describes these models, which are used in programming package and describes experiments carried out by the FSO SystSim.

Index Terms—FSO simulator, modeling, software package

I. INTRODUCTION

THE free space optical (FSO) systems operate in varying conditions, which parameters cannot be exactly estimated due to changing weather. It is necessary to know the behavior of the FSO transmission lines in all conditions and be able to choose suitable parameters for transmission. It is not the same if the transmission distance is several hundred meters, or several hundred kilometers. Behavior of FSO transmission line in certain areas, where we know the statistical parameters of the atmospheric transmission environment (ATE) for a sufficient long period, describes the so-called statistical model of FSO. Distance, with which will operate optical transmission system, regards to parameters of receivers and transmitters, such as transmitting power, receiver sensitivity, the diameters of transmitting and receiving lenses, laser beam directionality and also distance between the transmitter and receiver is described by steady model of FSO [1,2,6].

There are many types of program packages, which simulate atmospheric conditions and behavior of transmitted optical beams through the atmosphere e.g. LOWTRAN 7, FASCOD, OptiSIM and other. These programs are comprehensive, extensive, expensive but not good for students to understand basic relations and properties. Computer

program “FSO System Simulator” was created for study purposes. It contains all the elements and equipments of FSO link. Program is using the input parameters of technical facilities and distance conditions and transmission channel conditions, which calculate the availability of transmission channel, and unavailability of FSO lines in a given environment. Operate this program is simple, intuitive and program is free because it was developed at the Technical University in Košice. It is a good way how to obtain basic knowledge about effects of environment on the FSO.

Before the implementation of effective FSO communication links we need to know their availability and their reliability. Availability and reliability of FSO communication link depends on used systems, but also on atmospheric parameters such as rain, snow or fog [2,8,9]. This is the purpose of our study. Its output is a software FSO SystSim with input parameters (distance, Tx power, Rx sensitivity, Rx lens diameter, directivity of laser, weather conditions etc.), which allow to determine the availability of a communication link. Detailed description of the program is shown in the following sections of this article.

II. SOFTWARE PACKAGE FOR THE STEADY SIMULATION OF FSO LINK

From the input technical parameters of devices, distance and conditions of transmission channel, this program calculates availability or unavailability of communication links in a given environment. The program was created in a development environment Microsoft Visual C# 2008 Express Editions [11].

After opening the software package FSO System Simulator, we can see an initial window (Fig. 1).

The whole program consists of three basic parts – Steady and two Statistics (statistical) models. Switching between these models is done by switching the tabs in Windows applications (Fig. 1). This figure shows the steady model.

Window of steady model consists of two parts. On the left side there are options for filling the input data. The right side displays the calculated results. Following figure gives graphical representation of the entered and calculated parameters.

In the program section *Device Properties* the parameters of receiver and transmitter of system are entered manually or there is a possibility to choose systems parameters from the database.

Submitted Aug. 10, 2012, revised Jan. 14, 2013

F. M. Tatarko, Technical University in Košice, Department of Electronics and Multimedia Communications, Košice, Slovakia (phone: 055 602 4277; e-mail: matus.tatarko@tuke.sk).

S. L. Ovseník, Technical University in Košice, Department of Electronics and Multimedia Communications, Košice, Slovakia (phone: 055 602 4336; e-mail: lubos.ovsenik@tuke.sk).

T. J. Turán Technical University in Košice, Department of Electronics and Multimedia Communications, Košice, Slovakia (phone: 055 602 2943; e-mail: jan.turan@tuke.sk).

Software Package for Analyze FSO Links

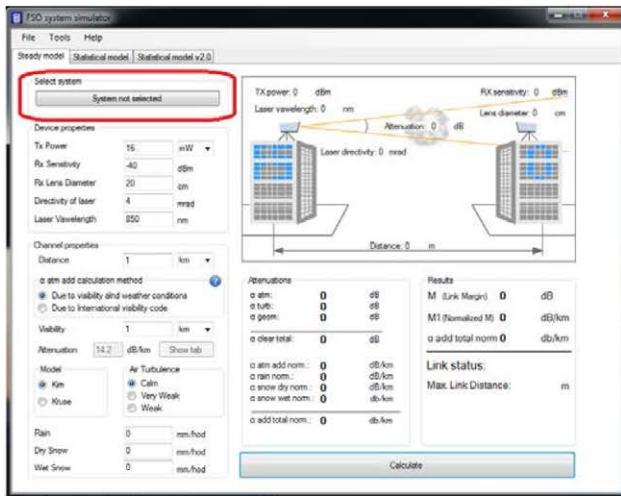


Fig. 1. Card of the Steady model.

Different parameters of *Device properties* are discussed below:

TX Power - is the mean of laser power generates by transmitter. It can be entered in mW or dBm.

RX Sensitivity - is the sensitivity of receiver equipment (values from -10 to 70 dBm).

RX Lens Diameter - is the diameter of the receiver lens (values from 1 to 100 cm).

Directivity of laser - is the laser beam directivity (values from 1 to 60 mrad).

Laser Wavelength - is parameter of system wavelength (values from 500 to 1600 nm) [3].

As was noted, each parameter has a limit for entering values. If you enter a value that exceeds the allowed range, the error message is displayed. You have to change the given value and enter new value, which will be in the desired range.

A. Description of system database

A new field was added to the original program and it was called *Selected system* (Fig. 1). This field contains a button that displays the name of the selected system. If there isn't any selected system, the field contains an inscription *System not selected*. When you click (in this case *System not selected*) on this field, it shows us the database of producers (Fig. 2).

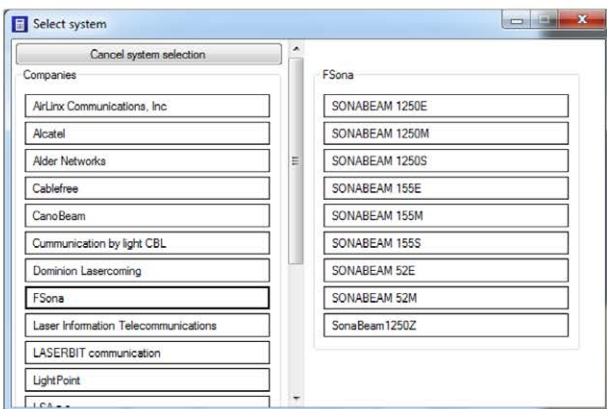


Fig. 2. Database of producers.

From Fig. 2 we can see that the database of systems consists of two parts. On the left side there is a button to deselect the option and a register of producers. The right side contains the database of the systems of producers. If any producer is selected, field *System of companies selected* displayed *Company not selected*. After selecting a certain producer it will show an overview of products, as is illustrated in Fig.2. When the system is chosen, parameters are copied into above-mentioned field *Device properties*.

To make the selection of systems easier, there is a possibility to display various parameters in the form of help. It allows us to choose a system based on the displayed parameters. The window help appears, when you let the cursor stands for a moment in any part of scheme. The window help contains the information about the system that we need for computing (Fig. 3).

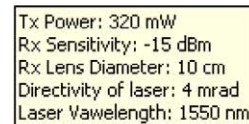


Fig. 3. Detail information about selected system.

After selecting and subsequently clicking on a system button, window for selecting of system will disappear and parameters of selected system can be seen in the *Device properties* and also name of system can be seen in the field *Select system* (Fig. 4).

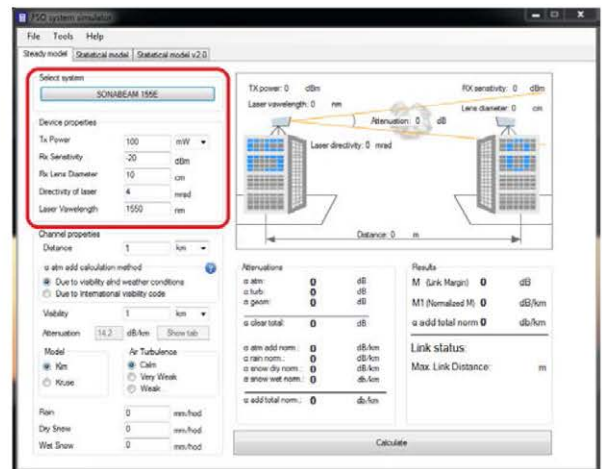


Fig. 4. Selected parameters from database.

After setting the properties of the channel, it is necessary to press a button *Calculate*. On the basis of the parameters of the system and properties of the transmission channel, the program will calculate availability of connection. Database of FSO systems in this program is suitably designed to allow easy addition of other producers and their systems. Whole database is located in the folder *Systems*. When we enter to this folder, database of all producers are displayed there (Fig. 5).

New systems are added to individual folders of producers in the form of .txt files with specific parameters. So if we create a new producer by creating new folder with the producer's

name and we want to specify the particular system, we will come into this folder and create .txt file as is shown on Fig. 6.

On Fig. 6 we can see nine .txt files of 9 specified systems from FSONA Company. Parameters and names of individual systems are added to this .txt files as can be seen from Fig. 7 in the following order: name of system, transmitted power and its unit, receiver sensitivity, receiver lens diameter, directionality of laser and laser wavelength.

After filling these parameters into .txt files the database is ready for further input, for example for adding new producers or for changing existing systems parameters, etc.

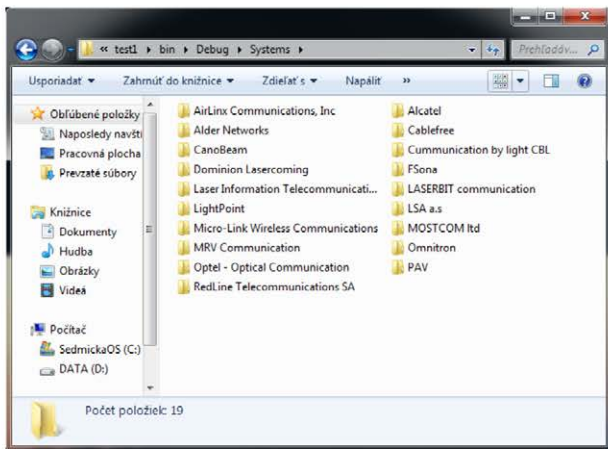


Fig. 5. Entering manufacturers.

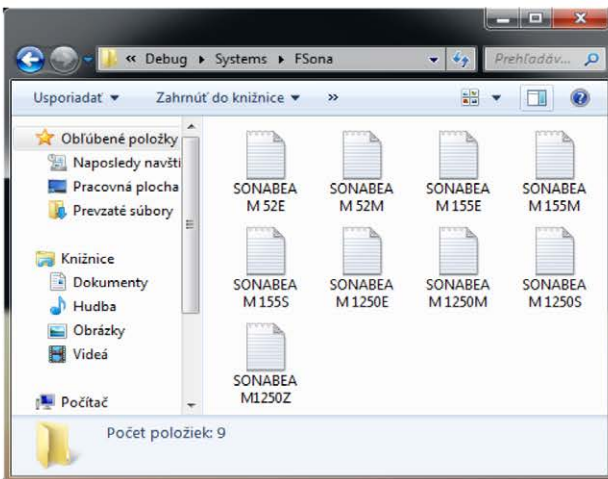
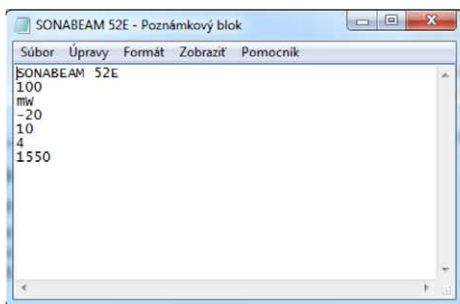


Fig. 6. Entering systems of the manufacturers.



III. EXPERIMENTS WITH THE STEADY MODEL

Different systems from database can be compared with each other under various weather conditions or we can only verify information provided by producers about their transmission properties.

In the steady model of simulator, you can set weather conditions in part *Channel properties*. The Fig. 8 shows a possibility how to set various weather conditions and how to add the item *α atm add calculation method*. If you choose the option *Due to visibility and weather condition* you can simulate different decreases of signal caused by rain or snow. You can also simulate turbulence by the selection of Kim or Kruse model [15].

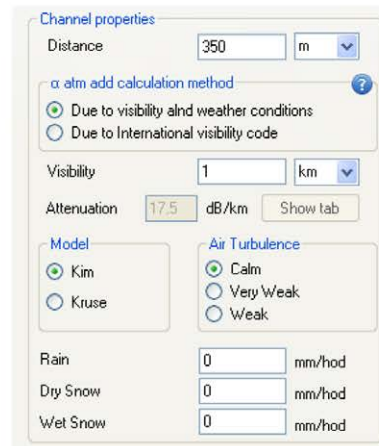


Fig. 8. Entering the atmospheric conditions and visibility due to weather conditions.

If you choose the option *Due to International visibility code* (Fig. 9) you can enter required attenuation to the field *Attenuation* or you can select the option *show table*. After selection this option a table will be subsequently displayed and we can determine the specific attenuation [dB/km] (Fig. 10). Other fields, except turbulence are hidden. It means that the final attenuation is entered directly to the field *attenuation*.

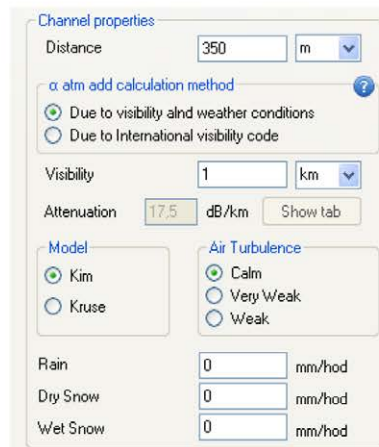


Fig. 9. Entering the atmospheric conditions for Due to visibility and weather conditions.

Weather conditions	Precipitation		Visibility	Attenuation (dB/km) at $\lambda = 785\text{nm}$
		mm/hod		
Dense fog			0 m	350
Thick fog			50 m	339,6
Moderate fog			200 m	84,9
Light fog			500 m	34,0
Very light fog	Storm	100	770 m	20,0
			1 km	14,2
Light mist	Strong rain	25	1,9 km	7,1
			2 km	6,7
Very light mist	Average rain	12,5	2,8 km	4,6
			4 km	3,0
Clear air	Light rain	2,5	5,9 km	1,8
			10 km	1,1
Very clear air	Drizzle	0,25	18,1 km	0,6
			20 km	0,53
			23 km	0,46
			50 km	0,21

Fig. 10. Table attenuation of weather conditions.

For testing the reported parameters we have chosen *Due to International visibility code* method. In this method we can exactly specify the required attenuation that is intended by producer. For this test we have chosen MRV Company and their products TereScope 5000 and TereScope 10GE. The producer indicates the availability of links for different attenuation as we can see in TABLE I.

TABLE I
TABLE OF DISTANCES PROVIDED BY THE MANUFACTURERS

Attenuation	Terescope 5000 Distance (m)	Terescope 10GE Distance (m)
3 dB/ km	5500 m	1000 m
10 dB/ km	2700 m	600 m
30 dB/ km	1200 m	300 m

Other calculation for systems Terescope 5000 and Terescope 10GE are shown in TABLE II.

TABLE II
TABLE OF RESULTS FROM THE FSO SIMULATOR

Attenuation	Terescope 5000 Distance (m)	Terescope 10GE Distance (m)
3 dB/ km	7214 m	2313 m
10 dB/ km	3154 m	1274 m
30 dB/ km	1339 m	637 m

By the comparison of TABLE I and TABLE II we can see, that calculated values are mainly different in system Terescope 10GE, where distances are twice bigger than producer offers. The system Terescope 5000 does not show so big deviations. For the attenuations 10 and 30 dB/km the deviations are 300 m and for the pure atmosphere it is around 1700 m. From the calculations we can say, that the system Terescope 10GE responds better to increase of turbulence than system Terescope 5000 because the increase of turbulence reach caused the decline only a few hundred meters.

A. Comparison of different systems among themselves

Comparison of different systems allows us to understand how deep influence has selected atmospheric conditions to the systems. According to calculations we can determine which product is suitable for the environment and which is not.

For comparison we choose these systems: CableFree Access A1000, Sonabeam 52E and PAV Light Gigabit. We set the same atmospheric conditions for all products, Kim’s model for turbulence *Calm* and visibility 1 km. Distance between transmitter and receiver to 1 km too. Results are shown in Fig. 12., Fig. 13. and Fig. 14.

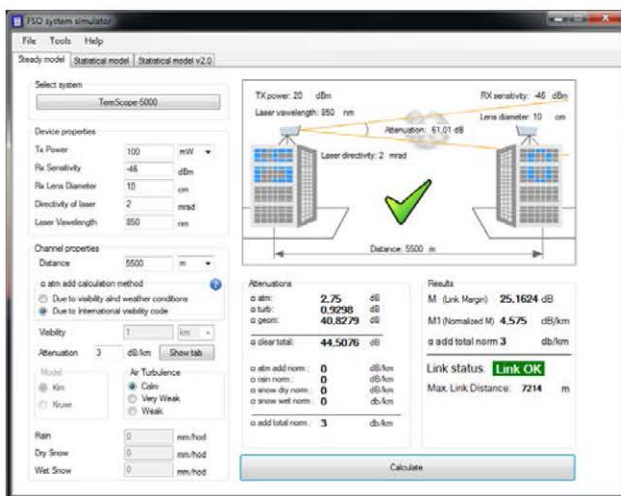


Fig. 11. Output of Steady model.

After selection the system Terescope 5000 and setting the attenuation to 3 dB/ km, which represents the clear atmosphere, simulator calculates the maximum reach of communication link to 7214 m for low turbulence (Fig. 11). With increased turbulence, reach of FSO link is falling down. With *Very Weak* turbulence, reach falls to 6380 m and with *Weak* turbulence reach falls even to 2600 m.

Attenuations		Results	
α atm:	0,5 dB	M (Link Margin)	25,9651 dB
α turb:	0,1843 dB	M1 (Normalized M)	25,9651 dB/km
α geom:	26,0206 dB	α add total norm	13,8212 dB/km
α clear total:	26,7049 dB	Link status:	Link OK
α atm add norm.:	13,8212 dB/km	Max. Link Distance:	1567 m
α rain norm.:	0 dB/km		
α snow dry norm.:	0 dB/km		
α snow wet norm.:	0 dB/km		
α add total norm.:	13,8212 dB/km		

Fig. 12. Output of steady model for PAV Light Gigabit.

Attenuations		Results	
α atm:	0,5 dB	M (Link Margin)	11,0035 dB
α turb:	0,1253 dB	M1 (Normalized M)	11,0035 dB/km
α geom:	32,0412 dB	α add total norm	10,3256 dB/km
α clear total:	32,6665 dB	Link status:	Link OK
α atm add norm.:	10,3256 dB/km	Max. Link Distance:	1034 m
α rain norm.:	0 dB/km		
α snow dry norm.:	0 dB/km		
α snow wet norm.:	0 dB/km		
α add total norm.:	10,3256 dB/km		

Fig. 13. Output of steady model for Sonabeam 52E.

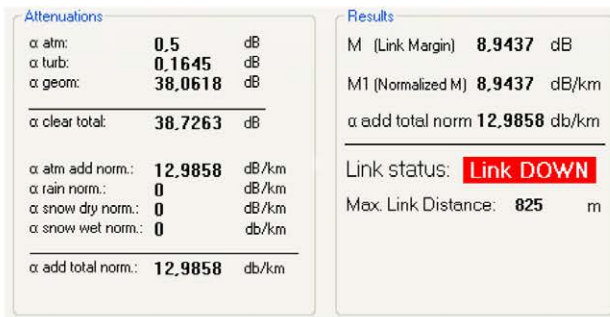


Fig. 14. Output of steady model for CableFree Access A1000.

From obtained data we can say, that first and second system is suitable for the considered environment. System PAV Light Gigabit still has some drawbacks and system Sonabeam 52E is located on the edge of functionality. Third system CableFree Access A1000 is not suitable with these properties for environment.

IV. SOFTWARE PACKAGE FOR THE STATISTIC SIMULATION OF THE FSO LINK

As was mentioned above in chapter two, FSO System Simulator includes two cards that deal with statistical parameters. First card of statistical models is named as "Statistical model" and works on the principle collecting data from databases. Collecting data is performed in two ways.

A. Statistical model

The first method uses data which are read from an artificial server that was created through the Wampeserver testing purposes. This database also runs on school website los.fei.tuke.sk. On this server we have created the MySQL database, which consists of two tables whose names are LZIB and LZIB_fade. Table LZIB consists of data downloaded from the websites of airports [3,4]. Downloaded data are about visibilities [m] from these airports.

The second table consists of established values because these values are not freely accessible on the Internet, so they have to be measured. With moving the cursor to set the Tools tab and then Database Fig. 15 we can see a table of input values, Fig. 16.

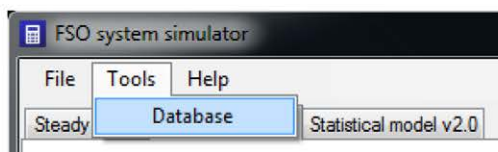


Fig. 15. Procedure to view a table.

As we can see the first tab called Database settings contains information about connecting to the server Fig 16.

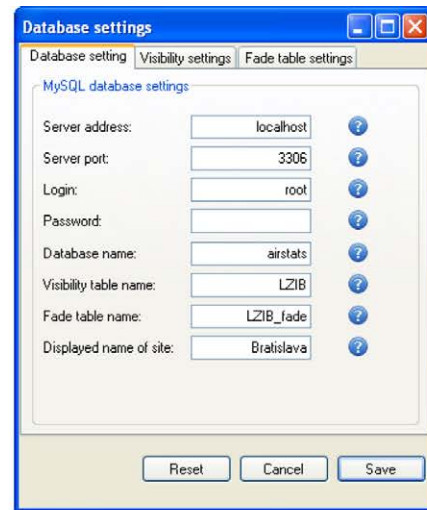


Fig. 16. Assign fields to connect to the database.

Here are described individual items:

Server address - the address of server where is given database. In this case it is a virtual server name in the program Wampserver

Server port- port number through which is your computer connects to the server. In this case it is the port number of our PCs because the database is running on our PC via the program Wampserver

Login- access name to the server

Password- password for the server

Database name- database name removal, in this case is a database airstats

Visibility table name- name of the first table which was downloaded from the websites of airports in this case it is LZIB

Fade table name- name of the other creating a table in this case it is LZIB_fade

These settings can be changed for any connection to the server if you know the necessary data.

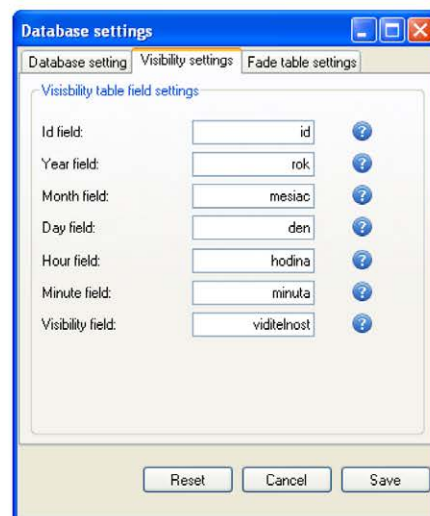


Fig. 17. Assign fields for column headings in table LZIB.

In the Fig. 17 is illustrated second tab *Visibility settings* represents the columns in the table with titled LZIB. LZIB column in the table are listed under the names we see inscribed in the fields to fill.

Tab in Fig. 18 under the card *Fade table setting* represents the columns in the table title LZIB_fade are listed under the names we see inscribed in the fields to fill.

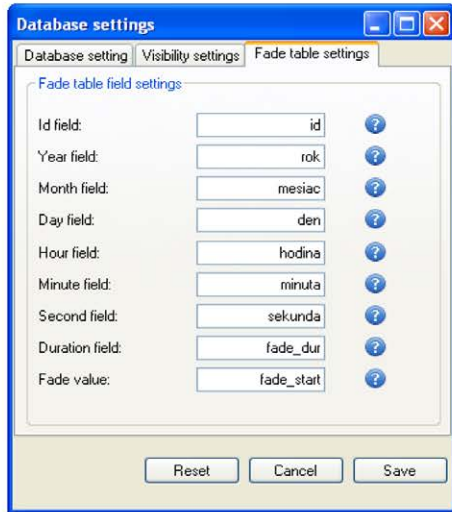


Fig. 18. Assign fields for column headings in table LZIB_fade.

Under the settings in the Fig. 17, Fig. 18 and Fig. 19 there are three buttons.

Reset- all user settings are canceled and set to the basic settings

Cancel- this button cancel the selection, alternative to this button is red cross into the top of the right corner

Save- all user settings are saved

Blue question mark belongs for each input field. After click on it, it provides a help for user.

The second way how to obtain data for calculation in the statistical model is downloading values from tables saved in the .txt file, Fig. 19. Values in row are in this order: id; year; month; day; hour; minute and visibility. Number "id" means the number of seconds from the current day. Every day has 86 400 seconds. The measuring starts with 0 and ends with 86 399.

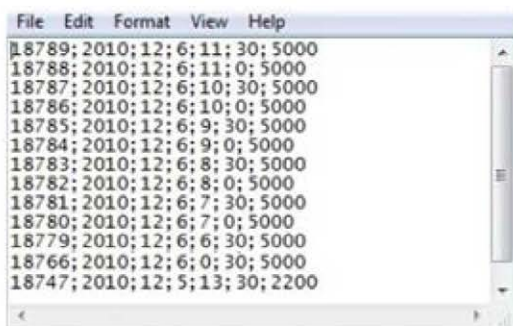


Fig. 19. Saved table in Data Name folder.

The output of the statistical model is shown in Fig. 20 where the first graph shows statistics of attenuation for one day every half hour. The second graph shows statistics of attenuation during one month. Blue curve shows the attenuation value and the red curve is the value of a safety margin. If the blue curve exceeds the red curve, connection will be interrupted. From the first graph we can say, that link was still active and without fades, but on the second graph there are several values which exceed Link margin border.

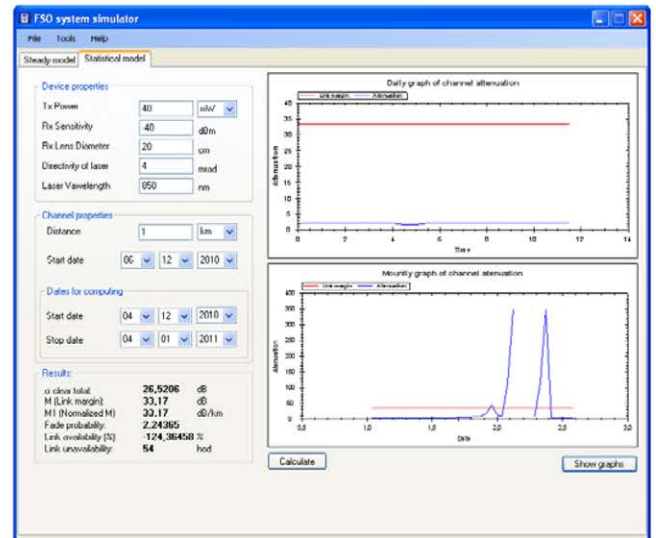


Fig. 20. The output of the statistical model.

The field *RESULTS* contains six values:

alpha clear total - this field displays the attenuation of pure atmosphere calculated from the output values. The value is displayed in dB and it is rounded to four decimal places.

M (Link margin) - this field displays the link margin; (output value in dB).

M1 (Normalized M) - this field shows the normalized M, it means that M is divided by the total distance.

Fade probability - it means the probability of fade and the failure of the connection during the chosen period. This value is rounded to five decimal places.

Link availability - displayed value indicated availability of link at percentage for a specified period. This value is rounded to five decimal places.

Link unavailability - is value of unavailability of connections for all the time. The value is displayed in seconds if the unavailability of link is less than 900 seconds. If the unavailability of link is greater than 900 seconds but less than 900 minutes the value is displayed in minutes and rounded. If the time stamp value is greater than 900 minutes is displayed in hours.

B. Statistical model v. 2.0

Second card of statistical models is named as "*Statistical model v. 2.0*" (Fig. 21) and works on the principle processing data from Fog sensor. It is a device for measuring density of fog [g/m³], temperature [C°] and relative humidity [%]. From information about density of fog it is able to calculate

availability of FSO link. Collecting data is performed by the Fog sensor, which measured data and then sending to server every second [13,14].

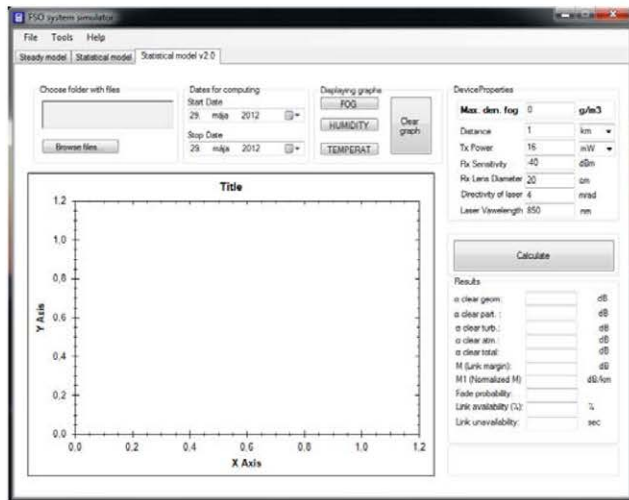


Fig. 21. Main window of Statistical model v. 2.0.

Every day is presented by one .txt file in folder. At the end of the day using .txt file is closed and new .txt file is opened for next day. In every .txt file are five columns. First three columns belong to measured data of density of fog, temperature and relative humidity. Next two columns give us information about average value and sequence number. Every day contains 86 400 values [12].

Before calculation it is necessary make some settings first. You have to do these settings from top left corner to bottom right corner (Fig. 22). At first it is needed to choose folder with files.

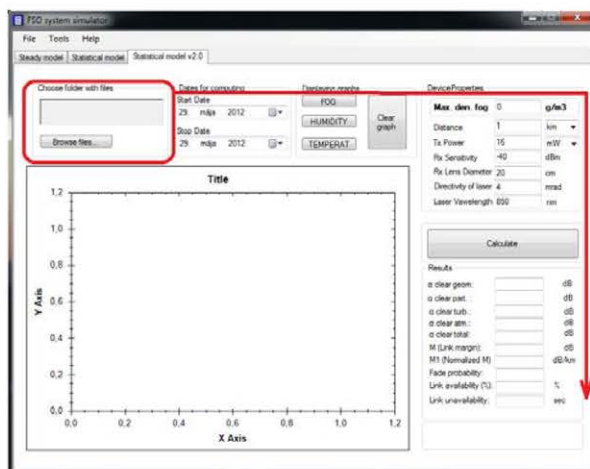


Fig. 22. Main window of Statistical model v. 2.0.

Then you choose actual date from what we want to use data for calculation (Fig. 23). There are two dates for filling, start and stop date. After selection a date is possible to create three types of graph. Graph about fog, humidity and temperature or all three types of graph in one.

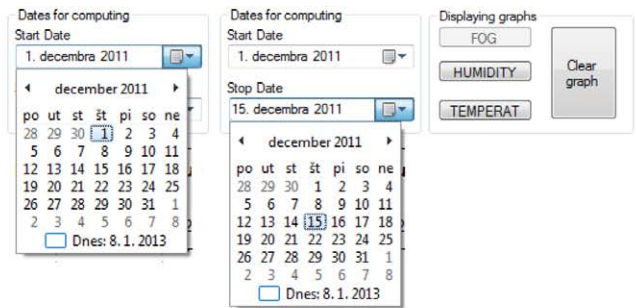


Fig. 23. Choosing dates for calculating from 1.12.2011 to 15.12.2011.

In Fig. 24 is illustrated graph of density of fog calculated from 1-15.12.2011.

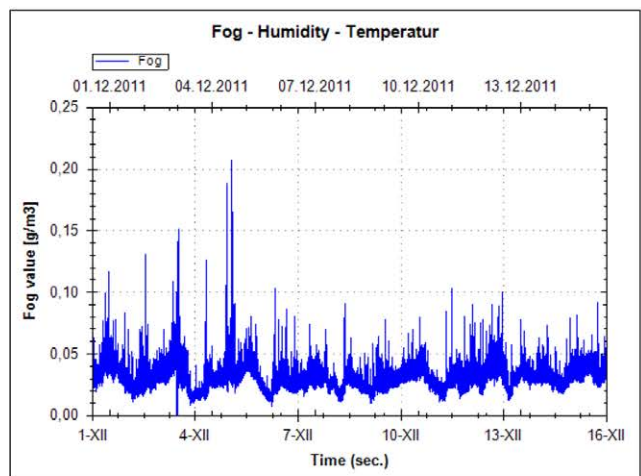


Fig. 24. Graph of fog from 1.12.2011 to 15.12.2011.

Next part of main window is called *Device properties*. There are seven fields for fill (Fig. 25).

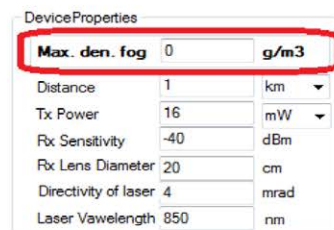


Fig. 25. Device properties.

In this section it is able to fill exact value of device for which you calculate availability of system. *Max. den. fog* is a threshold value for decision if the link is available or not. All values which are higher than threshold value cause decreasing of signal or totally damage of it. Other parameters are described below:

- Distance*- is distance between transmitter and receiver. It can be specified in meter or in kilometer
- Tx Power*- is power of transmitter in dB or mW
- Rx Sensitivity*- is sensitivity of receiver in dBm
- Rx Lens Diameter*- is diameter of receiving lens in cm
- Directivity of laser*- is directivity of laser beam in mrad
- Laser Wavelength*- is wavelength of laser beam in nm

Software Package for Analyze FSO Links

After filling all parameters it is able to push *Calculate* button and program gets results (Fig. 26).

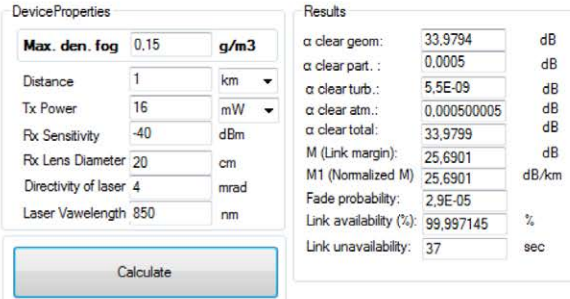


Fig. 26. Results of Statistical model v. 2.0.

Threshold value *Max.den. fog* makes a line in a graph of fog. As we can see in Fig. 27 some measured values of density of fog are higher than threshold. All values which exceed threshold are written in OverFog.txt (Fig.28). Values in row are in this order: measured value of *Max.den.fog*; exact time of fade, count of seconds from current day ("id") and duration of fade.

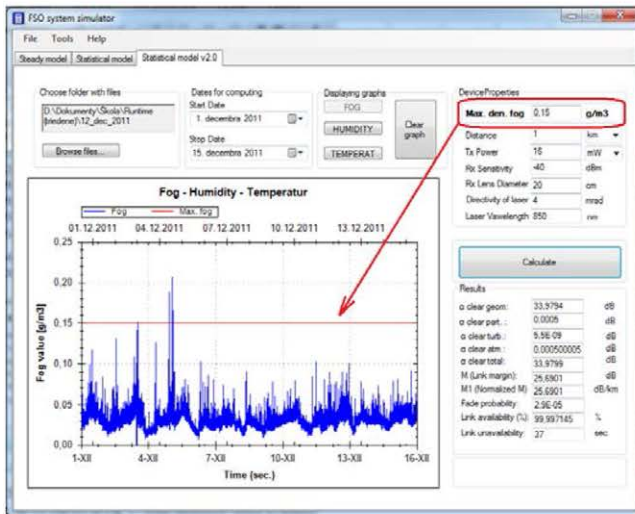


Fig. 27. Graph of fog from 1.12.2011 to 15.12.2011 with threshold.

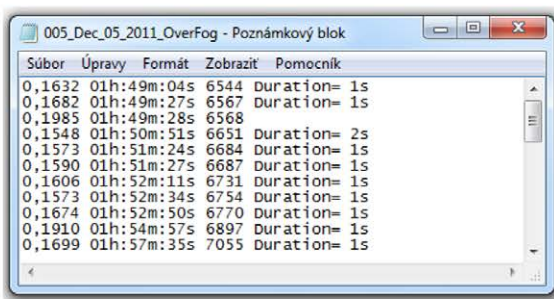


Fig. 28. Values higher than threshold.

In the Fig. 27 you can see a part named as *Results*. All of these parameters are described below:

α clear geom.- value of geometrical attenuation under clear atmosphere conditions in [dB]

α clear part.- attenuation value of particles under clear atmosphere conditions in [dB]

α clear turb.- value of attenuation due to turbulence under clear atmosphere conditions in [dB]

α clear atm.- value of atmospheric attenuation in [dB]

α clear total.- value of total attenuation under clear atmosphere conditions in [dB]

M (link margin)- value of link margin in [dB]

M1 (normalized M)- normalized value of link margin to unit length in [dB/km]

Fade probability- percentage probability of fade, or loss of signal between transmitter and receiver in [%]

Link availability- availability of link in [%]

Link unavailability-unavailability of link in [%]

ACKNOWLEDGMENT



We support research activities in Slovakia / Project is co-financed from EU funds. This paper was developed within the Project "Centrum excelentnosti integrovaného výskumu a využitia progresívnych materiálov a technológií v oblasti automobilovej elektroniky", ITMS 26220120055.

V. CONCLUSION

Optical wireless communications are evolving technology which rapidly spread from objects in need of reliable backup and high speed transmission (banks and large management companies) through various institutions located in the densely populated and built up areas for internet service provider. Transmission medium for laser beam of FSO systems is air and free environment. It is necessary to know details of each element of transmission channel. For obtaining optimal parameters for setting up the FSO systems is this FSO system simulator the best solution. Simulation of transmission channel of FSO systems is essential tool for designing and experimenting with such devices. FSO system simulator provides many setting for device properties, for weather parameters and making it possible to compare different devices from different manufacturers. Also from measured data about weather conditions allows calculate availability and reliability of FSO link. Statistical evaluation allows us to monitor certain areas during long time and output data gives us an image of potential uses FSO in this area.

REFERENCES

- [1] R. Kvicala, V. Kvicera, M. Grabner, O. Fiser, "BER and Availability Measured on FSO Link." Radioengineering, Vol. 16, No. 3, 2007.
- [2] P. Hovorák, O. Wilfert, "Free space optics - Measurement of Transmission Quality Link Parameters." Electronics'2005, 21-23 September, Sozopol, Bulgaria.
- [3] P. Hankovský, "Modelovanie optických komunikácií voľným prostredím I.," Diplomová práca, 2010.
- [4] R. German, "Modelovanie optických komunikácií voľným prostredím II.," Diplomová práca, 2010.
- [5] Z. Kolka, O. Wilfert, O. Fiser, "Achievable qualitative parameters of optical wireless links," Journal of Optoelectronics and Advanced Materials, Vol. 9, No. 8, August 2007, pp. 2419-2423.
- [6] M. O. Zatarí, "Wireless Optical Communication Systems in Enterprise Network," Telecommunications Review, 2003.
- [7] I. Kim, B. McArthur, E. Korevaar, "Comparison of Laser Beam Propagation at 785 nm and 1550 nm in Fog and Haze for Optical Wireless Communications," In Proceedings of SPIE, Volume 4241, Boston, USA, 2001, pp. 26-37.

[8] O. Bouchet, D. O'Brien, M. El Tabach, M. et al., "State of the Art-Optical Wireless," Deliverable D4.1, ICT- Omega, 2008.

[9] S. Hranilovic, "Wireless Optical Communication Systems, Spring, USA, 2005.

[10] O. Bouchet, et al., "Free- Space Optics Propagation and Communication," In Proceedings of ISTE, 2006.

[11] S. Bloom, E. Korevaar, J. Shuster, H. Willebrand, "Understanding the Performance of Free- Space Optics," Journal of Opt. Netw., Volume 2, No. 6, 2003, pp. 178-200.

[12] M. Tatarko, P. Mišenčík, „Measuring of Visibility by fog sensor,“ 12. Workshop of Elektrotechnical Research and practice : conference proceedings, April, 2012, Ostrava, Czech Republic, ISBN 978-80-248-2664-6.

[13] M. Tatarko, L. Ovseník, J. Turán, „Availability and Reliability of FSO links Estimation from Measured Fog Parameters,“ In MIPRO 2012, Jubilee 35. International convention, May, 2012, Opatija, Croatia, ISBN 978-953-233-069-4.

[14] M. Tatarko, „Measuring of availability and reliability of FSO links from measured weather parameters,“ In SCYR 2012, 12th Scientific Conference of Young Researchers, May, 2012, Herľany, Slovakia, ISBN 978-80-553-0943-9

[15] S. SHEIKH MUHAMMAD, „Investigation in Modulation and Coding for Terrestrial Free Space Optical Links,“ March 2007, Austria, 127 p

BIOGRAPHIES



Matúš TATARKO received Ing. (MSc.) degree in 2011 at Department of Electronics and Multimedia Telecommunications, Faculty of Electrical Engineering and Informatics of Technical University of Košice. Since September 2011 he has been at University of Technology, Košice as PhD. student. His research interests include free space optics systems and impact weather of them.



Ľuboš OVSEŇÍK (doc., Ing., PhD.) received Ing. (MSc.) degree in radioelectronics from the University of Technology, Košice, in 1990. He received PhD. degree in electronics from University of Technology, Košice, Slovakia, in 2002. Since February 1997, he has been at the University of Technology, Košice as Associate Professor for electronics and information technology. His general research interests include optoelectronic, digital signal processing, photonics, fiber optic communications and fiber optic sensors.



Ján TURÁN (Dr.h.c., Prof., RNDr., Ing. DrSc.) received Ing. (MSc.) degree in physical engineering with honours from the Czech Technical University, Prague, Czech Republic, in 1974, and RNDr. (MSc.) degree in experimental physics with honours from Charles University, Prague, Czech Republic, in 1980. He received a CSc. (PhD.) and DrSc. degrees in radioelectronics from University of Technology, Košice, Slovakia, in 1983, and 1992, respectively. Since March 1979, he has been at the University of Technology, Košice as Professor for electronics and information technology. His research interests include digital signal processing and fiber optics, communication and sensing.

CALL FOR PAPERS

Special Issue on Autonomic Communications

The explosion in the size of communication networks, including the Internet, and their increasing diversity, and the ever increasing burden imposed on communication networks by pervasive computing and the Internet of Things, means that networks that are statically organized are unable to cope with ever changing conditions. The speed at which conditions change are also making it very difficult, and extremely expensive, to rely on human intervention to provide the adaptation that is constantly needed. Autonomic Communications, and the underlying Autonomic Computing, with their requirements for system Self-Awareness, Learning and Adaptation, Self-Healing, and Adaptive QoS, offer a way forward to address this dilemma. Thus since the early 2000's significant work has been carried out both in research environments and in industry to define the principles and main component technologies for Autonomic Communications. Worldwide, numerous research projects have been conducted in this area, including in a series of successful EU FP6 and FP7 projects.

Thus our journal is calling for original and unpublished contributions to this important area that will be refereed. Selected papers will appear in a Special Issue to be published in September of 2013. Original and unpublished papers should be submitted by 1st of May, 2013 in the form of pdf files in IEEE format according to the formatting instructions available at http://www.ieee.org/publications_standards/publications/authors/authors_journals.html#sect2.

Submissions should be sent in the form of an email attachment to the Special Issue Editor Prof Erol Gelenbe at the following address: e.gelenbe@imperial.ac.uk. Authors will be informed of acceptance or rejection before the 1st of June 2013, and papers in final form will be due on 1st July 2013. Papers rejected for the Special Issue, may later be revised and resubmitted for consideration as regular papers in the Infocommunications Journal.

Guest Editor:

EROL GELENBE is the Professor in the Dennis Gabor Chair at Imperial College, London, and has actively developed the field of Autonomic Communications. His other areas of interest include neuronal networks and bioinformatics, performance engineering, energy modeling for computer systems and networks, and network security. He currently leads the EU FP7 Project NEMESYS on mobile network security. He participates in the ECROPS project on energy savings in computing and communications, and in the European Institute of Technology Project on Smart Networks at the Edge. A Fellow of IEEE and ACM, he was elected to Foreign Membership of the Hungarian Academy of Sciences, and is a member of the French National Academy of Engineering and of the Science Academy of Turkey.



CALL FOR PAPERS

Special Issue on Cognitive Infocommunications

CogInfoCom is a new interdisciplinary field of science defined as follows: Cognitive infocommunications (CogInfoCom) investigates the link between the research areas of infocommunications and cognitive sciences, as well as the various engineering applications which have emerged as the synergic combination of these sciences. The primary goal of CogInfoCom is to provide a systematic view of how cognitive processes can co-evolve with infocommunications devices so that the capabilities of the human brain may not only be extended through these devices, irrespective of geographical distance, but may also interact with the capabilities of any artificially cognitive system. This merging and extension of cognitive capabilities is targeted towards engineering applications in which artificial and/or natural cognitive systems are enabled to work together more effectively.

For more information on CogInfoCom please visit its home-site at www.coginfocom.hu

Contributions are expected from the following areas:

- 3D visualization and interaction
- Augmented cognition (AugCog)
- Brain-computer interface
- Cognitive informatics and media
- Cognitive robotics, etho-robotics
- Ethology-inspired engineering
- Human-computer and Human-robot interaction, interaction capabilities of CogInfoCom systems
- Interactive systems engineering
- Media Informatics
- Real and virtual avatars
- Social networks
- Vehicle informatics
- Virtual Reality Technologies and Scientific
- Affective computing
- Body area network
- Cognitive control
- Cognitive linguistics
- Cognitive science
- Future internet
- iSpace research
- Multimodal interaction
- Sensory substitution & sensorimotor extension
- Teleoperation
- Visualization

The authors are encouraged to submit full papers describing original, previously unpublished, complete research, not currently under review by another conference or journal, addressing state-of-the-art research and developments.

All papers will be reviewed and accepted papers will appear in the Infocommunications Journal. Papers must be submitted electronically in IEEE format (double column A/4, page limit 8-10 pages). For formatting instructions, please visit www.infocommunications.hu.

Authors' Schedule

Full paper submission: April 20, 2013, notification: May 20, 2013, final submission: June 10, 2013.

Paper submission

Please send manuscripts in PDF format to the Guest Editor of this Special Issue of Infocommunications Journal at baranyi@sztaki.hu.

Guest Editor:

PÉTER BARANYI

Computer and Automation Research Institute – Hungarian Academy of Sciences

13-17 Kende u., Budapest, H-1111 Hungary

Phone: +36 1 279 6111 Fax: +36 1 279 6218

E-mail: baranyi@sztaki.hu

CALL FOR PAPERS

Special Issue on Cryptology

This special issue will focus on the area of cryptology and will include selected papers from the 2013 Central European Conference on Cryptology. CECC 2013 covers various aspects of cryptology, including but not limited to:

- cryptanalysis,
- design of cryptographic systems,
- general cryptographic protocols,
- pseudorandomness,
- cryptographic applications in information security,
- encryption schemes,
- post-quantum cryptography,
- signature schemes and steganography.

Detailed information on submissions to CECC 2013 and other information is provided at <http://www.fi.muni.cz/cecc/>, with April 15, 2013 being the deadline for the submission of abstracts that will be reviewed by the program committee and authors will be informed about acceptance or rejection by April 29, 2013. The conference registration deadline will be May 22, 2013, and the conference dates are June 26-28.

Submissions and presentations at the conference will be evaluated by the program committee and authors will be informed about the evaluation results no later than June 30.

No more than 5 papers from the workshop shall be selected for the special issue of the Infocommunications Journal, and authors of these papers will have the opportunity to revise their papers (including typesetting in the IEEE format) after the conference - final versions for the special issue will be due July 22, 2013.

Papers from the general public are also welcome. The deadline for submission of such papers is May 15. Papers will be peer-reviewed as usual.

Guest Editors:



VÁCLAV (VASHEK) MATYÁS is a Professor at the Masaryk University, Brno (CZ), and serves as a Vice-Dean for Foreign Affairs and External Relations, Faculty of Informatics. His research interests relate to applied cryptography and security, publishing over a hundred peer-reviewed papers and articles, and co-authoring six books. He was a Fulbright Visiting Scholar with Harvard University, Center for Research on Computation and Society, and also worked with Microsoft Research Cambridge, University College Dublin, Ubilab at UBS AG, and was a Royal Society Postdoctoral Fellow with the Cambridge University Computer Lab. Vashek was one of the Editors-in-Chief of the Identity in the Information Society journal, and he also edited the Computer and Communications Security Reviews, and worked on the development of Common Criteria and with ISO/IEC JTC1 SC27. Vashek is a member of the Editorial Board of the Infocommunications Journal. He received his PhD degree from Masaryk University, Brno and can be contacted at matyas@fi.muni.cz.



ZDENEK RIHA is an Assistant Professor at the Masaryk University, Faculty of Informatics, in Brno (CZ). He received his PhD degree from the Faculty of Informatics, Masaryk University. In 1999 he spent 6 months on an internship at Ubilab, the research lab of the bank UBS, focusing on security and usability aspects of biometric authentication systems. Between 2005 and 2008 he was seconded as a Detached National Expert to the European Commission's Joint Research Centre in Italy, where he worked on various projects related to privacy protection and electronic passports. He was involved in the ePassport interoperability group known as the Brussels Interoperability Group. Zdenek has been working with the WG 5 (Identity management and privacy technologies) of ISO/IEC JTC 1/SC 27. Zdenek's research interests include smartcard security, PKI, security of biometric systems and machine readable travel documents. Zdenek can be contacted at zriha@fi.muni.cz.



MAREK KUMPOST is a Research Assistant at the Masaryk University, Faculty of Informatics, in Brno (CZ). He received his PhD in 2009 from the Faculty of Informatics, Masaryk University. The primary area of his doctoral research was oriented on privacy protection, anonymity and user profiling. He was involved in two European-wide project on privacy protection and identity management – FIDIS (Future of Identity in the Information Society) and PICOS (Privacy and Identity in Management for Community Services). He spent 3 months with the LIACC (Laboratory of Artificial Intelligence and Computer Science) group working on user profiling based on information from NetFlow. He is also interested in network security, web application security and cloud security. Marek can be contacted at kumpost@fi.muni.cz.

Guidelines for our Authors

Format of the manuscripts

Original manuscripts and final versions of papers should be submitted in IEEE format according to the formatting instructions available on

http://www.ieee.org/publications_standards/publications/authors/authors_journals.html#sect2, "Template and Instructions on How to Create Your Paper".

Length of the manuscripts

The length of papers in the aforementioned format should be 6-8 journal pages.

Wherever appropriate, include 1-2 figures or tables per journal page.

Paper structure

Papers should follow the standard structure, consisting of *Introduction* (the part of paper numbered by "1"), and *Conclusion* (the last numbered part) and several *Sections* in between.

The Introduction should introduce the topic, tell why the subject of the paper is important, summarize the state of the art with references to existing works and underline the main innovative results of the paper. The Introduction should conclude with outlining the structure of the paper.

Accompanying parts

Papers should be accompanied by an *Abstract* and a few *index terms (Keywords)*. For the final version of accepted papers, please send the *short cvs* and *photos* of the authors as well.

Authors

In the title of the paper, authors are listed in the order given in the submitted manuscript. Their full affiliations and e-mail addresses will be given in a footnote on the first page as shown in the template. No degrees or other titles of the authors are given. Memberships of IEEE, HTE and other professional societies will be indicated so please supply this information. When submitting the manuscript, one of the authors should be indicated as corresponding author providing his/her postal address, fax number and telephone number for eventual correspondence and communication with the Editorial Board.

References

References should be listed at the end of the paper in the IEEE format, see below:

- a) Last name of author or authors and first name or initials, or name of organization
- b) Title of article in quotation marks
- c) Title of periodical in full and set in italics
- d) Volume, number, and, if available, part
- e) First and last pages of article
- f) Date of issue

[11] Boggs, S.A. and Fujimoto, N., "Techniques and instrumentation for measurement of transients in gas-insulated switchgear," *IEEE Transactions on Electrical Installation*, vol. ET-19, no. 2, pp.87–92, April 1984.

Format of a book reference:

[26] Peck, R.B., Hanson, W.E., and Thornburn, T.H., *Foundation Engineering*, 2nd ed. New York: McGraw-Hill, 1972, pp.230–292.

All references should be referred by the corresponding numbers in the text.

Figures

Figures should be black-and-white, clear, and drawn by the authors. Do not use figures or pictures downloaded from the Internet. Figures and pictures should be submitted also as separate files. Captions are obligatory. Within the text, references should be made by figure numbers, e.g. "see Fig. 2."

When using figures from other printed materials, exact references and note on copyright should be included. Obtaining the copyright is the responsibility of authors.

Contact address

Authors are requested to send their manuscripts via electronic mail or on an electronic medium such as a CD by mail to the Editor-in-Chief:

Csaba A. Szabo
 Department of Networked Systems and Services
 Budapest University of Technology and Economics
 2 Magyar Tudosok krt.
 Budapest, 1117 Hungary
 szabo@hit.bme.hu



**IEEE INTERNATIONAL CONFERENCE
ON COMMUNICATIONS**
INDUSTRY FORUM & EXHIBITION
9-13 JUNE • BUDAPEST, HUNGARY



BRIDGING THE BROADBAND DIVIDE



IEEE ICC is dedicated to furthering the understanding of communications areas currently under research and to fostering next-generation theories and practices.

The **12 Technical Symposia** will feature presentations on current research and development results in areas of networks and the Internet, communications QoS, communication software and services, security, optical networks, and wireless communications and networking.

22 Tutorials, 20 Workshops and 10 Industry & Business Panels will provide more application and implementation-oriented information in a broad range of communication areas from cognitive radio networks, ultrawide bandwidth systems and automotive networking and telematics to cognitive and cooperative wireless networks and green communications.

Exciting and thought-provoking **Keynote & Invited Addresses** will be delivered by top industry executives and academic advisors.

KEYNOTES



Gerhard P. Fettweis
TU Dresden



Thomas Wiegand
TU Berlin



Peter Winzer
Bell Labs, Alcatel-Lucent

INVITED SPEAKERS



Jakob Hoydis
Alcatel-Lucent,
Bell Labs



Ove Edfors
Lund University



Michalis Matthaiou
Chalmers University
of Technology



David Gesbert
EURECOM



Ralf Müller
University of
Erlangen-Nuremberg



Giuseppe Caire
University of Southern
California, Los Angeles



Theodore S. Rappaport
Polytechnic Institute of
New York University



Amitabha Ghosh
Nokia Siemens Networks



Upamanyu Madhow
University of California,
Santa Barbara



Robert W. Heath Jr.
University of Texas,
Austin



Wonil Roh
Samsung Electronics

Register by 26 April 2013 to receive the reduced rate!
www.ieee-icc.org/2013

SCIENTIFIC ASSOCIATION FOR INFOCOMMUNICATIONS



Who we are

Founded in 1949, the Scientific Association for Infocommunications (formerly known as Scientific Society for Telecommunications) is a voluntary and autonomous professional society of engineers and economists, researchers and businessmen, managers and educational, regulatory and other professionals working in the fields of telecommunications, broadcasting, electronics, information and media technologies in Hungary.

Besides its more than 1300 individual members, the Scientific Association for Infocommunications (in Hungarian: HÍRKÖZLÉSI ÉS INFORMATIKAI TUDOMÁNYOS EGYESÜLET, HTE) has more than 60 corporate members as well. Among them there are large companies and small-and-medium enterprises with industrial, trade, service-providing, research and development activities, as well as educational institutions and research centers.

HTE is a Sister Society of the Institute of Electrical and Electronics Engineers, Inc. (IEEE) and the IEEE Communications Society. HTE is corporate member of International Telecommunications Society (ITS).

What we do

HTE has a broad range of activities that aim to promote the convergence of information and communication technologies and the deployment of synergic applications and services, to broaden the knowledge and skills of our members, to facilitate the exchange

of ideas and experiences, as well as to integrate and harmonize the professional opinions and standpoints derived from various group interests and market dynamics.

To achieve these goals, we...

- contribute to the analysis of technical, economic, and social questions related to our field of competence, and forward the synthesized opinion of our experts to scientific, legislative, industrial and educational organizations and institutions;
- follow the national and international trends and results related to our field of competence, foster the professional and business relations between foreign and Hungarian companies and institutes;
- organize an extensive range of lectures, seminars, debates, conferences, exhibitions, company presentations, and club events in order to transfer and deploy scientific, technical and economic knowledge and skills;
- promote professional secondary and higher education and take active part in the development of professional education, teaching and training;
- establish and maintain relations with other domestic and foreign fellow associations, IEEE sister societies;
- award prizes for outstanding scientific, educational, managerial, commercial and/or societal activities and achievements in the fields of infocommunication.

Contact information

President: **DR. GÁBOR HUSZTY** • ghuszty@entel.hu

Secretary-General: **DR. ISTVÁN BARTOLITS** • bartolits@nmhh.hu

Managing Director, Deputy Secretary-General: **PÉTER NAGY** • nagy.peter@hte.hu

International Affairs: **ROLLAND VIDA, PhD** • vida@tmit.bme.hu

Addresses

Office: H-1055 Budapest, V. Kossuth Lajos square 6-8, Room: 422.

Mail Address: 1372 Budapest, Pf. 451., Hungary

Phone: +36 1 353 1027, Fax: +36 1 353 0451

E-mail: info@hte.hu, Web: www.hte.hu